BOSTON UNIVERSITY

SCHOOL OF MEDICINE

Dissertation

DYNAMIC BRAIN NETWORK RECONFIGURATION SUPPORTS ABSTRACT REASONING AND RULE LEARNING

by

THOMAS M. MORIN

B.S., Tufts University, 2017

Submitted in partial fulfillment of the

requirements for the degree of

Doctor of Philosophy

2022

Approved by

First Reader

Chantal E. Stern, D.Phil.
Professor of Psychological and Brain Sciences
Boston University

Second Reader

Joseph T. McGuire, Ph.D.
Assistant Professor of Psychological and Brain Sciences
Boston University

Third Reader

David Badre, Ph.D.
Professor of Cognitive, Linguistic and Psychological Sciences
Brown University

DEDICATION

To all of my teachers.

Thanks for twenty-two extraordinary years of learning!

ACKNOWLEDGMENTS

I am tremendously grateful for the people in my life who made this work possible. I'm sure I'm not alone in saying that these last few years have been some of the most challenging and transformative of my life. Pursuing a PhD in these times has made me even more thankful for the communities of scholars, mentors, friends, and family that I am incredibly privileged to be a part of.

My thesis advisor, Chantal Stern has gone above and beyond to provide technical insight, professional guidance, and personal support to me and the other members of our lab. As I move forward in my own career, I aspire to emulate Chantal's composed demeanor in the face of difficulties, thoughtful approach to leadership, and unmatched understanding of the mind and brain. The members of my dissertation advisory committee, Mike Hasselmo, Joe McGuire, David Somers, and David Badre, have each inspired me intellectually and motivated me to ask deeper scientific questions. I'd like to especially thank David Somers for providing me with a second home in his lab at the beginning of my graduate career, and Joe McGuire for sparking several of the ideas that evolved into chapters of this dissertation.

Chantal Stern has a knack for recruiting incredible scientists to the Cognitive Neuroimaging Lab, and I am incredibly thankful to have worked alongside many: Allen Chang, Rachel Wehr, Justine Cohen, Matt Dunne, Stamati Liapis, Kylie Moore, Caroline Ahn, Kylie Isenburg, and Jing Guo. To Matt Dunne, thank you for teaching me all about hippocampal segmentations and for the countless scientific and personal conversations we've shared over five years of sharing an office. Thank you also to the many

undergraduate research assistants I've had the privilege to mentor and learn from over the last five years, especially Weida Ma who took a chance on a side project and developed it into a new line of research for the lab.

Thank you to Jun Shen and Denise Parisi for providing administrative support and a friendly face for students. Thank you to Eric Kolaczyk and Daniel Sussman for teaching invaluable courses in statistics and network science that inspired several of the projects in this dissertation. Thank you to the staff, past and present, in the Cognitive Neuroimaging Center, Stephanie McMains, Jay Bohland, Dustin Clark, and especially Shruthi Chakrapani whose friendship has made coming to work especially fun.

Thank you to Shelley Russek, Sandi Grasso, Nazifa Haque, and Lavell Blackwell for building such a wonderful community of scholars in the Graduate Program for Neuroscience. The primary reason I chose to pursue a PhD at Boston University was because of the incredible community of students studying neuroscience here. To the many students studying the brain at BU in the GPN and BBC programs, thank you for providing invaluable mentorship, advice, and friendship over the years. In particular, I'd like to recognize the members of my cohort: Lucas Carstensen, Kaitlyn Dorst, Margaret Minnig, Luis Ramirez, and Michael Rosario. Whether we were studying together for one of Doug Rosene's quizzes, kayaking at the annual GPN retreat, or streaming an episode of RuPaul's Drag Race over Zoom, it's been a great joy of my life to experience how the people I once considered "work-colleagues" are now my chosen family.

Thank you to my previous mentors Jacob Hooker and Monica Wey at the MGH Martinos Center for taking a chance on me and welcoming me into the world of

neuroimaging research. Thank you to Ani Patel at Tufts for the sage advice and teaching opportunities. Thank you also to Ayanna Thomas at Tufts for your professional wisdom and for inviting me to join the "Pandemic Writing Group." Thank you to my former high school teachers Meaghan Germain and Robert Marx for inspiring me to get a PhD in the first place and for making sure I knew I was capable.

To the experimental participants who allowed us to collect psychometric and MRI data, thank you. Without your contributions, our science would not be possible.

Finally, thank you to my family and to my partner, Darius, for their unwavering love and support.

Funding: This work was supported by the Office of Naval Research (grant numbers MURI N00014-16-1-2832, DURIP N00014-17-2304), and the National Science Foundation (grant number 1625552).

DYNAMIC BRAIN NETWORK RECONFIGURATION SUPPORTS ABSTRACT REASONING AND RULE LEARNING

THOMAS M. MORIN

Boston University School of Medicine, 2022

Major Professor: Chantal E. Stern, D.Phil., Professor of Psychological and Brain Science

ABSTRACT

Variability in the brain's functional network connectivity is associated with differences in cognition. The degree to which brain networks flexibly reconfigure, or alternatively remain stable, can differ across regions of cortex, across time, and across individuals. The goal of this dissertation was to investigate how the brain's functional network architecture is reconfigured to support abstract reasoning and rule learning. I proposed that flexibility within frontoparietal cortex, combined with a stable network core, is beneficial for effective reasoning and rule learning.

Experiment One investigated the activation patterns and dynamic community structure of brain networks associated with shifting task demands during abstract reasoning. Twenty-seven subjects underwent fMRI scanning during resting state and during a subsequent abstract reasoning task. When quantifying network reconfiguration between resting and task states, I found a stable system within default and somatomotor networks alongside a more flexible frontoparietal control network. The results motivated a novel understanding of how the brain performs reasoning tasks: an underlying stable functional network acts as a cognitive control mechanism, priming task-active nodes within frontoparietal cortex to variably activate for unique task conditions.

Experiment Two used a dynamic network analysis to identify changes in functional brain networks that were associated with context-dependent rule learning. During fMRI scanning, twenty-nine naïve subjects were challenged to learn a set of context-dependent rules. Successful learners showed greater stability in ventral attention and somatomotor regions, increased assortative mixing of cognitive control regions as rules were learned, and greater segregation of attention networks throughout the entire task. The results suggested that a stable ventral attention network and a flexible frontoparietal control network support sustained attention and the formation of rule representations.

In Experiment Three, I carried out a separate analysis of data from Experiment 2 to characterize the functional connectivity patterns with the hippocampus that emerged during successful rule learning. The results demonstrated that the hippocampal head became increasingly functionally connected to the lateral frontal pole and caudate in successful learners. Additionally, the entire hippocampus exhibited decreased functional connectivity with the mid-cingulate and precuneus in successful learners.

These three experiments demonstrated that stable functional connectivity in somatomotor and ventral attention networks, combined with flexible reconfiguration of frontoparietal cortex, is advantageous for successful rule learning and abstract reasoning. Altogether, this dissertation demonstrated that individual differences in dynamic functional connectivity are associated with learning, and that stability of brain networks across time and tasks supports higher order cognition.

TABLE OF CONTENTS

LIST OF TABLES

LIST OF FIGURES

LIST OF ABBREVIATIONS

AC-PC	Anterior Commissure-Posterior Commissure
AFNI	Analysis of Functional NeuroImages (Software)
ANOVA	Analysis of Variance
BIDS	Brain Imaging Directory Structure
BOLD	Blood Oxygenation Level Dependent
CAIPI	Controlled Aliasing in Parallel Imaging
CSF	Cerebrospinal Fluid
DTI	Diffusion Tensor Imaging
DVARS	Spatial root mean square of data after temporal differencing
EPI	Echo Planar Imaging
ETAC	Equitable Thresholding and Clustering
FD	Framewise Displacement
FDR	False Discovery Rate
fMRI	Functional Magnetic Resonance Imaging
FS-FAST	Freesurfer Functional Analysis Stream
FSL	FMRIB Software Library
FWHM	Full Width Half Maximum
GLM	General Linear Model
GM	Gray Matter
HRF	Hemodynamic Response Function
ICBM	International Consortium for Brain Mapping

INU	Intensity Non-Uniformity
ITK-SNAP	Insight Segmentation and Registration Toolkit (ITK) Library
MEMPRAGE RMS	Multi-Echo MP-RAGE Root Mean Square
MNI	Montreal Neurological Institute
MP-RAGE	Magnetization Prepared – Rapid Gradient Echo
MRI	Magnetic Resonance Imaging
MR/PET	Magnetic Resonance/Positron Emission Tomography
PFC	Prefrontal Cortex
PFIT	Parieto-Frontal Integration Theory
Pre-SMA	Pre-supplementary Motor Area
ROI	Region of Interest
RPM	Raven's Progressive Matrices
SD	Standard Deviation
SRT	Serial Reaction Time
SUMA	Surface Mapping (Software)
T1w	T1-weighted image
T2w	T2-weighted image
TE	Time to Echo
TR	Repetition Time
vlPFC	Ventrolateral Prefrontal Cortex
WM	White Matter

Yeo-7	7-network brain parcellation from Yeo et al. 2011
Yeo-17	17-network brain parcellation from Yeo et al. 2011

CHAPTER ONE: INTRODUCTION

Preamble

Variations in the functional connectivity of large-scale cortical brain networks may explain individual differences in higher-order cognitive abilities. Dynamic changes in functional connectivity within and between brain networks support the brain's ability to flexibly shift between cognitive tasks. Recent work has proposed that general human intelligence may arise from the brain's ability to both flexibly reconfigure and maintain stable functional connectivity as task demands evolve (Barbey, 2018). Studies have shown that both flexible reconfiguration (Bassett et al., 2011; Braun et al., 2015; Gerraty et al., 2018) and maintained stability (Hilger et al., 2020; Schultz & Cole, 2016; Thiele et al., 2021) of functional brain networks can be associated with better performance on a wide array of cognitive tasks.

The primary goal of this dissertation was to investigate the functional network reconfigurations that support abstract reasoning and rule learning. Using functional magnetic resonance imaging (fMRI), we characterized dynamic changes in functional brain networks as subjects performed abstract reasoning and rule learning tasks. A secondary goal of this dissertation was to characterize how variation in functional connectivity dynamics between subjects is associated with rule learning ability. The three experiments discussed in this dissertation provide evidence that regionally specific individual differences in the flexible reconfiguration of functional connectivity support higher-order cognition.

Network Neuroscience

The growing field of network neuroscience aims to provide a mathematical framework for understanding how the brain's structural and functional connections support cognition. Researchers in the field have developed a suite of graph theoretical tools that can be applied to functional MRI (fMRI) data to characterize functional connections, shifting communication patterns, and community structures that arise between brain regions (for review, see Bassett & Mattar, 2017; Betzel, 2022). Network neuroscience is based in graph theory and conceptualizes the brain as a set of interacting regions (nodes) that share information through structural or functional connections (edges). In this dissertation, brain networks are defined using fMRI. Nodes are defined as anatomically distinct brain regions. Edges connect nodes that have strong functional connectivity, where functional connectivity is typically defined as the Pearson correlation of blood oxygenation level dependent (BOLD) signal time courses. Other common metrics for quantifying functional connectivity include coherence, partial correlation, and mutual information. (For a review of different methods for constructing functional brain networks, see Betzel, 2022). Functional connectivity measures quantify the statistical linkage of interregional temporal fluctuations in BOLD signal. Functional connectivity is thought to be constrained by the anatomical connections that link brain regions, and may represent the exchange of information between distinct brain regions (Goni et al., 2014).

Depending on whether it is used in a graph theoretical or neuroscientific context, the word "network" can take on different meanings. In graph theory, the word "network" most often refers to an entire graph consisting of all nodes and edges (Kolaczyk, 2009). In

neuroscience, the word "network" most often refers to a group of brain regions exhibiting structural or functional connectivity (e.g., the frontoparietal network) (Mesulam et al., 1990; Passingham et al., 2002; Power et al., 2011; Uddin et al., 2019; Yeo et al., 2011). In this dissertation, I have primarily used the word "network" in the neuroscientific context, and have explicitly stated the type of network to which I refer (e.g., whole-brain network, frontoparietal network, etc.).

In graph theory, subcomponents of a network are referred to as communities. Communities can be defined *a priori* (e.g., assigning each brain region to a community in a pre-defined atlas). Communities can also be defined in a data-driven manner using clustering or community detection algorithms. Broadly, these algorithms typically attempt to group nodes based on factors that maximize connections within communities, and minimize connections between communities (Fortunato, 2010; Girvan & Newman, 2002; Newman & Girvan, 2004; M. A. Porter et al., 2009). When using data-driven communities, a node's community membership can change over time (Mucha et al., 2010; Palla et al., 2007). The flexibility of a brain region can be calculated by determining the number of times its community membership changes (Bassett et al., 2011).

Functional Brain Network Topography

Since the 1990s, neuroscientists have sought to divide the brain into large-scale networks based on the connectedness of disparate regions (Mesulam et al., 1990). Researchers have proposed that the function of a brain region, or more broadly the function of a brain network, is determined by its connections to other brain regions (Passingham et

al., 2002). Using resting state fMRI from large cohort studies including the Human Connectome Project, several groups have divided neocortex into large-scale functional networks (Gordon et al., 2017; Power et al., 2011; Schaefer et al., 2018; Uddin et al., 2019; Yeo et al., 2011). These standard network atlases are defined in a standard-template space, and can be applied to individuals using brain-registration techniques. The Yeo-7 parcellation contains the following seven networks: (1) visual, (2) somatomotor, (3) dorsal attention, (4) ventral attention/salience, (5) limbic, (6) frontoparietal control/cognitive control, and (7) default (see **Figure 1.1**) (Yeo et al., 2011). In the same work, Yeo and colleagues also defined a 17-network parcellation (see **Figure 1.1**). In the Yeo-17 parcellation, the Yeo-7 networks are subdivided into sixteen networks (e.g., frontoparietal control-A, frontoparietal control-B, frontoparietal control-C, etc.) and an additional temporal-parietal network is added (Yeo et al., 2011). Another functional network atlas put forth by Power et al. divides cortex into seventeen networks: default, medial visual, lateral visual, cingulo-opercular, salience, fronto-parietal, dorsal attention, ventral attention, anterior medial temporal lobe, posterior medial temporal lobe, context, auditory, hand sensorimotor, face sensorimotor, foot sensorimotor, premotor, and pre-memory (see **Figure 1.1**) (2011).

The network nomenclature from the Yeo and Power atlases is derived from the hypothesized function of the brain regions comprising each network. Generally, brain networks are divided into two main categories: unimodal and heteromodal. In the Yeo-7 atlas, the visual and somatomotor networks are considered unimodal. The visual network (purple) is located in the occipital lobe and consists of primary and secondary visual

cortices. The somatomotor network (blue) is located along the central sulcus and consists of primary motor and primary somatosensory cortices. The remaining networks make up heteromodal, or associative cortex. The dorsal and ventral attention networks (green and violet respectively) correspond to the dorsal and ventral attention streams that have been implicated in top-down and bottom-up attentional control (Corbetta & Shulman, 2002). The frontoparietal/cognitive control network (orange) consists of lateral prefrontal, lateral parietal, and dorsal anterior cingulate regions implicated in executive function behaviors such as working memory, and planning, and reasoning (Nyhus & Barceló, 2009; Vincent et al., 2008; Watson & Chatterjee, 2012). The limbic network (cream) consists of frontal pole and temporal pole regions implicated in feedback monitoring, reward, and emotional cognition (Kringelbach, 2005; Schnider et al., 2005). Finally, the default network (red), consisting primarily of medial prefrontal and medial parietal regions is named because initial studies documented the increased activation of these regions during "resting state" positing that this network maintained the brain's "default" state (Fox et al., 2005; Raichle, 2015).

Currently there is no universally agreed-upon functional network topography or naming system. For example, regions of the ventral attention network in the Yeo-7 parcellation are assigned to a mix of salience, cingulo-opercular, and ventral attention regions in the Power parcellation. Similarly, the frontoparietal control network as defined by Yeo has overlapping regions with the cingulo-opercular and frontoparietal networks in the Power parcellation (Power et al., 2011), and is sometimes instead referred to as the multiple demand system (Duncan, 2010). Network definitions can vary across atlases

because of the different methodological choices researchers made when constructing the atlases. For example, the Power atlas was constructed using a graph-theoretical clustering algorithm, known as infomap, to divide cortex into sub-networks (Fortunato, 2010; Lancichinetti & Fortunato, 2009; Power et al., 2011). The Yeo-atlas was constructed by projecting the brain-wide connectivity profiles of 18,715 vertices onto a hypersphere, and clustering vertices based on the distance from each other in hypersphere space. Notably, the Yeo-atlas's clustering approach required researchers to define the number of clusters ahead of time, and 7/17 networks were selected by measuring the stability of the clustering algorithm for all possible numbers of network assignments (Lashkari et al., 2010; Yeo et al., 2011).

Despite disagreement on the precise boundaries and naming conventions across cortical network parcellations, a concerted effort is currently underway to build consensus-based definitions of the most common cortical brain networks (Uddin et al., 2019, 2022). The universal network taxonomy proposed by Uddin and colleagues has only recently been proposed, and has not yet been widely adopted. The analyses in this dissertation use brain network definitions from the Yeo-7 cortical parcellations.

Cortical brain networks show robust within-subject reliability over time, with individual topographies that are consistent across hours, days, and weeks (Gordon et al., 2017). Additionally, some networks show greater inter-subject and within-subject variability than others. Primary sensory cortices (e.g., visual and somatomotor networks) show the greatest consistency, while associative cortex, especially the frontoparietal

control network, show the greatest variability (Krienen et al., 2014; Mueller et al., 2013; Yeo et al., 2011).

Functional Network Topology Differs (Slightly) Between Task and Rest

Importantly, one source of brain network variability stems from cognitive tasks (Salehi et al., 2020). While the core network structure of functional brain networks is largely maintained across resting and task states, there are small reliable changes in functional connectivity that are thought to be related to cognition (Krienen et al., 2014). During resting state and the transition from rest to task states, the majority of dynamic functional connectivity changes occur in frontoparietal (associative) brain regions (Bray et al., 2015; Gonzalez-Castillo et al., 2014; Hearne et al., 2017). Further research employing many repeated scanning sessions of individual subjects found that individually-defined variations in functional connectivity were maintained across both the resting and task states (Kraus et al., 2021). Cole and colleagues found that subjects showing fewer changes (higher stability) in functional connectivity between rest and task scored higher on fluid intelligence tests (Schultz & Cole, 2016). More recently, other groups have replicated this finding, building evidence that brain network stability is beneficial for higher order cognition (Hilger et al., 2020; Thiele et al., 2021). One interpretation of these findings is that more intelligent individuals have resting-state configurations that more closely relate to task-based functional connectivity states. Similarly, these results could be interpreted to show that the brain's ability to efficiently transition between resting state and task states is a key factor in cognitive performance and intelligence.

Functional Network Reconfiguration Supports Task Performance

Further research has investigated how the functional connectivity within and between cortical brain networks varies across task conditions. These studies have characterized the integration, segregation, and reconfiguration of brain networks that support a variety of higher order cognitive functions including frontoparietal control (Ray et al., 2020), reasoning (Hearne et al., 2015, 2017), working memory (Braun et al., 2015; Finc et al., 2020), and learning (Bassett et al., 2011; Gerraty et al., 2018).

One widely studied network motif is the decoupling of "task-positive" and "task-negative" networks, where a task-positive network is a group of brain regions that are functionally connected at rest and positively activated during tasks that require externally directed attention (Fox et al., 2005). Using the Yeo-7 nomenclature, this decoupling is referred to as an anticorrelation between the "task-positive" dorsal attention network and "task-negative" default network (Dixon et al., 2017, 2018). Decoupling of these networks is associated with better working memory performance (J. B. Keller et al., 2015) and is dysregulated in a number of disorders including schizophrenia, bipolar disorder, and major depressive disorder (Chai et al., 2011; Kaiser et al., 2015; Wotruba et al., 2014). Further evidence has implicated the frontoparietal control network (from the Yeo-7 atlas) (M. W. Cole & Schneider, 2007; Spreng et al., 2013) and/or the salience network (from the Power atlas) (Seeley et al., 2007) in regulating the decoupling of dorsal attention and default networks.

In addition to characterizing the coupling and decoupling patterns between networks, one can characterize the dynamic community structure of cortical brain networks

(Bassett et al., 2011; Fortunato, 2010; Mucha et al., 2010). With a sliding window analysis, functional connectivity measures can be calculated for multiple time points during either resting state or task, as well as for different task conditions. A multilayer brain network can be created where each node is connected to itself at previous and subsequent time points. Multilayer community detection can be used to quantify how the brain's community structure evolves over time (Mucha et al., 2010). In multilayer networks, a node is said to be flexible if its community membership changes frequently over time. Conversely, a node is said to be stable if its community membership remains consistent over time. Previous work has shown that increased flexibility within frontoparietal control regions is associated with increased learning on a motor sequence task (Bassett et al., 2011). Moreover, increased flexibility of fronto-striatal circuits was associated with increased learning rate on an associative learning task (Gerraty et al., 2018). An analysis of data from the MyConnectome Project (Poldrack et al., 2015) found that increased whole-brain network flexibility was also associated with positive mood and reduced event salience (Betzel et al., 2017). Together, these studies suggest that greater flexibility among associative regions may be beneficial for adaptive task control and integrating information across distal brain regions.

Hierarchical Organization of Frontoparietal Cortical Networks

Imaging work has demonstrated that associative networks located in frontoparietal cortex support executive function and frontoparietal control (for review see Menon & D'Esposito, 2021). The prefrontal cortex is hierarchically organized along a rostro-caudal

axis (Badre & D'Esposito, 2007; Badre & Nee, 2018; Koechlin et al., 2003). More caudal regions support motor-actions, mid-regions incorporate contextual information, and more rostral regions draw on learned schemas (Badre & Nee, 2018). A study by Choi et al. showed that this hierarchical organization is also reflected in lateral parietal cortex in the reverse direction (with more rostral parietal regions supporting motor actions and more caudal parietal regions implementing abstract schemas) (Choi et al., 2018). Using a hierarchical rule task, Choi and colleagues characterized the differential contributions of cortical brain networks to the hierarchical organization of frontoparietal cortex (2018). In their study, a single rule (first-order) elicited activation largely in dorsal attention and frontoparietal control network-A regions (as defined by the Yeo-17 parcellation). Higher up on the hierarchy, when four rules had to be considered at once (fourth order), brain activity increased in frontoparietal control network-A and B. These findings are supported by anatomical studies of frontoparietal activity, and correspond to fronto-striatal and parieto-striatal loops (Alexander et al., 1986; Goulas et al., 2014; Haber, 2003; Jarbo & Verstynen, 2015). These studies suggest that functional brain networks play an important role in the hierarchical control of behavior.

Organization of Dissertation

The remainder of this dissertation has been organized into four chapters. In Chapters Two, Three, and Four, I have presented results from neuroimaging studies of abstract reasoning and rule learning in humans. Specifically, I examined the dynamic network metrics and changes in functional connectivity that support abstract reasoning and

context-dependent rule learning. In Chapter Five, I summarized the research, discussed limitations, and outlined future directions.

Chapter Two investigated the brain activation and functional network reconfiguration that supports abstract reasoning. Building on previous work in our lab (Melrose et al., 2007), 27 participants were tested on a simplified Raven's Progressive Matrices task during fMRI scanning. The task investigated two types of reasoning: symbolic and perceptual. Notably, the results characterized regional variability in the amount of functional network reconfiguration when comparing resting state to the task. While default and somatomotor regions maintained a consistent community structure, frontoparietal and visual regions showed significant reconfiguration beginning with a highly fragmented community structure at rest, and forming a strongly connected community during the task. Altogether, results from this chapter suggested that the reconfiguration of frontoparietal functional connectivity supports abstract reasoning in the human brain.

Chapter Three investigated how variations in brain network dynamics are associated with learning context-dependent rules. For this study, 29 naïve participants were recruited to learn a set of context-dependent rules over the course of a single scanning session. Results from this study demonstrated that successful learners developed more stable functional community structures, particularly in ventral attention and somatomotor brain regions. As a working hypothesis, I proposed that successful learners quickly adopt effective representations of the context-dependent rules, and maintain those representations for the remainder of the task, resulting in the increased brain network stability.

Additionally, results demonstrated that successful learners benefit from a segregated community of attention nodes, as well as a community of frontoparietal control nodes that became more assortative (more highly interconnected with itself) during learning. Overall, the results demonstrated that a stable ventral attention community and flexible frontoparietal control community supported the formation of rule representations in successful learners.

Chapter Four presented a second analysis of the context-dependent rule learning task, focusing on how functional connectivity between the hippocampus and prefrontal cortex supports context-dependent rule learning. The human hippocampus exhibits an anterior-posterior axis of organization, with more anterior regions representing coarse information and more posterior regions representing fine information (Brunec et al., 2018; Poppenk et al., 2013; Strange et al., 2014) and stronger activation when implementing higher-order hierarchical rules (Brown et al., 2021). Results from this analysis demonstrated that a gradient of functional connectivity along the long axis of the hippocampus with the lateral frontal pole and caudate developed as participants successfully learned the context-dependent rules. Specifically, the hippocampal head shows an increase in functional connectivity with the lateral frontal pole and caudate in successful learners. The hippocampal body showed a less widespread increase in functional connectivity, with more caudal regions of prefrontal cortex. The hippocampal tail only showed increased functional connectivity changes with a small region of dorsolateral prefrontal cortex. The results also demonstrated that decreased functional connectivity between the hippocampal head and body (but not tail), with posterior regions of the default

network (precuneus and mid-cingulate) occurred during successful context-dependent rule learning. I showed that these functional connectivity changes were strongest during the cue period of the task, when subjects retrieved contextual information to determine which rule will apply. Finally, I showed that the rate of change in functional connectivity with the hippocampal head was associated with individual participants' overall learning rate. In Chapter Five, I discuss the main conclusions, limitations, and future directions of this work.

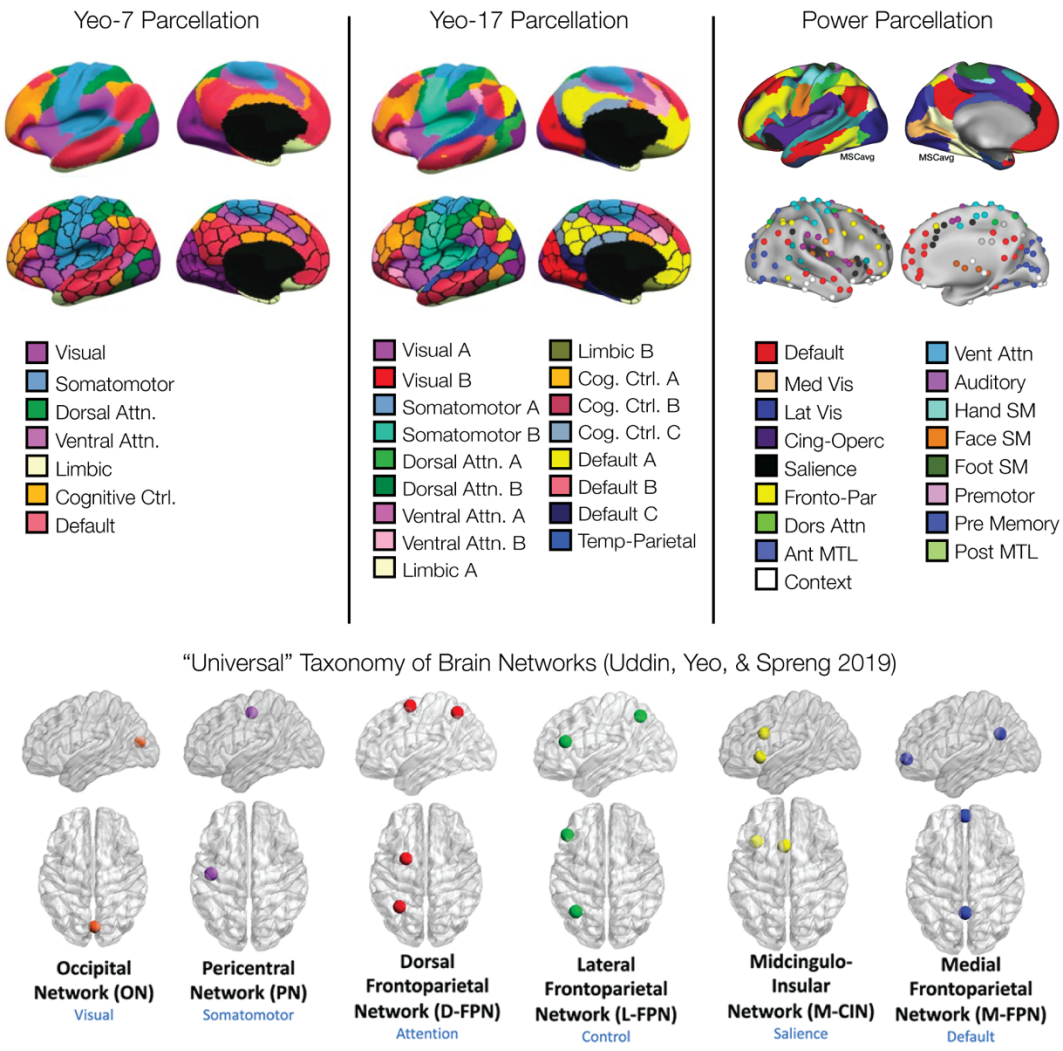

Figure 1.1 Functional Brain Network Taxonomy

Several of the most prominent functional brain network parcellations are displayed here. Top row from left to right: The Yeo-7, Yeo-17, and Power atlases are shown. Second row from top shows the Schaefer 2018 versions of the Yeo-7 and Yeo-17 atlases, along with a version of the Power atlas constructed using spherical ROIs. Atlases in this second row are convenient for constructing graph representations (e.g., extracting BOLD time series from each region of interest and forming nodes and edges). Bottom row: A "universal" taxonomy of brain networks, proposed by Uddin, Yeo, & Spreng in 2019. This taxonomy aims to unify the field through the use of an anatomically-defined nomenclature for six of the most common networks. This figure contains images from Schaefer et al. 2018, Power et al. 2011, Gordon et al. 2017, and Uddin, Yeo, & Spreng 2019, all used with permission.

CHAPTER TWO: FUNCTIONAL RECONFIGURATION OF A TASK-ACTIVE FRONTOPARIETAL NETWORK FACILITATES ABSTRACT REASONING

Introduction

The human brain has a remarkable reasoning capacity, allowing us to solve novel problems quickly by applying previously learned information, strategies, and ideas to new situations. Psychologists study abstract reasoning through a variety of tasks including the Raven's Progressive Matrices (RPM) task (Raven, 1941). Functional MRI (fMRI) studies have shown increased activation of frontoparietal cortex during variations of the RPM task (Christoff et al., 2001; Golde et al., 2010; Kroger et al., 2002; Melrose et al., 2007, 2018; Prabhakaran et al., 1997). A recent meta-analysis examining fMRI studies of human reasoning provided additional evidence for a frontoparietal system supporting abstract reasoning (Shin & Jeon, 2021). Evidence from human neuroimaging and computational modeling suggests that prefrontal cortex (PFC) in particular is essential for the more "abstract" portions of abstract reasoning, including representation and learning of specific rules (Hasselmo & Stern, 2018; Hoshi et al., 2000; Mansouri et al., 2020; Wallis et al., 2001; Zhu et al., 2020) and deduction of the relationship between analogous stimuli (Bunge et al., 2005; Green et al., 2010; Watson & Chatterjee, 2012). Moreover, anterior regions of PFC are activated more strongly as the relational complexity of a task (the number of rules that must be simultaneously considered) increases (Bunge et al., 2009; J. E. Cohen et al., 2018; Golde et al., 2010; Wendelken et al., 2012). This evidence supports theories of a hierarchical organization within the PFC, suggesting that more anterior regions of PFC

represent and process more abstract information, such as the integration of multiple rules (Badre & D'Esposito, 2007, 2009; Badre & Nee, 2018).

Studies of functional connectivity have demonstrated that the dynamic reconfiguration of frontoparietal cortex between resting and task states supports higher order cognition (Hearne et al., 2015, 2017; Ray et al., 2020; Vakhtin et al., 2014). During a Latin Squares matrix reasoning task, Hearne and colleagues demonstrated that increased functional connectivity between frontoparietal and visual cortices supported reasoning. Moreover, the strength of this connectivity increased with relational complexity: as the number of rules being integrated increased, so did functional connectivity (Hearne et al., 2017). In this study, they showed a significant reconfiguration of the brain's network community structure between rest and task, and relatively stable connectivity during the task. Previous work from our lab shows that the formation of stable brain network community structures also supports context-dependent rule learning (Morin et al., 2021). Additionally, task-based functional connectivity that more closely resembles resting state functional connectivity in individuals is associated with higher scores on tests of fluid intelligence, including the Raven's Progressive Matrices (Ferguson et al., 2017; Hilger et al., 2020; Schultz & Cole, 2016; Thiele et al., 2021).

In this study, we investigated how the brain's community structure dynamically shifted between resting and abstract reasoning task states. Subjects in our study underwent fMRI scanning first during resting state, followed by an abstract reasoning task. Using a univariate approach, we examined the separate activity patterns that support perceptual and symbolic reasoning. We then characterized the functional network reconfiguration

occurring as subjects transitioned between resting state and each of the different task conditions. Based on earlier results, we predicted that our univariate results would demonstrate activation in frontoparietal cortex in support of both symbolic and perceptual reasoning (Golde et al., 2010; Melrose et al., 2007; Shin & Jeon, 2021) and that prefrontal areas would activate more strongly for symbolic reasoning (Bunge et al., 2009; Prabhakaran et al., 1997), while inferior temporal areas would activate more strongly for perceptual reasoning (Sahyoun et al., 2010). At the network level, we predicted that a stable network core would be maintained across both resting state and the task conditions, with flexible reconfiguration of functional connectivity with frontoparietal regions supporting abstract reasoning (Hearne et al., 2017). Our results motivate a novel understanding of how the brain performs reasoning tasks: namely, nodes within frontoparietal cortex are functionally reconfigured, priming them to variably activate in different ways for unique task conditions.

Methods

Participants

Thirty-one healthy participants with normal or corrected to normal vision and no history or current diagnosis of neurological or psychiatric disorders were recruited from Boston University and the greater Boston area for the current study. Twenty-seven participants were included in the final analysis (mean age 25.7 years; SD 3.57 years; range 19 - 34 years; 17 females). One participant was excluded due to low accuracy on the behavioral task (< 80% in at least one condition). Three participants were excluded due to

excessive head motion (>3mm head displacement during at least two TRs within a single run). All participants gave written informed consent in accordance with Boston University's Institutional Review Board and were compensated for their time.

Simplified Raven's Progressive Matrices Task

During fMRI scanning, subjects performed a cognitive task designed to test their reasoning ability (see **Figure 2.1**). During each trial of the task, a stimulus with two answer choices appeared on the screen for 4.0s. During stimulus presentation, subjects indicated their response by pressing the left or right button on a response-box. The stimulus and answer choices remained on the screen for the full 4.0s time period, followed by feedback ("Correct," "Wrong," or "No Response") displayed for 1.0s. Following feedback, a blank grey screen with a fixation cross appeared for a random jitter lasting between 0.5 - 3.5s (values at 0.5s intervals). The jitter was optimized to maintain orthogonality between conditions using the tool optseq2 available through Freesurfer (version 5.3.0) (Charlestown, Massachusetts; http://surfer.nmr.mgh.harvard.edu) (Fischl, 2012).

Stimuli for the task were created with Adobe Illustrator (CS 5.1) and presented using PsychoPy (v1.90.3) (Peirce, 2007, 2008). Stimuli consisted of simplified versions of the Raven's Standard Progressive Matrices neuropsychological test (Raven, 1941). To investigate the neural correlates of reasoning, we designed the task with four conditions: symbolic reasoning, symbolic matching, perceptual reasoning, and perceptual matching (see **Figure 2.1**). In the symbolic reasoning and perceptual reasoning conditions, the stimulus pattern varied from left to right according to a sequential rule, with discrete stimulus patterns in the symbolic reasoning condition and a continuous stimulus in the

perceptual condition. Subjects were required to deduce and apply the sequence-rule to determine which of two answer choices correctly fit into a blank white square covering part of the stimulus. The symbolic matching and perceptual matching conditions were designed as control conditions to account for the visuospatial attention demands of the reasoning conditions. In the control conditions, there were no sequential rules for the stimuli, and the stimulus patterns were identical across the screen. Through behavioral piloting (data not shown) task stimuli were specifically chosen so that response times would be matched across all four conditions and accuracy would be at ceiling. Our goal was to reduce the effects of task-difficulty as much as possible within and across conditions.

The simplified RPM task was designed to test both symbolic and perceptual reasoning skills in order to specifically examine symbolic processing. Previously, studies have focused almost entirely on discrete symbolic versions of matrix reasoning, even though the first few trials of the Raven's Advanced Progressive Matrices task consist of continuous perceptual stimuli (Raven, 1941). Specifically, we were interested in comparing activation related to synthesizing multiple discrete symbols (unique to the symbolic conditions) with activation related to identifying sequential patterns (present in all conditions).

Patterns in the perceptual conditions took up the same amount of space on the screen as the sequences in the symbolic condition. The blank white square could appear on either the left or right side of the pattern or sequence, and this was counterbalanced across trials and conditions. The location of the correct answer (left or right) was also

counterbalanced across trials and conditions. Prior to scanning, the experimenter explained the task to the subject and guided them through eight sample trials using pen and paper. While in the MRI scanner, subjects completed 384 trials (96 in each of the four conditions). The experiment was divided into six runs, each lasting 6 minutes and 42 seconds. Conditions were counterbalanced within and across runs, and run order was randomized for each subject.

MRI Data Acquisition

Data was acquired on a 3 Tesla Siemens MAGNETOM Prisma magnetic resonance scanner located at the Cognitive Neuroimaging Center at Boston University in Boston, Massachusetts. A 64-channel head coil was used for all scans. A T1-weighted MEMPRAGE RMS structural image was acquired for each subject [TR = 2200ms, TE = 1.67ms, Flip Angle = 7°, Voxel size = 1.0mm isotropic]. Each subject underwent up to three runs of resting state fMRI (rs-fMRI) prior to task-based scans. During rs-fMRI scans, subjects were asked to lie still with their eyes open for six minutes per run, while a fixation cross was displayed on the screen in front of them. For rs-fMRI scans, T2*-weighted echo-planar (BOLD) images were acquired using a multiband sequence (slice acceleration factor, 6) [TR = 1000ms, TE=30ms, Flip Angle = 60°]. Twenty-four subjects underwent three consecutive six-minute resting state runs prior to completing the task scans. Due to time constraints, two subjects completed two resting state runs, and one subject completed one run. For task-based fMRI scans, T2*-weighted echo-planar (BOLD) images were acquired using a multiband sequence (slice acceleration factor, 3) [TR = 2000ms, TE = 30ms, Flip Angle = 60°, partial-fourier acquisition]. For both the rest and task scans, a total

of 78 slices were acquired, covering the whole brain. Images were acquired with 2mm isotropic voxels (matrix size 96 x 96) and the z-axis was aligned to the AC-PC line. Two opposite phase-encoded EPI fieldmaps (one anterior-to-posterior, the other posterior-to-anterior) were acquired for each subject to be used for distortion correction of the functional images [TR = 8540ms, TE = 66ms, Flip Angle = 90°].

fMRI Preprocessing

Both resting state and task fMRI data were preprocessed using a standardized pipeline available through fMRIprep (v1.4.1) (Esteban et al., 2019). Preprocessing steps included skull-stripping, distortion correction using magnetic field-maps, co-registration of each subject's functional data with their anatomical scan using boundary-based registration with 12-degrees of freedom, estimation of head-motion parameters, slice-time correction, spatial normalization of the subject's anatomical and functional data to standard template space (MNI152NLin2009cAsym template from templateflow), and projection onto a standardized cortical surface (fsaverage) (Ciric et al., 2021). Full details of the fMRIprep pipeline are outlined in the **Appendix**. After minimal preprocessing with fMRIprep, we performed spatial smoothing on the data (3mm FWHM gaussian kernel) using FSL (Y. Zhang et al., 2001).

Univariate Statistical Analyses

Voxelwise analysis was performed on single subject data using a general linear model (GLM) implemented with AFNI's 3dDeconvolve command. GLM regressors included: a boxcar predictor function for each task condition (symbolic reasoning,

symbolic matching, perceptual reasoning, and perceptual matching) spanning the 4s period when the stimuli were displayed, a 3-degree polynomial (cubic) baseline term, six nuisance regressors per run for motion (x, y, and z translations and rotations), and four amplitude-modulated task regressors (one for each task condition) to account for signal related to response-time on each trial. High motion time points (> 0.5mm frame-to-frame head movement; or outlier fraction > 0.1), as well as incorrect trials, were censored from the GLM analysis. Notably, the Feedback phase of each trial was not explicitly modeled in the GLM, and it is included in the baseline. This could result in Feedback-related activity influencing the estimate of beta-weights for the four task conditions. However, because subjects achieved ceiling-levels of accuracy, we do not expect Feedback-related signal to differ across conditions.

Two-sided t-tests were conducted at each voxel to determine differences in activation between conditions using AFNI's 3dttest++ command. Group statistical maps were thresholded using AFNI's equitable thresholding and clustering (ETAC) method (Cox, 2019). For visualization, we also included results projected onto inflated cortical surface maps (thresholded at $p < 0.05$, cluster size > 20 vertices) (see **Figure 2.3**).

Yeo-7 Network ROI Analysis

We examined differences in BOLD signal within functional brain network ROIs as defined by the Yeo-7 functional network atlas available in Freesurfer (Yeo et al., 2011). Each network in the atlas was converted into gifti format for use in the SUMA program that is available with AFNI (Cox, 1996; Saad & Reynolds, 2012). The mean BOLD percent signal change in the perceptual and symbolic reasoning vs. matching contrasts was

extracted from each Yeo-7 network ROI (visual, somatomotor, dorsal attention, ventral attention, limbic, cognitive control, and default) for each subject. The mean BOLD percent signal change was plotted as a bar-graph and results are displayed in **Figure 2.4**. Error bars represent a 95% confidence interval based on between-subjects mean and variance. T-tests were conducted to determine which of the seven networks showed statistically significant changes in BOLD signal between the symbolic and perceptual conditions. Results were corrected for multiple comparisons using Bonferroni-correction.

Functional Connectivity Measures

Prior to calculating task and resting state functional connectivity measures, preprocessed data was further denoised using linear regression. All denoising and functional connectivity calculations were implemented in the CONN Toolbox (Whitfield-Gabrieli & Nieto-Castanon, 2012). In the denoising procedure, confound regressors included six head-motion parameters and their first-order temporal derivatives, linear drift, and five noise components from CSF and white matter ROIs (the mean signal as well as the first four components from a principal component analysis in each ROI) (Chai et al., 2012). High-motion time-points (> 0.5mm frame-to-frame head movement or outlier fraction > 0.1) were censored as part of the denoising procedure. For the task-based scans, task-related signal from each of the four task conditions was also removed from the time series using HRF-convolved boxcar functions and their first-order derivatives. Regression of task-related signal is essential to ensure that functional connectivity observations were due to low-frequency coupling, rather than interregional similarities in task-based activation (Gonzalez-Castillo & Bandettini, 2018; Tomasi & Volkow, 2019). Finally, the

denoised time series was band-pass filtered (0.008-0.09 Hz) to isolate the frequency-band of interest that is most commonly associated with BOLD signal.

For resting state scans, functional connectivity between two regions *i* and *j* was defined as the Fisher-Z transformed Pearson correlation between the ROI timeseries. For task scans, a weighted GLM was employed to first isolate the signal associated with each condition in our event-related design. Weights were constructed as condition-specific boxcar timeseries convolved with a canonical HRF. Pearson correlation was calculated between the condition-specific signal extracted from each pair of ROIs, and this was Fisher-Z transformed. For each subject, the result was a functional connectivity matrix A_{ij} (400 x 400 ROIs in size) for each of the five conditions: resting state, symbolic reasoning, symbolic matching, perceptual reasoning, and perceptual matching.

Network Reconfiguration Analysis

We conducted a network reconfiguration analysis based on methods from Hearne et al. (Hearne et al., 2017). The goal of this analysis was to divide the functional connectivity network into communities and track community-membership across resting state and task conditions. A community is defined as a group of nodes that exhibit stronger connectivity to each other in the whole-brain network than they do in a relevant null model (Hearne et al., 2017; Newman & Girvan, 2004). The five weighted connectivity matrices for each subject were thresholded so that only the top 20% of connections remained in the matrix. Because the threshold level can influence network statistics (Rubinov & Sporns, 2011), we repeated all statistics at 5, 10, 15, 20, 25, and 30% thresholds. This ensured that when comparing different networks across subjects and conditions, differences in network

statistics were not influenced by differing edge densities (Garrison et al., 2015). Varying the threshold did not result in any significant changes to the network measures described below, so we present results at the 20% threshold in the main text. See **Figures 2.7** and **2.8** for results presented at each of the other thresholds. The thresholded, weighted matrices were subjected to a Louvain community detection algorithm implemented in the Brain Connectivity Toolbox (Rubinov & Sporns, 2010). The Louvain community detection algorithm generates community assignments that maximize the modularity, Q, which is defined as (Fortunato, 2010; Newman & Girvan, 2004):

$$Q(\gamma) = \frac{1}{2m}\sum_{ij}[A_{ij} - \gamma P_{ij}]\delta(\sigma_i\sigma_j),$$

where A_{ij} is the weighted and thresholded functional connectivity matrix, $2m$ is the sum of all the edge weights in the graph, $P_{ij} = \frac{k_i k_j}{2m}$ is the expected number of edges between nodes i and j according to a null model that preserves degree sequence of the graph, and $\delta(\sigma_i\sigma_j) = 1$ if the community assignment of node i is the same as the community assignment of node j ($\sigma_i = \sigma_j$), and is zero otherwise. The resolution parameter γ determines the size of the final communities, with $\gamma < 1$ leading to larger communities and $\gamma > 1$ leading to smaller communities. In line with previous work, we fixed $\gamma = 1$.

Because the outcome of Louvain community detection is dependent on initial conditions (e.g., which node is first assigned to a community), we repeated this process 1000 times for each connectivity matrix. To obtain a single set of community assignments for each subject and condition, we ran the following consensus procedure: First, an agreement matrix B was calculated in which each element B_{ij} represents the probability

that two nodes were classified into the same community across all 1000 iterations of Louvain community detection for a particular subject and condition. Then, we performed module-based consensus partitioning on the agreement matrix to obtain a single set of community assignments for each subject and condition. The entire consensus procedure was repeated across subjects to obtain a single set of community assignments per condition that was consistent across the entire group of subjects. The changing community memberships were plotted in an alluvial flow diagram (using the R packages *easyalluvial* and *parcats*) (Rosvall & Bergstrom, 2010) (**Figure 2.5**). Finally, to demonstrate fluctuating activity levels within stable task communities, we extracted the mean BOLD signal from each consensus community during each of the four task conditions (**Figure 2.6c**). (See **Figure 2.8** for results plotted across edge threshold levels.) A repeated measures ANOVA with paired T-test post-hoc testing was conducted to assess which communities exhibited significantly different activity levels across conditions. Results were corrected for multiple comparisons using Bonferroni correction.

Statistical Analysis of Community Structure

To evaluate the extent to which community structure changed between resting state and each task condition within subjects, we calculated the information theoretic distance (variation of information, V_{In}) between the consensus community assignments for each condition (Braun et al., 2015). V_{In} is defined as (Meilă, 2007):

$$V_{In} = \frac{H(X)+H(Y)-2MI(X,Y)}{\log(n)},$$

where X and Y are vectors listing the community assignments of n nodes in two different conditions, H is the entropy, and MI is the mutual information.

To assess the significance of V_{In} measures, we followed the procedure outlined by Hearne et al. to generate a null distribution of V_{In}. Briefly, we generated 10,000 permutations of community assignments by randomly selecting half of the subjects to switch their condition labels (e.g., when comparing symbolic reasoning and resting state community assignments, the condition labels were switched for half of the subjects, and a new consensus community structure and V_{In} metric were computed and added to the null distribution).

To compare the extent to which individual communities exhibited change between resting state and the task conditions, V_{In} was also computed separately for each of the three task communities, repeated across all four task conditions. Results are plotted in **Figure 2.6b**. (See **Figure 2.7** for results plotted across edge threshold levels.) A repeated measures ANOVA was employed to determine whether there was a difference in V_{In} across task communities and/or task conditions. Results from paired T-test post hoc testing were corrected for multiple comparisons using Bonferroni correction.

Results

Behavioral Performance

To examine brain activity and network reconfiguration across different abstract reasoning conditions, we developed a simplified version of the Raven's Progressive Matrices task suitable for fMRI scanning. Additionally, we wanted brain activity and

connectivity differences to be related to the reasoning conditions, not task difficulty. Through behavioral piloting in a separate cohort of subjects (data not shown), we balanced the four task conditions so that participants' accuracy was maximized, and so that the distributions of response times were similar across all four conditions. The 27 subjects included in the final analysis achieved > 80% accuracy on each of the four conditions. To compute accuracy measures, trials in which the subject did not respond were considered incorrect. "No Response" trials were omitted from calculations involving response times. Across all subjects "No Response" trials only occurred 49 times out of 10,368 trials (M +/- S.D. 1.73 +/- 2.76 trials/subject). There was a statistically significant difference in accuracy between conditions as determined by a one-way ANOVA ($F(3, 26) = 4.241$, $p < 0.01$). Pairwise-T post hoc testing showed that accuracy on the perceptual matching condition was significantly lower than accuracy on the symbolic matching condition ($T(26) = -4.28$, $p < 0.01$) and the symbolic reasoning condition ($T(26) = -2.32$, $p < 0.05$). All other contrasts were found to not be significantly different from each other. Additionally, mean accuracy for each condition was above 92%, and considered to be at ceiling (Symbolic reasoning: 94.7 +/- 3.55 percent correct, symbolic matching: 96.0 +/- 3.28 percent correct, perceptual reasoning: 94.7 +/- 3.55 percent correct, perceptual matching: 92.8 +/- 3.98 percent correct).

There was no significant difference in response times between conditions as determined by a one-way ANOVA, ($F(3, 26) = 2.02$, $p = 0.116$). Subjects' response times were consistent across the perceptual matching (1.74 +/- 0.219s), perceptual reasoning (1.79 +/- 0.173s), symbolic matching (1.67 +/- 0.180s), and symbolic reasoning (1.78 +/-

0.231s) conditions. Accuracy and response time measures are displayed in **Figure 2.2**. Overall, the behavioral results demonstrated that across all task conditions, subjects achieved high accuracy and similar response times, in line with our goal of generating different reasoning conditions with similar levels of difficulty.

Task-based fMRI

From previous research on abstract reasoning**,** we expected that frontoparietal cortex would be active during reasoning conditions on our task. To test this, we generated brain activity maps using a univariate approach. Our results also identified prefrontal regions and inferior temporal regions that are uniquely activated for symbolic and perceptual reasoning respectively. The full results of the univariate analysis are described below.

Symbolic Reasoning and Symbol Matching

A random-effects group analysis of the fMRI data contrasting the symbolic reasoning with the symbol matching task conditions demonstrated significant clusters of increased signal (symbolic reasoning > symbolic matching) throughout left lateral prefrontal cortex (peak MNI coordinates = [-28, -2, 64] $Z = 6.60$), right lateral prefrontal cortex (peak MNI coordinates = [56, 10, 24], $Z = 5.37$), bilateral lateral parietal cortex/cerebellum (peak MNI coordinates = [48, -40, 54], $Z = 6.47$), bilateral dorsomedial prefrontal cortex (peak MNI coordinates = [-4, 26, 46], $Z = 5.48$), left anterior insula (peak MNI coordinates = [-38, 18, 0], $Z = 4.87$), and right frontal pole (peak MNI coordinates = [46, 52, -10], $Z = 4.47$). Significant negative clusters (symbolic matching > symbolic reasoning) were present in left medial prefrontal cortex (peak MNI coordinates = [-8, 54, -

4], Z = --5.17), right medial prefrontal cortex (peak MNI coordinates = [-2, -46, 26], Z = -4.71), left frontopolar cortex (peak MNI coordinates [-24, 44, 42], Z = -4.27), and bilaterally in the precuneus (peak MNI coordinates = [2, -18, 42], Z = -4.41). Voxelwise activation maps are presented in **Figure 2.3a**.

Perceptual Reasoning and Perceptual Matching

A random-effects group analysis of the fMRI data contrasting the perceptual reasoning with the perceptual matching conditions of the task demonstrated significant positive clusters (perceptual reasoning > perceptual matching) throughout bilateral lateral parietal and inferior temporal cortices (peak MNI coordinates = [30, -60, -12], Z = 6.41), left dorsolateral prefrontal cortex (peak MNI coordinates = [-50, 36, 18], Z = 4.37), right dorsolateral prefrontal cortex (peak MNI coordinates = [-26, 6, 60], Z = 4.77), left cerebellum (peak MNI coordinates = [-28. -68, -52], Z = 4.16), and right cerebellum (peak MNI coordinates = [8, -56, -50] Z = 4.60). Significant negative clusters (perceptual matching > perceptual reasoning) were found in bilateral occipital cortex (peak MNI coordinates = [-18, -100, -8], Z = -5.68), left medial prefrontal cortex (peak MNI coordinates = [-4, 56, 16], Z = -4.56), and bilateral precuneus (peak MNI coordinates [2, -24, 36], Z = -5.65). Voxelwise activity maps are displayed in **Figure 2.3b**.

Interaction Maps

A random-effects group analysis of the fMRI data contrasting the symbolic conditions (symbolic reasoning > symbolic matching) with the perceptual conditions (perceptual reasoning > perceptual matching) was used to identify brain regions important for symbolic reasoning or perceptual reasoning, but not both types of reasoning in general.

Brain regions that were significant for symbolic reasoning included bilateral occipital cortex (peak MNI coordinates = [16, -100, 0], $Z = 5.72$), right dorsolateral prefrontal cortex and insula (peak MNI coordinates = [48, 8, 24], $Z = 4.58$), bilateral dorsomedial prefrontal cortex (peak MNI coordinates = [0, 34, 46], $Z = 5.20$), right lateral parietal cortex (peak MNI coordinates = [62, -32, 50], $Z = 4.14$), and right frontal pole (peak MNI coordinates = [48, 44, -2], $Z = 4.68$). Brain regions that were significantly more active for perceptual reasoning included bilateral parieto-occipital sulcus (peak MNI-coordinates = [12, -88, 28], $Z = -5.08$), right inferior temporal cortex (peak MNI-coordinates = [30, -58, -10], $Z = -5.74$), and left inferior temporal cortex (peak MNI-coordinates = [-20, -76, -8], $Z = -5.76$). Voxelwise activity maps are displayed in **Figure 2.3c**.

Yeo-7 Network ROI Analysis

A region of interest (ROI) analysis was conducted to determine which functional brain networks (as defined by Yeo et al. 2011) were contributing to successful abstract reasoning behavior on the simplified Raven's Progressive Matrices task. ROI analysis showed increased activation in visual, dorsal attention, and cognitive control networks during the reasoning conditions compared to the matching conditions for both the symbolic and perceptual stimuli. Moreover, activation in the cognitive control network was greater for the symbolic contrast than for the perceptual contrast ($T = 3.48$, $p < 0.05$, Bonferroni corrected) (**Figure 2.4b**). The results from this analysis are shown in **Figure 2.4**.

Network Reconfiguration

To determine whether functional connectivity was stable across task conditions, we performed a network reconfiguration analysis based on work by Hearne et al. (2017). An alluvial flow plot in **Figure 2.5** displays the results from this analysis. Using Louvain community detection, we identified twelve communities during resting state (A – L), and three communities during each of the four task conditions (A – C). During pre-task resting state, the communities roughly correspond to the default network (community A), somatomotor network (community B), visual network (community C), along with eight communities (D – K) that when combined, form the frontoparietal networks dorsal attention, ventral attention, and cognitive control (Yeo et al., 2011). During the task, communities A and B remained largely intact, trading a small number of nodes with the frontoparietal communities (see **Figure 2.5**). The remaining task community (community C) formed a robust frontoparietal-visual system from the strengthened connections amongst resting state communities C – K, reflecting stronger connections between frontoparietal and visual nodes during the task compared to rest. In **Figure 2.6a**, we show the topography of each community A – C for the symbolic reasoning condition of the task. This topography is nearly identical to communities A – C in each of the other three task conditions (not shown).

Using the variation of information metric (V_{In}), we quantified the similarity between the community partitions for each of the task conditions and the resting state. When considering the entire brain network, we found that the community structure during each of the four task conditions was significantly different from the community structure

during resting state (V_{In} Symbolic Reasoning vs. Rest = 0.17; V_{In} Symbolic Matching vs. Rest = 0.17; V_{In} Perceptual Reasoning vs. Rest = 0.18; V_{In} Perceptual Matching vs. Rest = 0.17; $p < 0.01$, Bonferroni corrected for all contrasts).

Since the whole-brain community structure was significantly different between rest and the task conditions, we quantified the relative amount of reconfiguration in task communities A – C. To do so, we calculated V_{In} individually for each task community across each of the four task conditions (see **Figure 2.6b**). All p-values below are Bonferroni-corrected for multiple comparisons. A repeated measures ANOVA showed a main effect of task community ($F(2,26) = 30.78$, $p < 0.01$) but no main effect of task condition ($F(3,26) = 0.717$, $p = 1.0$). Post-hoc testing with pairwise t-tests showed that across all four task conditions, community C (the frontoparietal-visual community) had the highest overall V_{In} and that it was significantly higher than the V_{In} of both other task communities (compared to community A: $T(134) = 14.99$, $p < 0.01$, and compared to community B: $T(134) = 16.19$, $p < 0.01$). Additionally, there was also a significant difference in the V_{In} metric between communities A and B ($T(134) = 2.86$), $p < 0.05$). Together, these results demonstrate that the change in community structure between resting state and the reasoning task is driven by reconfiguration of nodes in community C (the frontoparietal-visual community) (see **Figure 2.6b**).

ROI Analysis of Reconfigured Communities

To determine how each of the communities differentially contributed to the various reasoning conditions, we calculated the average BOLD signal within each community for

each of the four task conditions. All p-values below are Bonferroni-corrected for multiple comparisons.

A repeated measures ANOVA showed significant differences in the activity of community A across the four task conditions ($F(3,26) = 29.15$, $p < 0.01$). Post-hoc analysis revealed significant differences between symbolic reasoning vs. perceptual reasoning ($T(26) = 6.65$, $p < 0.01$), symbolic reasoning vs. perceptual matching ($T(26) = 5.18$, $p < 0.01$), symbolic matching vs. perceptual reasoning ($T(26) = 6.60$, $p < 0.01$), and symbolic matching vs. perceptual matching ($T(26) = 6.98$, $p < 0.01$).

A repeated measures ANOVA also showed significant differences in the activity of community B across the four task conditions ($F(3,26) = 9.33$, $p < 0.01$). Post-hoc analysis showed significant differences between symbolic reasoning vs. perceptual matching ($T(26) = 5.31$, $p < 0.01$), and symbolic matching vs. perceptual matching ($T(26) = 3.87$, $p < 0.01$).

Finally, a repeated measures ANOVA showed significant differences in the activity of community C across the four task conditions ($F(3,26) = 92.24$, $p < 0.01$). Notably, community C showed the highest levels of activity on the task, and post-hoc analysis showed that it was the only community with significant activity differences between same-domain reasoning and matching conditions. Post-hoc analysis revealed significant differences between all six contrasts: symbolic reasoning vs. symbolic matching ($T(26) = 9.05$, $p < 0.01$), symbolic reasoning vs. perceptual reasoning ($T(26) = -11.20$, $p < 0.01$), symbolic reasoning vs. perceptual matching ($T(26) = -4.74$, $p < 0.01$), symbolic matching vs. perceptual reasoning ($T(26) = -16.50$, $p < 0.01$), symbolic matching vs. perceptual

matching ($T(26) = -9.12$, $p < 0.01$), and perceptual reasoning vs. perceptual matching ($T(26) = 4.52$, $p < 0.01$).

Together, these results demonstrate that each community identified in the network reconfiguration analysis has an activity pattern that is consistent in its direction (always positively activated or negatively activated), but variable in its intensity across the task conditions. Namely, community A (default) is negatively activated, community B (somatomotor) is not significantly activated, and community C (frontoparietal-visual) is positively activated. Community C showed increased activity during symbolic and perceptual reasoning conditions compared to their respective matching conditions.

Discussion

In this study, we investigated regional variability in brain network activation and reconfiguration during an abstract reasoning task. By analyzing fMRI data during both resting and task states, we demonstrated that regions of the default and somatomotor networks remained stable, while simultaneously frontoparietal and visual regions flexibly reconfigured into a task-ready state. When examining task-based activity patterns, we found that frontoparietal and visual regions, which had flexibly reconfigured from resting to task states, exhibited the strongest task-based activation. Overall, these results demonstrated that flexible reconfiguration of underlying networks supports the transition from rest to task, and that activation of frontoparietal cortex supports abstract reasoning.

A Stable Network Core Persists During Resting State and the Reasoning Task

Consistent with prior work, we found that overall, functional brain network topology was largely conserved between resting state and task (M. W. Cole et al., 2014; C. Gratton, Laumann, et al., 2018; Hearne et al., 2017; Krienen et al., 2014; Salvo et al., 2021). Across both resting state and task scans, we identified two stable communities primarily consisting of regions in the default and somatomotor networks (**see Figure 2.5**). Previous work suggests that these regions form a stable network "core" and that they exhibit the fewest changes in functional connectivity when comparing resting and task states (Krienen et al., 2014). Recent work from our lab further suggests that successful rule learning ability is associated with increased stability of specific brain networks, including the somatomotor network (Morin et al., 2021). Considering the whole brain, previous work has shown that increased whole-brain network stability between resting and task states is strongly associated with higher fluid intelligence scores (Ferguson et al., 2017; Hilger et al., 2020; Schultz & Cole, 2016; Thiele et al., 2021). As a working hypothesis, we propose that stability in somatomotor and default regions allows the brain to spend more energy reconfiguring the functional connectivity of other regions, such as frontoparietal and visual cortices, that show increased activation during the task. Future studies employing network control theory (Gu et al., 2015; Scheid et al., 2021) or activity flow mapping (M. W. Cole et al., 2016) may be able to model the "energy savings" that are afforded when the underlying functional connectivity network is reconfigured into a task-ready state.

Frontoparietal and Visual Cortices Flexibly Reconfigure to Support Reasoning

During the resting state scans, we found a largely fragmented community structure among frontoparietal and visual regions, consisting of nine small communities. While these regions were part of many different communities at rest, they joined together to form a single strongly connected community during the task (see **Figure 2.5**). This task-based community was maintained across all four task conditions. This result is consistent with previous work from Hearne and colleagues, who found that frontoparietal and visual cortical regions exhibited increased reconfiguration, forming a single community structure during a Latin Squares reasoning task (2017). Previous work has shown that generally, frontoparietal cortex shows increased reconfiguration compared to other brain regions, and that increased flexibility of frontoparietal cortex is associated with better performance on motor sequence learning, associative learning, and working memory tasks (Bassett et al., 2011; Betzel et al., 2017; Braun et al., 2015; Gerraty et al., 2018). Moreover, patterns of task-based network reconfiguration occurring in frontoparietal control regions is predictive of individual differences in fluid intelligence scores (Greene et al., 2018).

Frontoparietal cortical regions are uniquely positioned to integrate information across distal regions of cortex (for review, see Avena-Koenigsberger et al., 2017; Parks & Madden, 2013). During abstract reasoning, the brain must balance global integration of information with local specialization. Functional brain networks facilitate this balance with a rich-club organization where hub regions (regions with strong network-wide connectivity) are also highly interconnected with each other (van den Heuvel & Sporns, 2011). Frontoparietal cortex contains hubs that are well-positioned to facilitate interaction

between functional networks (C. Gratton, Sun, et al., 2018). We propose that the formation of a strong frontoparietal-visual community during our reasoning task facilitates the brain-wide integration of information across networks that is necessary for abstract reasoning.

Frontoparietal Network Activity and Reconfiguration Supports Reasoning

In our study, frontoparietal cortex was significantly more active for reasoning conditions compared to matching conditions (see **Figure 2.6**). Moreover, activation of the cognitive control network, as defined *a priori* in the Yeo-7 atlas, was greater for the symbolic reasoning contrast compared to the perceptual reasoning contrast (see **Figure 2.4**). Frontoparietal cortical regions are activated in a variety of abstract reasoning paradigms including tasks of analogical reasoning (Green et al., 2010; Watson & Chatterjee, 2012), rule learning (Wallis et al., 2001), and matrix reasoning (Christoff et al., 2001; Golde et al., 2010; Melrose et al., 2007, 2018; Prabhakaran et al., 1997). Functional MRI studies have demonstrated lateral parietal activity during tasks of top-down directed attention (Bisley & Goldberg, 2003), mental rotation and spatial reasoning (Schendan & Stern, 2007, 2008), and magnitude processing (including numerical, temporal, and spatial magnitudes) (Ansari et al., 2006; Holloway et al., 2010; Maloney et al., 2010; Sokolowski et al., 2017; Van Opstal & Verguts, 2013; Walsh, 2003). Lateral prefrontal cortex has also been implicated in abstract reasoning behavior and exhibited higher activation associated with increased rule complexity, relational integration, and working memory demands (Bunge et al., 2009; Christoff et al., 2001; Prabhakaran et al., 1997; Wendelken et al., 2012). More generally, researchers have proposed that frontoparietal cortex functionally contributes to general human intelligence, which is often measured with reasoning tasks

like the one used in our experiment (Fraenz et al., 2021; Jung & Haier, 2007; Vakhtin et al., 2014).

Highly Activated Regions Exhibited the Greatest Network Reconfiguration

We found that frontoparietal control regions exhibited not only increased activation during symbolic and perceptual reasoning, but also increased reconfiguration between resting and task states (see **Figure 2.6**). As discussed above, frontoparietal nodes enjoy a privileged hub status within functional brain networks, with increased functional connectivity to each other and to many regions throughout the brain (van den Heuvel & Sporns, 2011). Previous work proposed that network nodes exhibiting both hub status and increased task activation are uniquely positioned to exert cognitive control (C. Gratton et al., 2016). With increased functional connectivity to many other brain regions, task-based activation within these network hubs can be highly influential. We propose that the robust community structure of frontoparietal nodes that formed during our reasoning task facilitates the integration of information across distal brain regions and results in increased task activation of the community.

Notably, the regions that showed the largest task-based community reconfiguration also showed the largest magnitude change in task-based activation (see **Figure 6**). Conceivably, task-related co-activation could increase coupling between brain regions. With this in mind, we adopted an analysis approach that was previously used by Hearne et al. to compare network organization at rest with network organization during an event-related task design (2017). Task-related signal from each of the four task conditions was removed from the time series using HRF-convolved boxcar regressors and their first-order

derivatives (M. W. Cole et al., 2014). Notably, this nuisance regression procedure only removes linear task signal, and remaining nonlinear portions of task-related signal may contribute to functional connectivity patterns. Preprocessing and denoising procedures were identical across task and resting state data, except for regression of task-related signal in the task data, and bandpass filtering of resting-state data. Task-based functional connectivity was calculated using a weighted GLM approach that created condition-specific (weighted) time-series of fMRI data. This approach keeps (as opposed to other approaches such as beta-series correlation) the data in a similar format as the resting state data (namely a 4D series of BOLD signal volumes, rather than statistically derived beta-weights). Notably, we cannot rule out differences in signal to noise ratio (SNR) between resting and task data that may contribute to increased functional connectivity during the task. Future studies could benefit from methodological choices that consider the relationship between SNR, cognitive tasks, and functional connectivity.

While a more continuously presented task (e.g., movie-watching) may have been ideal for analyzing both resting state and task fMRI data using identical analysis pipelines, we chose an event-related task so we could simultaneously analyze task activation. Additionally, the results from our network reconfiguration analysis (stable unimodal regions and reconfigured frontoparietal regions) are supported by previous work that analyzed continuously presented tasks (Krienen et al., 2014).

As a conceptual framework, we propose that the brain's functional connectivity is reconfigured when transitioning from rest to task in order to facilitate more efficient task activation. Previous studies using connectome fingerprinting have established that resting-

state functional connectivity is predictive of task-based activation (Osher et al., 2019; A. Porter et al., 2021; Tobyne et al., 2018). Moreover, individual network connectivity is predictive of task-based activity patterns (Salvo et al., 2021). While functional connectivity is largely maintained between resting and task states in individuals, regional changes to the brain's functional connectivity are functionally relevant (M. W. Cole et al., 2014; C. Gratton, Laumann, et al., 2018). Modeling work using activity flow mapping has also shown that task activation patterns can be predicted from the underlying network of functional connectivity (M. W. Cole et al., 2016). Studies have also shown that changes to the underlying functional connectome (e.g., due to task-reconfiguration) can affect task activation patterns (Arbabshirani et al., 2013; M. W. Cole et al., 2021; Tomasi & Volkow, 2019). Together with previous literature, our results suggest that task activations occur on top of an underlying functional connectivity network that has been flexibly reconfigured into a task-ready state.

Conclusion

Using a simplified Raven's Progressive Matrices task, we demonstrated that while unique cortical regions are activated by symbolic and perceptual reasoning, a common, stable functional connectivity network architecture supports both types of reasoning. We identify a significant role for the frontoparietal control network in functionally reconfiguring from a fragmented set of communities at rest, into a task-active strongly-connected community structure during abstract reasoning.

Figures

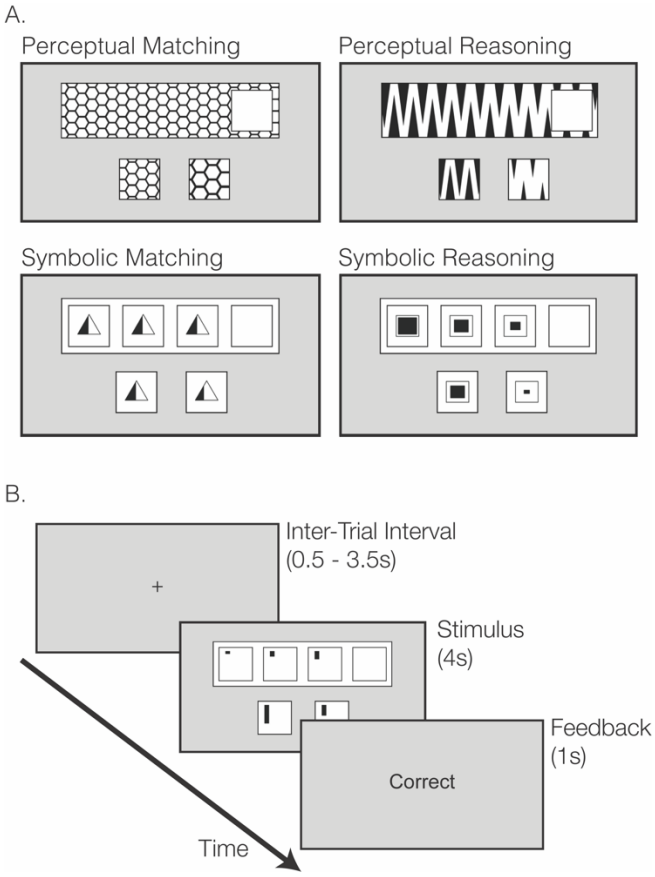

Figure 2.1 Simplified Raven's Progressive Matrices Task

A. During the task, subjects decided which of two answer choices best fit into the blank white square missing from the pattern at the top of the screen. A 2x2 task design was employed to test reasoning in two domains: symbolic and perceptual. Symbolic stimuli consisted of discrete squares each containing a symbol; perceptual stimuli consisted of continuous patterns. Reasoning stimuli progressed according to a pattern from left to right. As a control, matching conditions consisted of stimuli that were unchanging across the screen. **B.** During a single trial, subjects first viewed a fixation cross (0.5 – 3.5s jitter). Next, they viewed the problem and selected an answer choice with a button box (4.0s). Finally, they were presented with feedback ("Correct", "Wrong", or "No Response") (1.0s). Subjects completed 396 trials over the course of a 1-hour fMRI scanning session divided into six task runs.

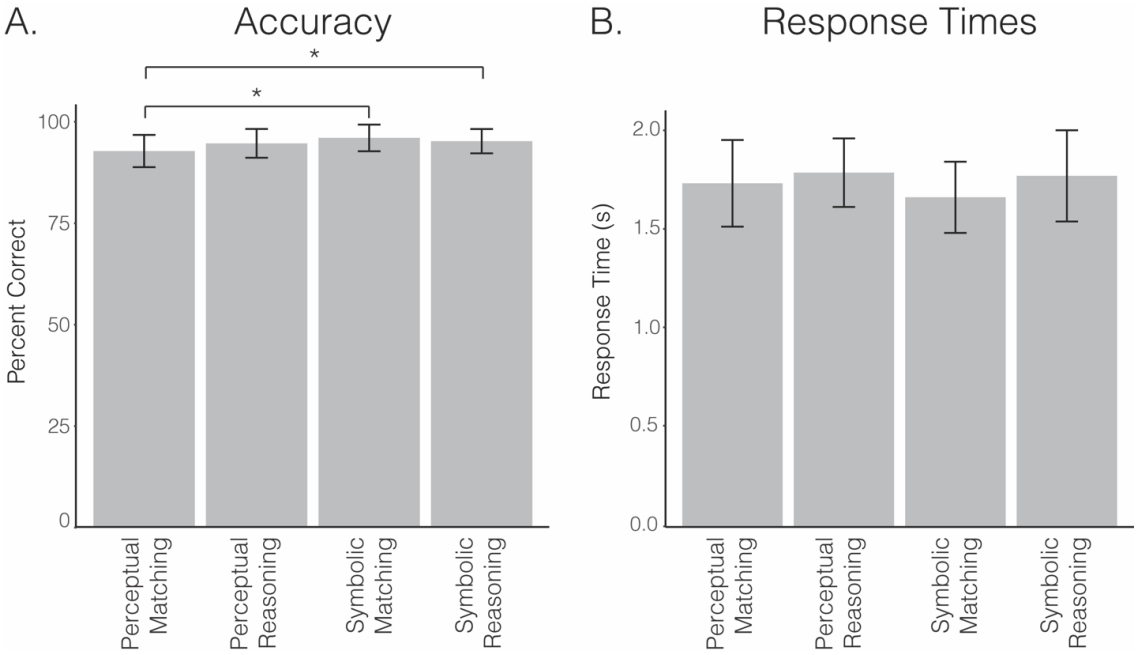

Figure 2.2 Behavioral Performance Measures

A. Mean accuracy measures are plotted for each stimulus condition. **B.** Mean response times are plotted for each stimulus condition. Error bars indicate 95% confidence interval. * denotes statistical significance ($p < 0.05$ on a one-way ANOVA $F(3,26)$ with pairwise T-test post-hoc testing).

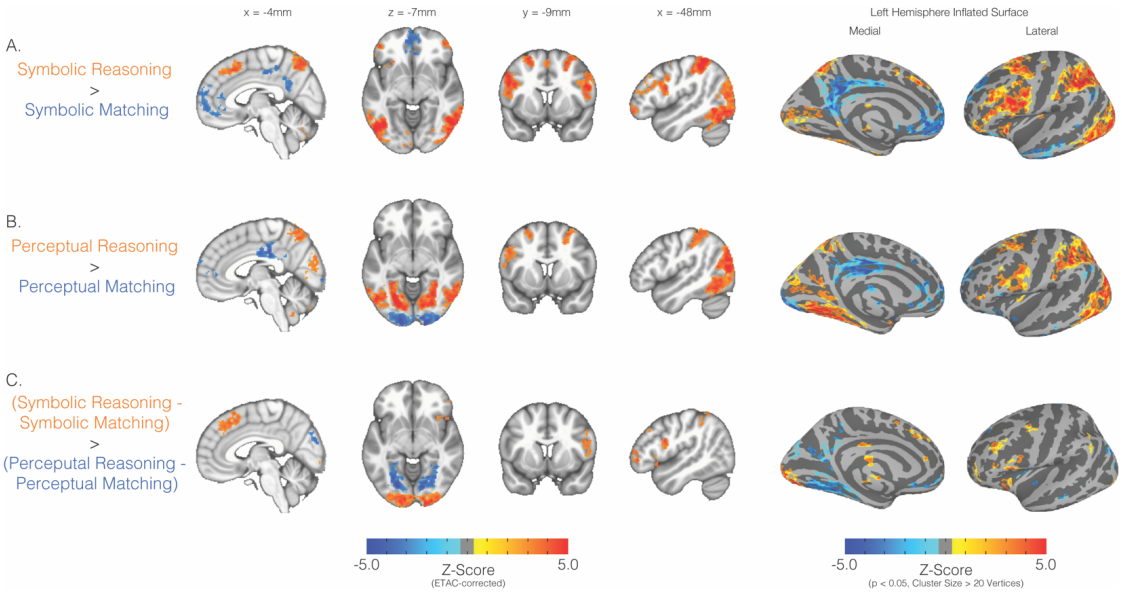

Figure 2.3 fMRI Activity Maps

Colored voxels indicate regions with a significant difference in activity between conditions for each of the following contrasts: **A.** Symbolic Reasoning > Symbolic Matching, **B.** Perceptual Reasoning > Perceptual Matching, and **C.** Interaction Maps: (Symbolic Reasoning – Matching) > (Perceptual Reasoning – Perceptual Matching). Voxel shading represents Z-score magnitude. For the volumetric maps (left), activation was thresholded at $p < 0.05$ and corrected for multiple comparisons using AFNI's equitable thresholding and clustering (ETAC) method. Surface maps (right), shown for visualization purposes, were thresholded at $p < 0.05$, and for clusters with > 20 vertices.

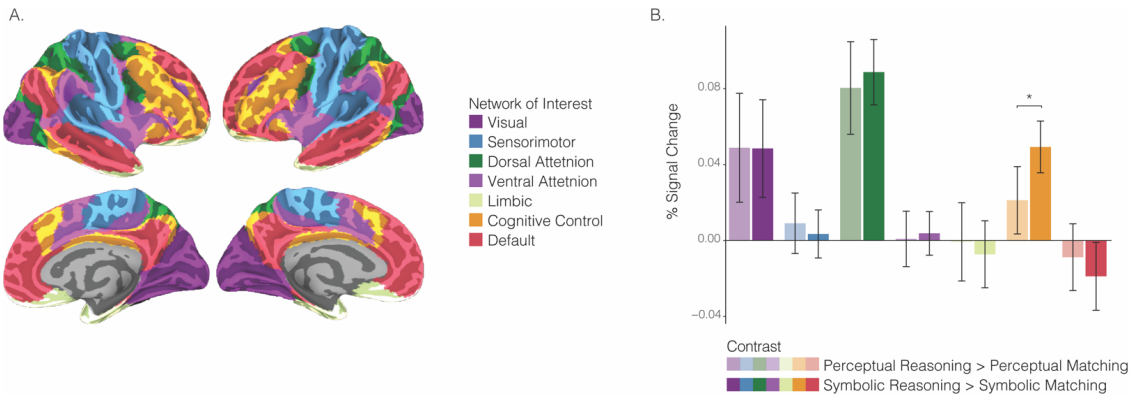

Figure 2.4 Resting State Network ROI Analysis

A. Regions of interest were defined a priori from the Yeo 7-network resting state parcellation (2011). **B.** Bars represent BOLD percent signal change in each ROI for the perceptual contrast (lighter colors), and symbolic contrast (darker colors). Error bars indicated 95% confidence interval. * denotes significant difference in percent signal change between contrasts ($p < 0.05$, Bonferroni corrected for multiple comparisons).

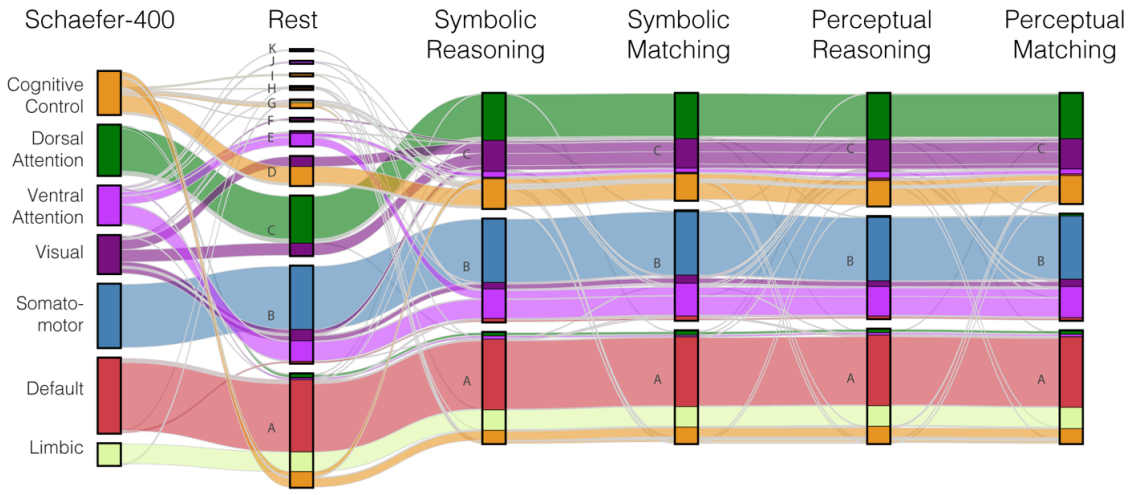

Figure 2.5 Task-Based Network Reconfiguration

We plotted network reconfiguration on an alluvial flow diagram to demonstrate the changing community memberships of nodes in the brain network. Canonical community memberships are shown in the left column for the 400 ROIs in the Schaefer-400 cortical parcellation with Yeo-7 labels (Schaefer et al., 2018). A Louvain community detection algorithm was used to define network communities during resting state and each of the four task conditions (labeled here as respective columns in the flow diagram). During resting state, the brain network was divided into 11 communities (labeled A – K). During each task condition, three communities (A – C) were detected. Communities are outlined in black. Connecting flows show the changing community memberships across rest and task conditions. To visualize the makeup of each community, colors represent the canonical Yeo-7 memberships for each of the Schaefer-400 regions (Orange = Cognitive Control, Green = Dorsal Attention, Violet = Ventral Attention, Purple = Visual, Blue = Somatomotor, Red = Default, Cream = Limbic).

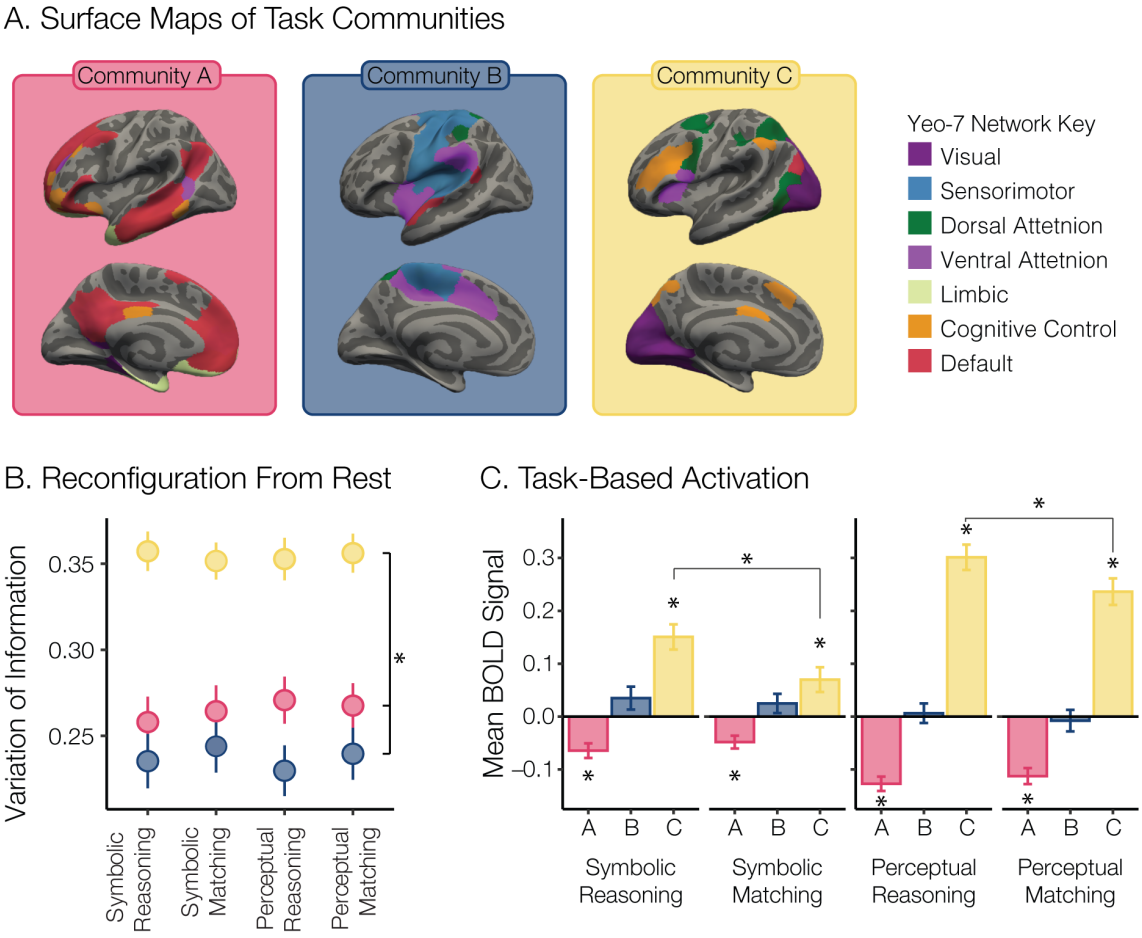

Figure 2.6 Community Layout, Reconfiguration, and Activity

A. Three communities were detected during each of the task conditions. Projected here on a cortical surface are the communities from the symbolic reasoning condition. Individual nodes from the Schaefer-400 cortical parcellation are colored according to their canonical Yeo-7 network membership (Schaefer et al., 2018). Although only the communities for symbolic reasoning are shown here, the condition-specific A, B, and C communities were used to calculate the statistics shown in panels B and C. **B.** To quantify the difference in parcellation between each task condition and the resting state we plotted the variation of information (V_{In}) for each of the task communities. Points represent mean V_{In} across subjects. Error bars represent standard error. Nodes in community C showed the largest change in community assignment for all four conditions, compared to rest. * denotes significant differences in V_{In} between communities ($p < 0.05$, Bonferroni corrected). **C.** The mean BOLD signal within each task community is plotted for each of the task conditions. Bar height represents the mean BOLD signal across subjects for each community. Error bars represent standard error. Across all graphs, Red = community A, Blue = community B, Yellow = community C. * denotes mean BOLD signal significantly different from zero ($p < 0.05$, Bonferroni corrected).

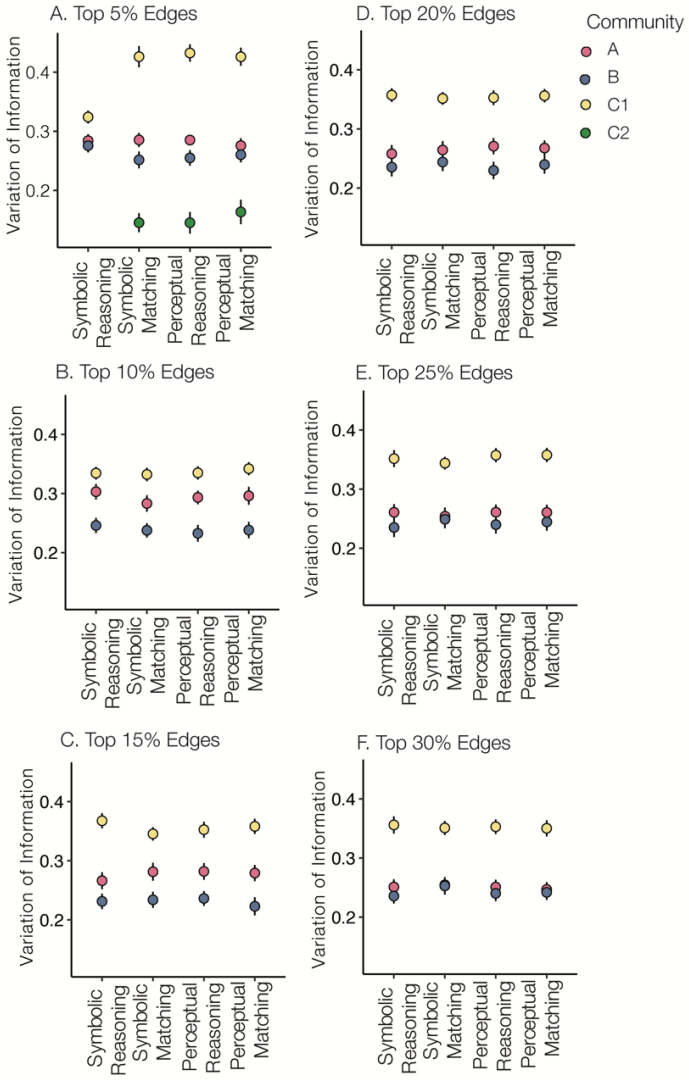

Figure 2.7 Variation of Information Across Edge Thresholds

To quantify the difference in community assignment between each task condition and the resting state we plotted the variation of information (V_{In}) for each of the task communities. Points represent mean V_{In} across subjects. Results are presented for subjects' functional connectivity networks thresholded at six levels (top 5, 10, 15, 20, 25, and 30% of edges in the network) (A-F). Error bars represent standard error. Nodes in community C showed the largest change in community assignment for all four conditions, compared to rest across all six thresholds. Red = community A, Blue = community B, Yellow = community C. For the 5% thresholded network (panel A), Community C remained intact during symbolic reasoning, but split into two subnetworks C1 (Yellow) and C2 (Green) for the other three task conditions.

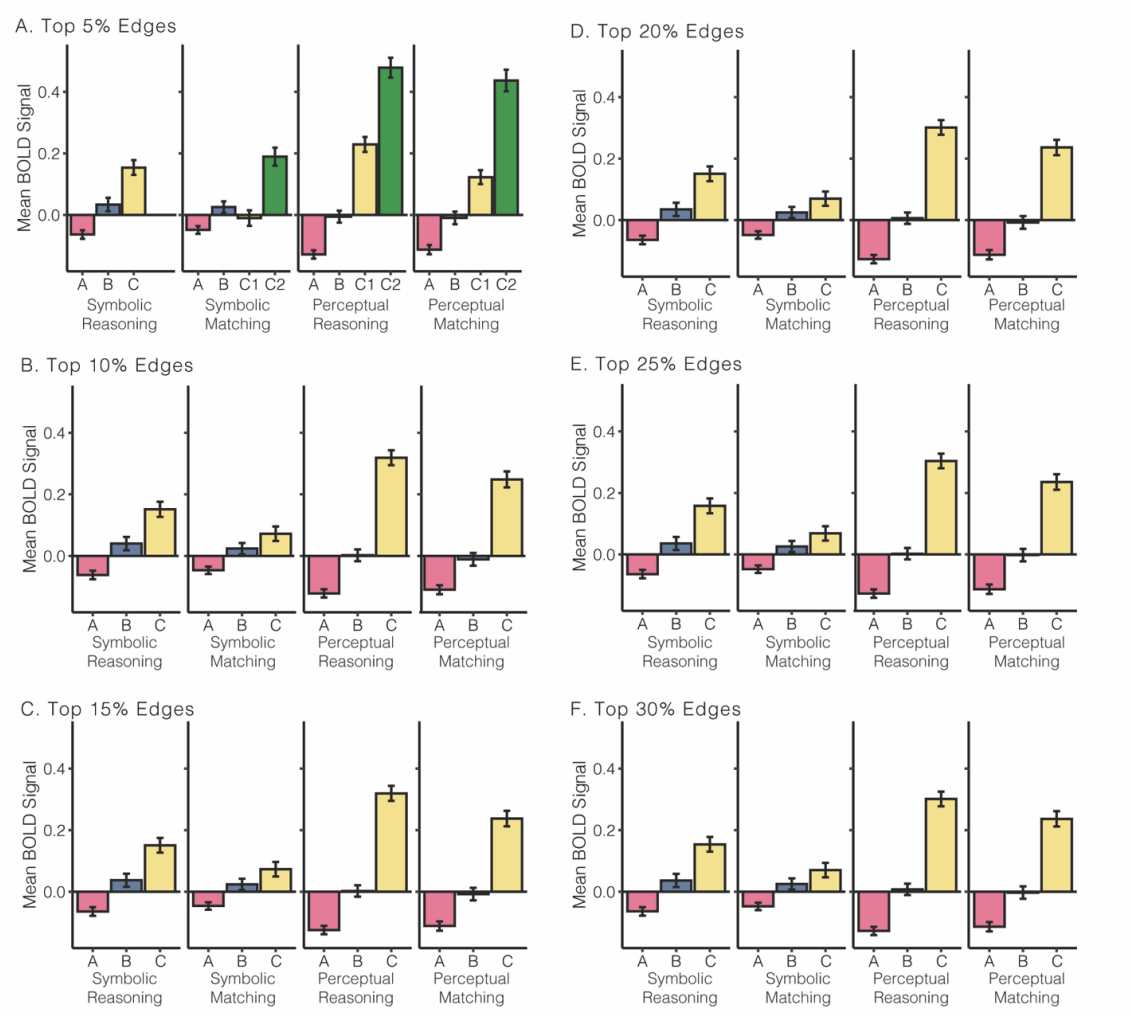

Figure 2.8 Community Activation Across Edge Thresholds

The mean BOLD signal within each task community is plotted for each of the task conditions. Bar height represents the mean BOLD signal across subjects for each community. Results are presented for subjects' functional connectivity networks thresholded at six levels (top 5, 10, 15, 20, 25, and 30% of edges in the network) (A-F). Error bars represent standard error. Red = community A, Blue = community B, Yellow = community C. For the 5% thresholded network (panel A), Community C remained intact during symbolic reasoning, but split into two subnetworks C1 (Yellow) and C2 (Green) for the other three task conditions.

CHAPTER THREE: DYNAMIC NETWORK ANALYSIS DEMONSTRATES THE FORMATION OF STABLE FUNCTIONAL NETWORKS DURING RULE LEARNING[1]

Introduction

We often encounter situations where we must learn and apply rules. For example, imagine searching for parking on an unfamiliar road. Depending on the context of the situation – the location, time of day, and status of your parking permit – a "no-parking" rule may or may not apply. Here, we examine the changes in functional network connectivity associated with learning a set of context-dependent rules.

Studies of rule learning have described a coordinated system of prefrontal cortical regions essential for representing and utilizing rules (for review, see (Mansouri et al., 2020). Electrophysiological recordings in non-human primates have identified neurons in orbitofrontal cortex, ventrolateral prefrontal cortex (vlPFC), and dorsolateral prefrontal cortex (dlPFC) that selectively fire for different abstract rules (Hoshi et al., 2000; Wallis et al., 2001). Recordings from dlPFC neurons demonstrate that as rules become learned, the onset of neuronal firing shifts earlier in the trial (Cromer et al., 2011; Pasupathy & Miller, 2005).

In humans, network neuroscience offers an array of methods to study the dynamic network changes associated with learning (for review, see Bassett & Mattar, 2017). With

[1] This work was previously published as Morin TM, Chang AE, Ma W, McGuire JT, and Stern SE (2021). Dynamic Network Analysis Demonstrates the Formation of Stable Functional Networks During Rule Learning. *Cerebral Cortex*. DOI: 10.1093/cercor/bhab175

these methods, the brain is conceptualized as a network of nodes (brain regions), connected by weighted edges (functional connectivity strength). Nodes can be assigned to different cortical networks, which we call communities. Canonical communities (e.g., default, dorsal/ventral attention, and cognitive control communities) have been defined previously from large samples of resting state fMRI data (Power et al., 2011; Yeo et al., 2011). Dynamic network analyses have been extensively employed in studies of implicit motor sequence learning, showing that during a serial reaction time (SRT) task sensory systems become functionally segregated, and PFC becomes functionally integrated (Bassett et al., 2015). Moreover, the degree of community switching (flexibility) in frontoparietal cortical regions was predictive of subsequent performance on the task (Bassett et al., 2011). Task-specific network reconfiguration has been observed when comparing difficulty levels on an n-back working memory task (Braun et al., 2015), on an abstract reasoning task (Hearne et al., 2017), and during reinforcement learning (Gerraty et al., 2018). Studies of associative memory have shown that the functional relationships within and between communities can be indicative of learning rate and task-performance (Fatima et al., 2016; Gerraty et al., 2018). Broadly, decoupling of default and dorsal attention communities is a strong marker of cognitive states (Dixon et al., 2017) and is a predictor of performance on working memory (J. B. Keller et al., 2015) and fluid intelligence tasks (M. W. Cole et al., 2012). The cognitive control community regulates this decoupling by supporting switching between different mental representations (M. W. Cole & Schneider, 2007; Spreng et al., 2013) and becomes active during memory-guided attention (Rosen et al., 2016).

Here, we applied network neuroscience techniques to a context-dependent rule learning task. During the task, naïve participants learned a novel set of context-dependent rules in order to correctly identify paired-associates (Zhu et al., 2020). In contrast with previous studies, which have primarily examined rule retrieval, we designed the task to include minimal instruction and no training before scanning to specifically investigate rule learning. Overall accuracy on the task varied significantly over time and across individuals, allowing us to compare the brain network organization of successful and unsuccessful learners. Through a dynamic network analysis, we characterized shifts in network metrics associated with successful learning.

The primary goals of our network analysis were to (1) assess how network dynamics differed between successful and unsuccessful learners, and (2) characterize how network measures shifted as subject performance improved on the task. We predicted that successful learners would form stable functional representations of the rules, which would correspond to lower-levels of community switching (network flexibility). This hypothesis is supported by previous literature showing that performance on language, reasoning, and working memory tasks is associated with increased stability of functional networks (Ferguson et al., 2017; Schultz & Cole, 2016). As a general framework, we predicted that the task would become more automatic for successful learners as their performance improved, corresponding to (1) greater functional segregation (network assortativity) and decreased centrality of cognitive control regions as learning occurred, and (2) decoupling of the default and attention communities. Our results provide a new perspective, identifying

a key role for brain-wide functional networks that are shown to decouple and stabilize during rule learning.

Methods

Participants

A total of 32 participants were scanned for the study (Age, Mean = 22.78, SD = 3.97; 14 female) and 29 were included in the final analysis. Participants were recruited from the Boston area and were English language speakers between the ages of 18 and 35. All subjects had normal or corrected-to-normal vision and reported no past or current neurological or psychiatric disorders. All procedures were approved by the Boston University Institutional Review Board and all subjects provided written informed consent. For the three participants not included in the final analysis, one withdrew during scanning, one was excluded for undisclosed prior knowledge about the task, and one was excluded for excess head motion (>3mm Framewise displacement during two or more scanning runs).

Cognitive Task

Before fMRI scanning, participants were not pre-trained or provided with task instructions. During scanning, subjects performed a cognitive task designed to test their ability to learn context-dependent associative rules (**Figure 3.1**). Our lab has previously used this task for computational modeling and behavioral testing of context-dependent rule learning (Zhu et al., 2020). During the task, a cue image appeared on the screen (2.0s),

followed by a delay (2.0s) and then an associate image (2.0s). Subjects were then allowed 2.0s to decide whether or not the cue image was correctly paired with the associate image. Subjects indicated their response (match or mismatch) by pressing the left or right button on a response-box, and were provided with feedback ("Correct," "Incorrect," or "No Response") for 0.5s. Between each trial, a fixation cross was displayed for 4.0s. There were four context-dependent cue-associate pairings that subjects encountered during the scan, and they are described in **Figure 3.1**. Scanning consisted of nine runs, with 32 trials per run.

Behavioral Data Analysis

Accuracy was calculated for each subject across each of the nine scanning runs. Each scanning run consisted of 32 trials of the context-dependent rule learning task, and subject performance was used as a measure of when (and if) subjects shifted from "learning" to "learned" phases. With the task set up in a 2-alternative forced choice format, we assumed that subjects who hadn't yet learned the context-dependent rules would achieve about 50% accuracy (16 correct responses per run) purely by chance. Using the binomial distribution, we determined the observed level of accuracy per run that would have a 0.1% likelihood of occurring by chance, and set the threshold for above-chance performance to 26 correct responses out of 32 trials per scanning run (or 81.25% correct). If a subject responded correctly to at least 26 trials during one run, then that run was classified as "learned." Subjects were considered "successful" learners if they achieved at least one "learned" scanning run. Subject performance is presented in **Figure 3.3**.

MRI Data Acquisition

Scanning was conducted using a 3 Tesla Siemens TIM Trio magnetic resonance scanner and a 32-channel head coil at the Center for Brain Science at Harvard University in Cambridge, Massachusetts. High-resolution T1-weighted multi-planar rapidly acquired gradient echo (MP-RAGE) scans were acquired for each subject (TR = 2530 ms; TE = 1.64 ms; flip angle = 7º; slices = 176; resolution = 1 mm isotropic). T2*-weighted EPI (BOLD) images were acquired using a slice-accelerated EPI sequence that permitted simultaneous multi-slice acquisitions using the blipped-CAIPI technique (TR 2 s; TE 26 ms; flip angle 80º; 6/8 partial-fourier acquisition) (Setsompop et al., 2012). A total of 69 slices were acquired with a slice acceleration factor of 3 and no skip, covering the whole brain. Images were acquired at a nominal 2 mm isotropic spatial resolution (matrix size: 108 x 108).

fMRI Preprocessing

Functional data were analyzed using the Freesurfer FS-FAST software package (version 6.0, Charlestown, MA; http://surfer.nmr.mgh.harvard.edu/) (Fischl, 2012). The following preprocessing steps were performed: slice-time correction, motion correction, spatial smoothing (3mm FWHM), boundary-based registration with 12-degrees of freedom to co-register each subject's functional and anatomical data, and spatial normalization of each subject's reconstructed surface to Freesurfer's standard template (fsaverage) using spherical surface registration. Functional data were further preprocessed in MATLAB (The MathWorks). Head-motion regression (6 motion parameters and their 6 temporal derivatives), whole-brain signal regression, and ventricular and white matter signal regression were performed (Van Dijk et al., 2010). Additionally, our matrix of nuisance

regressors included two event-related regressors corresponding to the Response and Feedback events in the task. For the Response events, regressors were created by convolving a standard hemodynamic response function with a duration-modulated boxcar, where boxcars were scaled by the subject's response time on a per-trial basis. Similarly, the Feedback regressors were created by convolving the same standard hemodynamic response function with a boxcar enveloping the length of the feedback period (0.5s). We included these event-related regressors to ensure that observed changes in network connectivity were associated with rule learning, rather than differences in response times or feedback presentation between successful and unsuccessful learners. We then calculated framewise displacement by taking the sum of the absolute derivatives of the 6 motion parameters for each time point (Power et al., 2012). A threshold of 0.5 mm was set to identify time points with excessive motion. To avoid artifact spread during wavelet decomposition, high motion timepoints were replaced using linear interpolation (Carp, 2013).

Network Construction

From the 2018 Schaefer-parcellation, we defined 400 cortical regions of interest across the two brain hemispheres (200 per hemisphere, see **Figure 3.2**) (Schaefer et al., 2018). For each subject and each run of data, these 400 brain regions formed the nodes of a network. To define edges between the nodes, the mean BOLD signal time-course was extracted from each region and the wavelet correlation between time-courses for each pair of regions (*i, j*) was calculated. Maximum overlap discrete wavelet transform was used to decompose a time-course into scales corresponding to frequency bands (this is identical to

the methods used in Bassett et al. 2011. The software for this method can be found at: http://grinsted.github.io/wavelet-coherence/). We used scale 2 (0.0625 – 0.125 Hz) in our analysis because this frequency overlaps most with the canonical hemodynamic response function. In line with previous research using wavelet methods to define network edges, we calculated the Pearson correlation between scale 2 time-courses (Bassett et al., 2011; Z. Zhang et al., 2016). Our choice of wavelet correlation over wavelet coherence means that the network does include negative edges. Wavelet correlation was most appropriate for our analysis because we calculated functional connectivity measurements over an entire scanning run (450s of data, 225 TRs), and the non-stationarity of fMRI time-courses makes coherence measures inappropriate for this large time-scale (Bullmore et al., 2004; Z. Zhang et al., 2016). Edge weights in the network were subjected to significance testing using the *rcorr.adjust* function in R. For a pair of nodes *i* and *j*, if functional connectivity was deemed statistically different from zero according to a liberal statistical threshold (alpha = 0.05, Holm corrected for multiple comparisons), then the weight of edge (*i, j*) remained the same. Otherwise, it was set to zero, eliminating the edge from the graph. For each subject, this resulted in nine network layers, spanning the nine runs of fMRI scanning. For all network statistics and clustering methods described below (except for betweenness centrality), we included both positive and negative edge-weights. When calculating betweenness centrality, we only included positive edge-weights. This is because betweenness centrality calculations depend on deriving shortest paths between pairs of nodes, a problem that is ill-defined for nodes connected by negatively-weighted edges. Although including negative edge weights can complicate the interpretation of network

measures, we chose to include negative edge weights when possible. Previous work indicates that negative edges are physiologically meaningful, indicating segregation or competition between regions (Fox et al., 2005; C. J. Keller et al., 2013; Rubinov & Sporns, 2011). (For additional discussion on the inclusion of negative edges, see: (Fornito et al., 2015; Schwarz & McGonigle, 2011). Finally, only 3.5% of the within-layer edges were negatively weighted in our subjects' networks, suggesting that their overall influence on network measures is small.

Dynamic Community Detection & Flexibility

For community detection and node flexibility calculations, we combined the nine network layers into a single dynamic network for each subject. In the dynamic network, each layer corresponded to one of the nine scanning runs, ordered in time. Networks were linked across time by connecting each node in one layer to itself in the immediately adjacent layers. Inter-layer edges were equally weighted, $\omega = 1$.

To determine the community membership(s) of each node over time, we used a Louvain community detection algorithm that is generalized for multi-layered networks (Mucha et al., 2010). MATLAB code for the algorithm was produced by Mucha and Porter, and is freely available online: http://netwiki.amath.unc.edu/GenLouvain/GenLouvain. The algorithm detects communities by optimizing multilayer modularity, Q_{ml} (originally presented in this format by Bassett et al. 2011):

$$Q_{ml} = \frac{1}{2\mu}\sum_{ijlr}\left\{\left(A_{ijl} - \gamma_l \frac{k_{il}k_{jl}}{2m_l}\right)\delta_{lr} + \delta_{ij}\omega_{jlr}\right\}\delta(g_{il}, g_{jr}),$$

where the adjacency matrix of layer l (e.g. scanning run number l) has components A_{ijl}, γ_l is the resolution parameter of layer l, g_{il} gives the community assignment of node i in layer l, g_{jr} gives the community assignment of node j in layer r, the function $\delta(g_{il}, g_{jr})$ is 1 when $g_{il} = g_{jr}$ and 0 otherwise, ω_{jlr} is the connection strength between node j in layer r and node j in layer l, k_{il} is the strength of node i in layer l, m_l is half the sum of all the edge-weights in layer l, $2\mu = \sum_{jr} \kappa_{jr}$, $\kappa_{jl} = k_{jl} + \omega_{jl}$, and $\omega_{jl} = \sum_r \omega_{jlr}$. We set $\omega = 1$ for edges connecting the same node in adjacent layers and set the resolution parameter $\gamma_l = 1$.

By this definition, modularity is minimized when strongly connected groups of nodes (both within and between layers) are part of the same community. The between-layer connectivity strength is summarized by the term $\delta_{ij}\omega_{jlr}$, and the within-layer connectivity strength is summarized by the term $\left(A_{ijl} - \gamma_l \frac{k_{il}k_{jl}}{2m_l}\right)\delta_{lr}$. This algorithm allows a node to change its community allegiance across layers. See Mucha et al. (2010) for details on precise methods and implementations. Note, the community detection algorithm discussed here is a data-driven approach. The communities it assigns are unrelated to the canonical resting state communities (Yeo-communities) that are discussed elsewhere in this paper. The Yeo-communities were determined a priori with a parcellation developed by Schaefer et al. (2018), without any influence from our subjects' fMRI data.

After running the community detection algorithm, we calculated flexibility for each node by counting the number of times a node switched communities and dividing by the possible number of switches (there were eight possible switches, since our network had nine layers). Because the outcome of the community detection algorithm depends on initial

conditions (e.g., which node is first assigned to a community), we ran the algorithm 100 times for each subject, calculating average flexibility for each node across iterations.

Whole brain average flexibility was determined for each subject by taking the mean flexibility across all vertices. The average flexibility was also determined for each of the seven Yeo-communities (Yeo et al., 2011). Average flexibility for the whole brain is plotted against accuracy on the cognitive task for each subject in **Figure 3.4a**. To visualize the spatial distribution of flexibly-changing nodes on cortex, and the relationship of flexibility with accuracy, we projected the group mean correlations between the flexibility of an individual node and subject accuracy onto the cortical surface in **Figure 3.4b**. Average flexibility for each of the seven Yeo-communities is plotted against task accuracy in **Figure 3.4c**. The relationship between flexibility and learning was assessed through Pearson correlation using the *cor.test* function in R, the results of which are summarized in **Table 3.1** (p-values FDR corrected).

Assortative Mixing

To determine whether brain regions connected mostly to other regions in the same Yeo-community and the extent to which this differed over time and across successful and unsuccessful learners, we calculated assortative mixing for each Yeo-community. We performed these calculations within each layer of a subject's network to determine the assortative mixing of Yeo-communities for each scan run. To calculate assortative mixing, we used the assortativity function in the *igraph* package available for R which uses Newman's definition of assortativity (Newman, 2003):

$$r = \frac{\sum_i e(i,i) - \sum_i a(i)b(i)}{1 - \sum_i a(i)b(i)}$$

Where $e(i,j)$ is the fraction of edges connecting nodes labeled *i* and *j*, $a(i) = \sum_j e(i,j)$, and $b(j) = \sum_i e(i,j)$. When calculating $e(i,j)$, negative edges subtract from the numerator, but add to the denominator. In this way, negative within-category edges decrease assortativity. Assortativity *r* is equal to one when there is perfect assortative mixing (all edges are within-category). Similarly, it is equal to zero when the mixing is completely random and *r* approaches -1 when mixing is disassortative (edges on the graph connect vertices with other vertices outside of their category). We calculated separate assortativity measures for each Yeo-community by re-labeling the nodes of the graph with only two labels: nodes within the community being measured, and those outside of the community being measured. Assortativity across communities, subjects, and scan runs is plotted in **Figure 3.5a** and summarized in **Table 3.2** (p-values FDR corrected).

Centrality

To determine which brain regions integrated information from many other brain regions, and whether this was altered with time and task performance, we calculated the average betweenness centrality for each of the seven Yeo-communities across subjects and scanning runs. Betweenness centrality was originally defined by (Freeman, 1978) and is defined by (Kolaczyk, 2009) as:

$$c_B(v) = \sum_{s \neq t \neq v \in V} \frac{\sigma(s,t|v)}{\sigma(s,t)}$$

where $\sigma(s,t|v)$ is the number of shortest paths from *s* to *t* that include *v*, and $\sigma(s,t)$ is the total number of shortest paths from *s* to *t*. Betweenness centrality is high for vertices that are on the shortest paths between many other nodes. Betweenness centrality is ill-defined for networks with negative edge-weights, so we eliminated all negative edges from our networks for this analysis. Additionally, because betweenness centrality relies on a shortest path metric, edges on the graph were transformed from a metric of strength (wavelet correlation) to a metric of distance, using the inverse transform ($1 / A_{ij}$). We then calculated betweenness centrality using the betweenness function available in the *igraph* library for R. Betweenness centrality across communities, subjects, and scan runs is plotted in **Figure 3.5b** and displayed in **Table 3.3** (p-values FDR corrected).

Inter-community Edge Strength

To determine how connectivity between the Yeo-communities changed with learning, we calculated the average weight of inter-community edges for each scanning run. The inter-community edge strength between two communities i and j is defined as:

$$s(i,j) = \frac{\sum_{i \neq j} w_{ij}}{n_{ij}}$$

where w_{ij} is the weight of an edge connecting a node in community i with a node in community j and n_{ij} is the total number of edges connecting communities i and j. This was calculated using the simplify function available in the *igraph* library for R. Negative edges decrease the overall inter-community edge strength between two communities. We plotted the time-varying inter-community edge strength for each pair of communities in

both successful and unsuccessful learners in **Figure 3.6**. Statistics are reported in **Table 3.4** (p-values FDR corrected).

Dynamic Network Statistics

To test how assortative mixing, betweenness centrality, and inter-community edge strength differed between learning groups and changed throughout learning, we estimated two linear mixed effects models implemented with the lme4 package in R. With the first model (Model 1) we examined the effects of learning group (successful or unsuccessful) and time on each of the network measures. The model included fixed effects for learning group, time (scan run), and the interaction between learning group and time, as well as a random effect of subject. We report results where the intercept varied across subjects. We also conducted a version of Model 1 allowing slope to vary for each subject, but this model failed to converge and fit poorly in most circumstances, so we do not report it here. A second model (Model 2) was used to test the effect of each subject's unique learning curve (measured as each subject's accuracy on each scan run) on the network metrics. This model included fixed effects for run-to-run accuracy as well as overall task accuracy to control for between-subject differences in overall performance. The model also included a random effect of subject. Both models were fit to data for each of the seven Yeo-communities (or each pair of communities, in the case of inter-community edge strength). We applied a false discovery rate (FDR) correction for multiple comparisons across communities and model parameters (Benjamini & Hochberg, 1995). Unless otherwise noted, all reported p-values have been corrected using FDR correction.

Results

Behavioral Results

As expected, performance on the cognitive task varied considerably across subjects. Subject accuracy over time is displayed in **Figure 3.3**. A few subjects learned the context-dependent rules and achieved ceiling-levels of accuracy in just two or three scanning runs. Other subjects remained at chance-levels of accuracy throughout. Subjects who remained at chance-level performance throughout all nine scanning runs were considered "unsuccessful" learners, and subjects who achieved above-chance performance on at least one scan run were considered "successful" learners. Overall, 20 subjects met criteria as successful learners, and 9 subjects were unsuccessful. The variation in learning ability provided us with a natural control group for identifying functional network characteristics associated with successful rule learning.

Network Stability and Community Switching

To examine functional network architecture changes over the course of the task, we can measure the community switching (flexibility) of a given brain region. As a working model, we proposed that during learning, brain regions flexibly adapted their community allegiance as subjects adopted different task strategies. Once the task was learned, the community structure became more rigid (less flexible). Subjects with greater accuracy spent more time in the "learned" phase than the "learning" phase. Therefore, we predicted that overall accuracy would be inversely related to flexibility and hypothesized that

subjects with greater accuracy on the cognitive task would exhibit decreased brain network flexibility, consistent with the rapid development of stable rule representations.

We plotted mean flexibility across the whole brain against subject accuracy in **Figure 3.4a**. We did not observe a significant association between overall accuracy on the task and whole-brain mean flexibility. In **Figure 3.4b** we projected the correlation between accuracy and flexibility for each node in the Schaefer-400 atlas onto the cortical surface. A regional pattern emerged with certain areas showing consistently high or low correlation between accuracy and flexibility. To determine if certain Yeo-communities were driving this result, we plotted the average flexibility for each community against accuracy in **Figure 3.4c**. We found a statistically significant Pearson correlation coefficient between flexibility and accuracy in the ventral attention community ($r = -0.524$, $p < 0.05$) as well as in the somatomotor community ($r = -0.527$, $p < 0.05$) (FDR corrected for multiple comparisons). We failed to detect a significant correlation in any of the other Yeo-communities. The correlation coefficients and corresponding p-values for all seven Yeo-communities and the whole brain are displayed in **Table 3.1**.

Assortative Mixing

Assortative Mixing is defined here as the degree to which nodes are highly connected with other nodes in the same Yeo-community. A positive value for assortative mixing indicates that nodes within a community are more strongly connected to each other than they are to nodes outside of their community. We predicted that assortative mixing would be stronger in successful learners, which would correspond to the formation of stable, modular networks and the predicted decrease in node flexibility. For each of the seven Yeo-

communities, we calculated assortative mixing during each scanning run. Results are displayed in **Figure 3.5a**. Using two linear mixed effects models, we tested the effects of learning, time, and the interaction between learning and time on assortativity (Model 1), as well as the effect of run-to-run accuracy on assortativity while controlling for the effect of overall accuracy (Model 2). Model results are presented in **Table 3.2**. Model 1 showed a significant interaction between learning and time on assortativity in the cognitive control community ($T = 2.70$, $p < 0.05$). Post-hoc testing with the *lstrends* command in R showed that the slope of assortativity over time was significantly different between successful learners, who showed an increase in assortativity over time, and unsuccessful learners, who showed a decrease in assortativity over time. However, each group's slope itself did not significantly differ from zero (Successful learners: Slope = 0.0022, $T = 1.69$, $p = 0.093$; Unsuccessful learners: Slope = -0.0034, $T = -1.73$, $p = 0.086$). This result indicated that the interconnectivity of cognitive control nodes showed a more positive trend over time in successful learners than in unsuccessful learners, albeit without supporting strong conclusions about the sign of the trend in each group individually. Echoing this finding, Model 2 showed a significant positive effect of run-to-run accuracy on assortativity in the cognitive control community, even when controlling for overall accuracy ($T = 2.60$, $p < 0.05$). This indicates that changes in assortativity of the cognitive control community were significantly associated with individual learning curves across subjects.

Centrality

Centrality measures the degree to which a brain region acts as a mediator between distantly connected brain regions. We calculated mean betweenness centrality across nodes

in each of the seven Yeo-communities during each scanning run. Results from this analysis are plotted in **Figure 3.5b**. Using two linear mixed effects models, we tested the effects of learning, time, and the interaction between learning and time on betweenness centrality (Model 1), as well as the effect of time-varying accuracy on betweenness centrality while controlling for the effect of overall accuracy (Model 2). Model results are presented in **Table 3.3**. Model 1 did not reveal any significant interactions between learning and time. Model 2 showed that when controlling for overall accuracy, increased run-to-run accuracy is significantly associated with reduced betweenness centrality in the ventral attention community ($T = -2.32$, $p < 0.05$).

Inter-community Edge Strength

Inter-community edge strength is a measure of connectivity between a pair of Yeo-communities, and can tell us how communication between two communities changes during learning. We predicted that in successful learners, we would observe a greater decoupling of the default community from the dorsal/ventral attention communities. Previous research has indicated that decoupling of default and attention systems is associated with better working memory and overall fluid intelligence scores (M. W. Cole et al., 2012; J. B. Keller et al., 2015). Inter-community edge strength is plotted over time for each pair of Yeo-communities and for both successful and unsuccessful learners in **Figure 3.6**. Using two linear mixed effects models, we tested the effects of learning, time, and the interaction between learning and time on inter-community edge strength (Model 1), as well as the effect of time-varying accuracy on inter-community edge strength while controlling for the effect of overall accuracy (Model 2). Model results are presented in

Table 3.4. The results support our hypothesis, showing that successful subjects had greater decoupling between default and attention communities. However, the results indicate that this is largely driven by an overall decoupling of the dorsal and ventral attention communities from most other Yeo-communities in successful learners, rather than a specific decoupling of attention systems from the default community. Model 1 showed that compared to unsuccessful learners, the dorsal attention community in successful learners showed significantly reduced inter-community edge strength with visual (T = -2.71, p < 0.05), somatomotor (T = -3.67, p < 0.01), ventral attention

(T = -2.92, p < 0.05), and limbic (T = -3.01, p < 0.05) communities. Reduced inter-community edge strength between the dorsal attention and default communities was only significant before FDR correction for multiple comparisons (T = -2.40, p = 0.06). Similarly, the ventral attention community in successful learners showed significantly reduced inter-community edge strength with visual (T = -3.01, p < 0.05), dorsal attention (T = -2.92, p < 0.05), cognitive control (T = -3.58, p < 0.01), and default (T = -2.55, p < 0.05) communities. Reduced inter-community edge strength between the ventral attention and limbic communities was only significant before FDR correction (T = -2.39, p = 0.06). Interestingly, Model 2 showed several pairs of Yeo-communities in which inter-community edge strength was strongly associated with time-varying accuracy on the task. These pairs were somatomotor – default (T = 3.39, p < 0.01), somatomotor – limbic (T = 3.06, p < 0.01), and ventral attention – cognitive control (T = 2.58, p < 0.05).

Discussion

We performed a dynamic network analysis to identify functional brain network changes associated with individual differences in learning a set of context-dependent rules. We propose that a stable ventral attention community supports maintenance of sustained attention in successful learners, and that dynamic changes in assortativity and inter-community edge strength of the cognitive control community are associated with the formation of context-dependent rule representations, and task automaticity. These results highlight key brain network features that are associated with successful learning.

Network Stability

In line with our predictions, we found that participants with greater overall accuracy on the task exhibited decreased average community switching (flexibility) within the ventral attention and somatomotor communities (see **Figure 3.4c, Table 3.1**). We view decreased network flexibility as increased network stability, and in successful subjects this stability correlates with their high accuracy and representation of the context-dependent rules.

Considering the ventral attention community, previous work on rule learning has identified vlPFC and pre-SMA as regions important for representing specific rules, and suppressing activity from a previous task set respectively (Crone, Donohue, et al., 2006; Crone, Wendelken, et al., 2006). Moreover, recently published work in non-human primates shows that neuronal population activity in the dorsal anterior cingulate cortex, another prominent node in the ventral attention community, reflects the search for new rules in a categorical rule-learning task (Cohen et al., 2021). For successful learners on our

task, it is likely beneficial for these regions to have stable connectivity and reduced community switching as they actively represent learned rules. Considering the somatomotor community, previous work using recordings from motor cortex in non-human primates demonstrates that rules are most easily learned when they are aligned with the intrinsic network activity of this region (Sadtler et al., 2014). Reduced flexibility observed in our successful subjects could reflect a reduced change in somatomotor community activity during rule implementation compared to rest.

Our results complement previous studies of network flexibility where lower overall flexibility was observed in somatomotor cortex compared to other brain regions (Bassett et al., 2011; Betzel et al., 2017; Gerraty et al., 2018). Several studies have also identified a positive association between learning and flexibility in frontoparietal cortical regions (Bassett et al., 2011; Braun et al., 2015; Gerraty et al., 2018). While not statistically significant in our study, we did observe a positive association between flexibility and accuracy in the cognitive control community ($r = 0.22$, $T = 1.81$, $p = 0.22$). In our study, we identified two communities that showed greater stability associated with overall accuracy on the task. This is in line with several large-scale studies have identified network stability as a key feature contributing to general intelligence and overall cognitive ability (Ferguson et al., 2017; Schultz & Cole, 2016).

Previously, studies of network flexibility and learning have employed homogeneous samples of learners whose learning improved over time (Bassett et al., 2011; Gerraty et al., 2018). Our study expands upon previous work with the inclusion of unsuccessful subjects who never learned the context dependent rules. These subjects

comprised a natural control group that allowed us to identify individual differences in brain network structure associated with learning. Additionally, in our study we capture the full learning curves of successful subjects, from the beginning phases of learning, up until performance has plateaued and high accuracy is achieved.

While we highlight the reduced flexibility of the ventral attention community as a key feature of successful learning, we also found changes in the centrality and inter-community edge strength of this community that are associated with learning. It is not necessarily true that a node with low flexibility has unchanging functional connectivity. Rather, a node with low flexibility is part of a stable community. With Louvain community detection in particular, emphasis is put on creating modular networks, where intra-community connections are stronger than inter-community connections (Mucha et al., 2010). A stable community might exhibit low flexibility (the nodes within the community stay a part of that community), but be changing its connectivity with other communities. The community maintains low flexibility by ensuring that all members alter their connectivity patterns together.

Cognitive Control

In the cognitive control community, we observed a significant interaction effect between learning group and time on assortative mixing (Table 3.2, Model 1). Assortative mixing showed a greater increase over time in successful learners than in unsuccessful learners. Complementing this result, we also found a significant positive association between assortative mixing in the cognitive control community and run-to-run accuracy on the task (Table 3.2, Model 2).

Brain regions within the cognitive control community are understood to be responsible for higher order executive functioning, including response inhibition, working memory, and planning (Nyhus & Barceló, 2009; Vincent et al., 2008; Watson & Chatterjee, 2012). A large body of work proposes that rules are represented in prefrontal cortex for the purpose of directing top-down attention (for review, see (Miller & Buschman, 2014). Additionally, frontoparietal cortex is implicated in strategic access to memory (Badre & Wagner, 2007) and memory guided attention (Rosen et al., 2016).

Successful context-dependent rule learning on our task could be conceptualized as the ability to create a task-set structure during uninstructed learning. Modeling work suggests that the creation of task sets could be accomplished through cognitive control and executive functioning (Collins & Frank, 2013). A potential mechanism by which the cognitive control community could direct attention is by mediating the decoupling of default and dorsal attention communities, and titrating the balance between inward and outward awareness (Spreng et al., 2013). For successful learners, the context-dependent rule task quickly became automatic, and an increase in assortativity may be reflective of decreased dependence on, or more efficient processing within the cognitive control community for directing top-down attention. This framework is in line with theories suggesting that cognitive control connectivity adaptively reconfigures to meet task demands, primarily through a set of connector hubs (Gordon et al., 2018; C. Gratton et al., 2016; C. Gratton, Sun, et al., 2018; G. Gratton et al., 2018). As a working hypothesis, we propose that as learning occurs, executive control over network configuration becomes more efficient and the cognitive control community becomes more strongly connected to

itself and less widely integrated in the whole brain network. Similarly, in unsuccessful learners, decreased assortative mixing of the cognitive control community over time is reflective of continual strategy updating as attempts at implementing rules remain unsuccessful.

Interactions Between Attention and Cognitive Control

We observed a positive association between run-to-run accuracy on the task and inter-community edge strength of the cognitive control and ventral attention communities (Table 4, Model 2). Additionally, successful learners exhibited significantly lower inter-community edge strength between attention communities and most other communities throughout the brain (Table 4, Model 1).

The vlPFC, pre-SMA, and dorsal anterior cingulate are prominent regions in the ventral attention community that contribute to rule learning (Y. Cohen et al., 2021; Crone, Donohue, et al., 2006; Crone, Wendelken, et al., 2006; Passingham et al., 2000). The ventral attention community is often associated with orienting, as it is activated by novel stimuli and stimulus-driven shifts in attention (Corbetta & Shulman, 2002; H. Kim, 2014; Mantini et al., 2009). While the Schaefer-400 atlas includes the vlPFC, pre-SMA, and dorsal anterior cingulate as part of the "ventral attention" community, other groups use varying labels and definitions (Power et al., 2011; Yeo et al., 2011). One common framework refers to the ventral attention community as the cingulo-opercular network, and suggests that both the cognitive control community and cingulo-opercular network work together to achieve executive control (C. Gratton et al., 2016; C. Gratton, Sun, et al., 2018).

Research from Crittenden and colleagues showed increased activity in both cingulo-opercular and cognitive control regions during a rule-based associative memory task (Crittenden et al., 2016). Interestingly, they found that specific task rules were most accurately decoded using signals from voxels within cognitive control regions (which they call the frontoparietal network). This led them to suggest that cognitive control regions contain more specific rule-based representations, while cingulo-opercular regions are more important for emphasizing event salience and maintaining focused attention (Crittenden et al., 2016). This interpretation complements other work conceptualizing the ventral attention community as a salience network (Seeley et al., 2007) that plays a top-level role directing changes in functional connectivity between cognitive control and other communities throughout the brain (Menon & Uddin, 2010; Sridharan et al., 2008). Our study adds new evidence to this conceptual framework, demonstrating that a stable ventral attention community contributes to steady maintenance of attention throughout the task, and a more flexible cognitive control community demonstrates dynamic changes in assortativity and inter-community edge strength associated with successful rule learning.

We also observed a negative association between the centrality of the ventral attention community and run-to-run accuracy on the task (Table 3.3, Model 2). This suggests that as subjects learn the context-dependent rules, ventral attention regions reduce their long-ranging functional connections with other brain regions. Within the frameworks discussed above, decreased centrality of the ventral attention community could be reflective of more targeted salience to specific features of the task. In concert with the increased inter-community edge strength we observe between ventral attention and

cognitive control regions, these results suggest more targeted attention to rule representations in successful learners.

Finally, we also observed reduced inter-community edge strength between the dorsal/ventral attention communities and most other communities in successful learners throughout the entire task (Table 3.4, Model 1). This observation reflects the well-known dissociation between default and attention systems of the brain that is present at rest (Fox et al., 2005) and is modulated by various tasks (Dixon et al., 2017; J. B. Keller et al., 2015; Spreng et al., 2013). Miller and Buschman suggest that local synchrony of neurons in attention and primary sensory areas is essential for synchronizing mental representations with the external world (Miller & Buschman, 2014). More broadly, functional segregation of attention communities could be advantageous for maintaining focused attention during learning.

Conclusion

Our work expands upon previous studies of rule learning by using a dynamic network analysis and focusing on brain-wide connectivity. We identified several brain network characteristics associated with individual differences in learning context-dependent rules. These include decreased flexibility of the ventral attention and somatomotor communities, functionally segregated attention systems, and shifts in the cognitive control connectivity associated with successful learning.

Figures

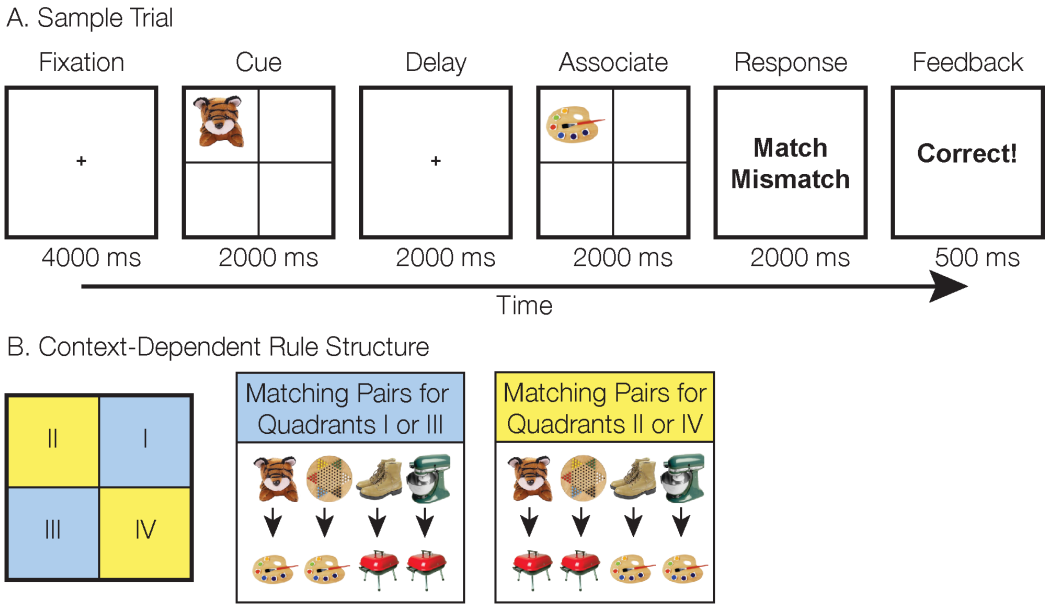

Figure 3.1 Context-Dependent Rule Learning Task

(A) During each trial, the subject saw a fixation (4000ms), followed by a cue stimulus (2000ms), delay (2000ms), and an associate stimulus (2000ms). Then, the subject was given 2000ms to decide whether or not the cue image was correctly paired with the associate image. Subjects indicated their response by pressing the left or right button on a response box. The trial ended with 500ms of feedback ("Correct," "Incorrect," or "No Response"). **(B)** Subjects were naïve to the fact that a context-dependent rule structure dictated whether cue and associate stimuli were correctly paired. If the cue and associate appeared in Quadrant I or III (highlighted here in blue for emphasis), they obeyed one set of rules (e.g., the tiger and paint-palette are a pair). If instead the cue and associate appeared in Quadrant II or IV (yellow), they obeyed an alternate set of rules (e.g., the tiger and grill are now a match). Subjects were tasked with learning these context-dependent pairings over the course of nine scanning runs. Each scanning run consisted of 32 trials of the task.

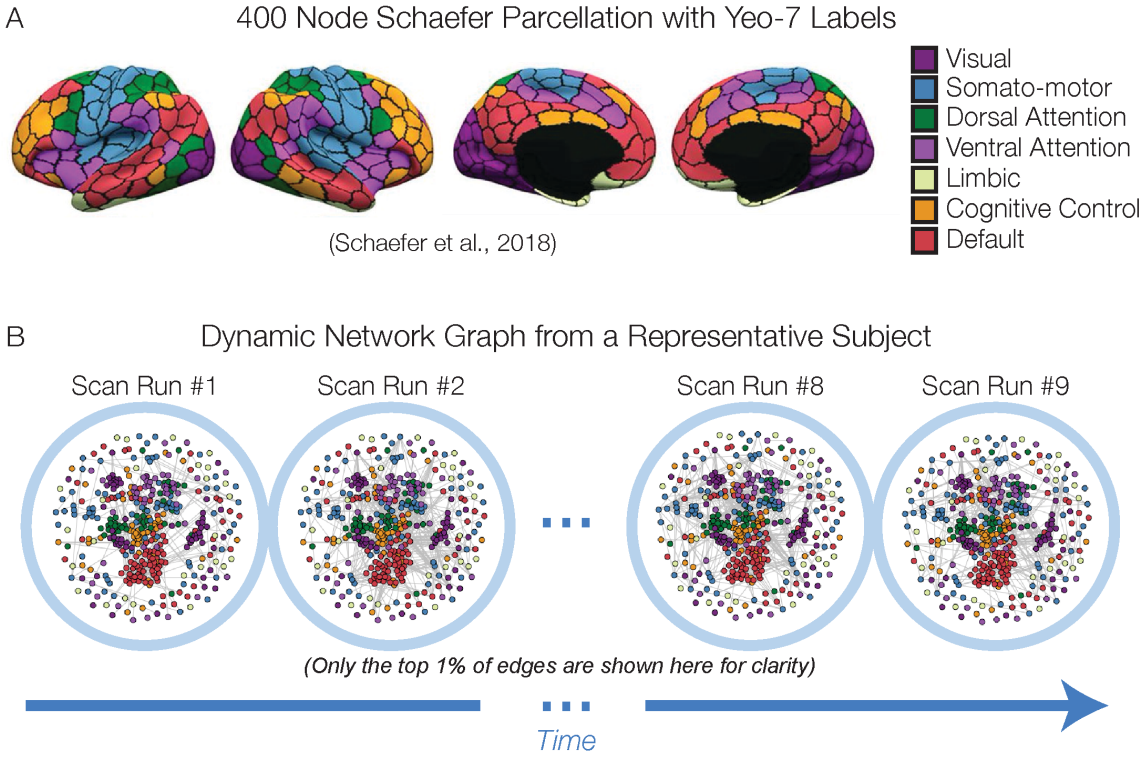

Figure 3.2 Network Construction

(A) Inflated representation of cortex divided into 400 regions, each assigned to a Yeo-community (adapted with permission from https://github.com/ThomasYeoLab/CBIG/tree/master/stable_projects/brain_parcellation/Schaefer2018_LocalGlobal). **(B)** Multilayer network of the connectivity between regions in a single subject. Each brain region from (A) is represented by a node. Edges represent functional connectivity between regions. For clarity, only the top 1% of strongest edges in each layer are shown here.

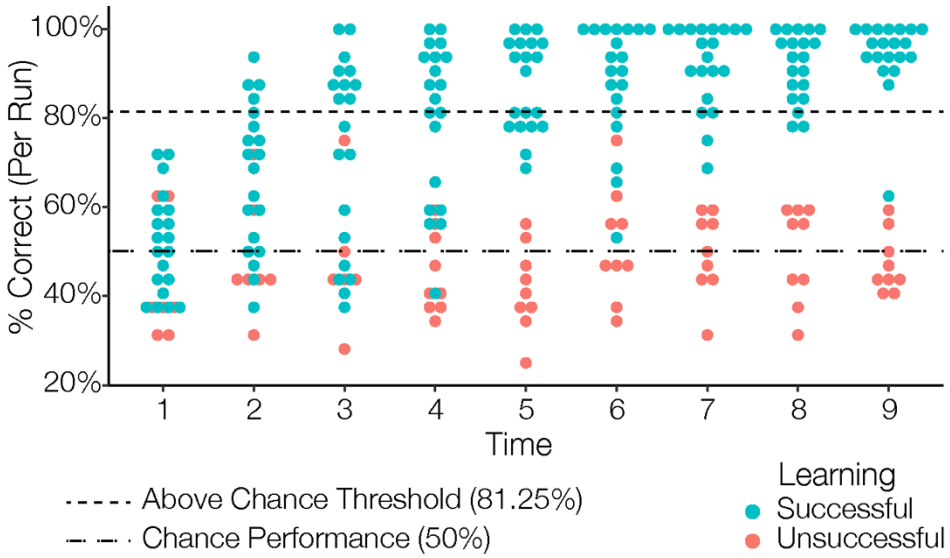

Figure 3.3 Rule Learning Ability

Behavioral results. Subject accuracy is plotted here over time. Time points represent each of the 9 scanning runs (32 trials per run). Subjects who achieved accuracy significantly above chance in at least one run are considered successful learners and plotted in blue (n = 20). Accuracy measurements for unsuccessful learners are plotted in red (n = 9).

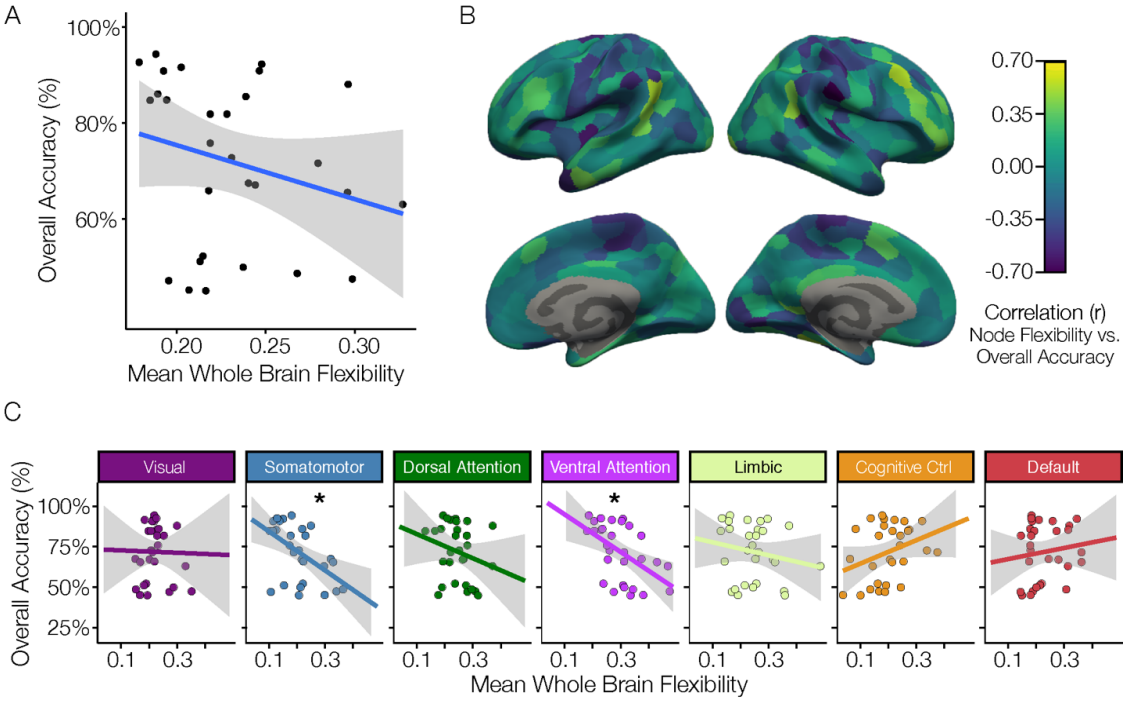

Figure 3.4 Flexibility

(A) Whole-brain average flexibility is plotted against accuracy on the cognitive task for each subject. **(B)** Cortical map of the correlation between flexibility for each of the nodes in the Schaefer400 atlas and overall accuracy. **(C)** Average flexibility within each of the seven Yeo-communities is plotted against task accuracy. Trend lines show a linear regression between flexibility and accuracy. Grey area represents a 95% confidence interval. * denotes statistically significant correlation; $p < 0.05$, FDR corrected. All correlation statistics are presented in **Table 3.1**.

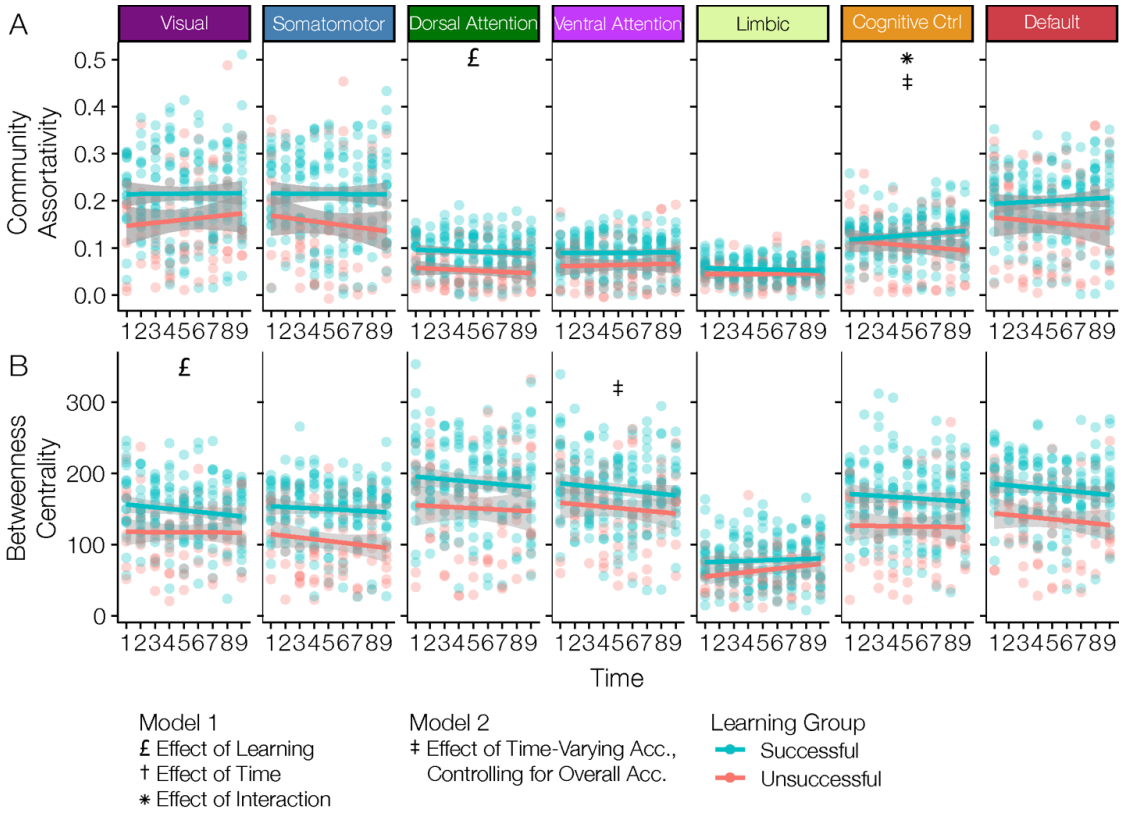

Figure 3.5 Community Assortativity and Betweenness Centrality

(A) Community assortativity and **(B)** mean betweenness centrality of the nodes in each Yeo-community were calculated for each of the 9 scanning runs for each subject. Points are colored blue for subjects who successfully learned the task, and red for subjects who did not learn the task. Linear regression of changes in assortativity and betweenness centrality for each group over time are plotted. Grey area surrounding regression lines represents a 95% confidence interval. Two linear mixed effects models were used to assess the effects of learning group and time (Model 1) as well as the effect of run-to-run accuracy (Model 2) on the network measures. Model results are presented in **Tables 3.2** and **3.3**. **£** = Effect of Learning Group; † = Effect of Time; ∗ = Effect of Learning Group x Time Interaction; ‡ = Effect of Run-to-Run Accuracy, Controlling for Overall Accuracy ($p < 0.05$, FDR corrected).

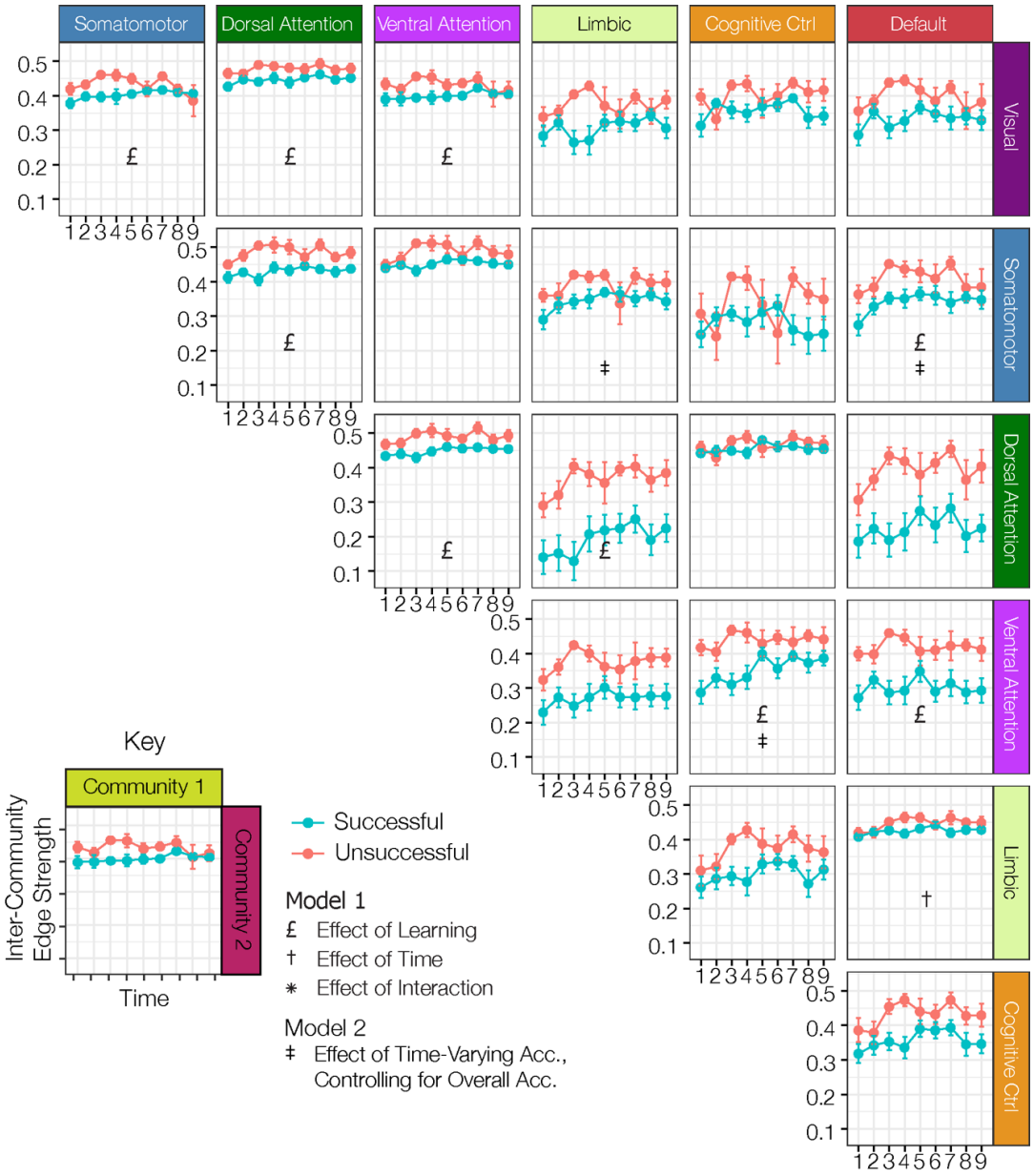

Figure 3.6 Inter-community Edge Strength

Inter-community edge strength plotted over time for each pair of Yeo-communities. Points represent mean inter-community strength across subjects in each group: successful learners are colored blue and unsuccessful learners are colored red. Time points represent each of the 9 scanning runs (32 trials per run). Error bars represent standard error. Two linear mixed effects models were used to assess the effects of learning group and time (Model 1) as well as the effect of run-to-run accuracy (Model 2) on the network measures. Model results are presented in **Table 3.4**. £ = Effect of Learning Group; † = Effect of Time; ∗ = Effect of Learning Group x Time Interaction; ‡ = Effect of Run-to-Run Accuracy, Controlling for Overall Accuracy ($p < 0.05$, FDR corrected).

Tables

Community	Correlation of Accuracy vs. Flexibility		
	r	*T* (28)	*p*
Visual	-0.02	-0.11	0.92
Somatomotor	**-0.53**	**-3.23**	**< .05**
Dorsal Attention	-0.25	-1.31	0.32
Ventral Attention	**-0.52**	**-3.20**	**< .05**
Limbic	-0.19	-1.01	0.43
Cognitive Control	0.33	1.81	0.22
Default	0.14	0.71	0.55
Whole Brain Avg.	-0.25	-1.36	0.32

Table 3.1 Relationship Between Accuracy and Flexibility

Pearson correlation was calculated to assess the relationship between accuracy on the cognitive task and flexibility of brain regions; repeated for each Yeo-community and across the whole brain. [r = Pearson correlation coefficient; T (28) = T-statistic with degrees of freedom of 28; p = adjusted p-value (FDR corrected). **Bold** results show a statistically significant relationship between accuracy on the task and brain-region flexibility, $p < 0.05$, FDR corrected for multiple comparisons.

	Model 1						Model 2			
	Learning		Time		Learning * Time		Overall Acc.		Acc. Per Run	
Community	Effect	*p*	Effect	*p*	Effect	*p*	Effect	*p*	Effect	*p*
Visual	0.07	0.12	0.003	0.43	-0.003	0.54	**0.20**	**< .05**	0.01	0.90
Somatomotor	0.04	0.36	-0.004	0.36	0.004	0.45	**0.22**	**< .05**	0.01	0.90
Dorsal Attn.	**0.04**	**< .05**	-0.001	0.43	0.000	0.82	**0.12**	**< .05**	-0.002	0.90
Ventral Attn.	0.03	0.15	0.001	0.73	-0.001	0.82	0.07	0.13	0.014	0.55
Limbic	0.01	0.20	0.000	0.90	-0.001	0.62	**0.05**	**< .05**	-0.017	0.19
Cognitive Ctrl	-0.003	0.90	-0.003	0.20	**0.005**	**< .05**	0.01	0.90	**0.041**	**< .05**
Default	0.03	0.54	-0.003	0.41	0.004	0.28	**0.20**	**< .05**	-0.008	0.90

Table 3.2. Linear Mixed Effects Models for Assortativity

Results from two linear mixed effects models that were run for each of the seven Yeo-communities. Model 1 treated each subject as a random effect and included fixed effects for learning group (successful or unsuccessful), time, and the interaction between learning group and time. Model 2 treated each subject as a random effect and included fixed effects for overall accuracy and time-varying accuracy (per run). p = adjusted p-value (FDR corrected). **Bold** results show a statistically significant effect, adjusted $p < 0.05$.

	Model 1						Model 2			
	Learning		Time		Learning * Time		Overall Acc.		Acc. Per Run	
Community	Effect	*p*	Effect	*p*	Effect	*p*	Effect	*p*	Effect	*p*
Visual	**40.60**	**0.04**	-0.122	0.952	-1.98	0.39	**119.87**	**< .01**	-22.53	0.21
Somato.	37.84	0.06	-2.406	0.165	1.37	0.56	**149.08**	**< .01**	-0.98	0.95
Dorsal Attn.	41.07	0.15	-1.049	0.727	-0.80	0.86	**129.02**	**< .05**	-13.75	0.57
Ventral Attn.	27.54	0.25	-1.899	0.391	-0.23	0.95	**145.43**	**< .01**	**-41.09**	**< .05**
Limbic	21.95	0.12	2.233	0.097	-1.60	0.35	**59.91**	**< .05**	7.46	0.57
Cog. Ctrl	45.41	0.06	-0.280	0.952	-1.05	0.73	**150.84**	**< .01**	-2.14	0.95
Default	41.30	0.06	-2.039	0.286	0.11	0.95	**151.09**	**< .01**	-11.32	0.57

Table 3.3. Linear Mixed Effects Models for Betweenness Centrality

Results from two linear mixed effects models that were run for each of the seven Yeo-communities. Model 1 treated each subject as a random effect and included fixed effects for learning group (successful or unsuccessful), time, and the interaction between learning group and time. assessed the effects of learning, time, and the interaction between learning and time. Model 2 treated each subject as a random effect and included fixed effects for overall accuracy and time-varying accuracy (per run). p = adjusted p-value (FDR corrected). **Bold** results show a statistically significant effect, adjusted $p < 0.05$.

		Model 1						Model 2			
		Learning		Time		Learning * Time		Overall Acc.		Acc. Per Run	
Comm. 1	Comm. 2	Effect	*p*	Effect	*p*	Effect	*p*	Effect	*p*	Effect	*p*
VIS	SOM	**-0.07**	**< .01**	-0.004	0.16	**0.007**	**< .05**	**-0.14**	**< .01**	0.031	0.21
VIS	DAN	**-0.04**	**< .05**	0.001	0.50	0.001	0.72	**-0.13**	**< .01**	0.032	0.07
VIS	VAN	**-0.06**	**< .05**	-0.002	0.39	0.005	0.09	**-0.13**	**< .05**	0.031	0.21
VIS	LIM	-0.09	0.09	0.002	0.76	0.004	0.59	**-0.29**	**< .01**	0.031	0.51
VIS	CTRL	-0.03	0.52	0.005	0.32	-0.004	0.56	**-0.18**	**< .05**	0.015	0.72
VIS	DEF	-0.09	0.09	-0.001	0.86	0.004	0.48	**-0.32**	**< .01**	0.038	0.38
SOM.	DAN	**-0.06**	**< .01**	0.002	0.56	0.001	0.72	**-0.19**	**< .01**	0.022	0.35
SOM.	VAN	-0.04	0.13	0.002	0.31	0	0.90	**-0.13**	**< .01**	0.016	0.44
SOM.	LIM	-0.06	0.155	0.003	0.50	0.003	0.63	**-0.25**	**< .01**	**0.102**	**< .01**
SOM.	CTRL	-0.01	0.863	0.006	0.47	-0.01	0.32	-0.08	0.59	-0.08	0.27
SOM.	DEF	**-0.09**	**< .05**	0.001	0.86	0.005	0.33	**-0.36**	**< .01**	**0.114**	**< .01**
DAN	VAN	**-0.05**	**< .05**	0.002	0.28	0.001	0.76	**-0.16**	**< .01**	0.031	0.10
DAN	LIM	**-0.19**	**< .05**	0.009	0.28	0.003	0.76	**-0.64**	**< .01**	0.076	0.29
DAN	CTRL	-0.01	0.788	0.003	0.25	-0.001	0.76	-0.08	0.08	0.02	0.37
DAN	DEF	-0.16	0.06	0.007	0.32	-0.002	0.84	**-0.67**	**< .01**	0.046	0.48
VAN	LIM	-0.11	0.061	0.003	0.59	0.001	0.90	**-0.40**	**< .01**	0.018	0.72
VAN	CTRL	**-0.13**	**< .01**	0.003	0.63	0.009	0.10	**-0.41**	**< .01**	**0.106**	**< .05**
VAN	DEF	**-0.12**	**< .05**	0	0.95	0	0.97	**-0.46**	**< .01**	0.003	0.94
LIM	CTRL	-0.07	0.204	0.006	0.32	-0.001	0.90	**-0.28**	**< .05**	0.023	0.64
LIM	DEF	-0.01	0.495	**0.003**	**< .05**	-0.002	0.49	-0.07	0.08	0.009	0.59
CTRL	DEF	-0.07	0.158	0.005	0.26	-0.001	0.86	**-0.32**	**< .01**	0.05	0.29

Table 3.4 Linear Mixed Effects Models for Inter-Community Edge Strength

Results from two linear mixed effects models that were run for each pair of the seven Yeo-communities. Model 1 assessed the effects of learning, time, and the interaction between learning and time, on inter-community edge strength. Model 2 assessed the effects of overall accuracy and time-varying accuracy (on a per-run basis) on inter-community edge strength. *p* = adjusted p-value (FDR corrected). **Bold** results show a statistically significant

effect, adjusted $p < 0.05$. VIS = Visual, SOM = Somatomotor, DAN = Dorsal Attention, VAN = Ventral Attention, LIM = Limbic, CTRL = Cognitive Control, DEF = Default.

CHAPTER FOUR: HIERARCHICAL GRADIENTS IN PREFRONTAL CORTEX AND HIPPOCAMPUS SUPPORT CONTEXT-DEPENDENT RULE LEARNING

Introduction

Humans continuously adapt their behavior to meet environmental demands. Imagine you are packing a bag for work. If the weather calls for rain, you might choose to pack an umbrella. Working late? Don't forget to pack an extra lunch! The rule for whether an item belongs in your bag will depend on the context of the day (e.g., Will it rain? Will I be working late?). In this study, we propose that interactions between the hippocampus, prefrontal cortex, and the basal ganglia support context-dependent rule learning.

Electrophysiological recordings from the rat hippocampus have demonstrated that hippocampal neurons represent specific item-place coding (Bulkin et al., 2016; Komorowski et al., 2009; Manns & Eichenbaum, 2009). Komorowski and colleagues tested rats on a context-dependent memory task where they had to determine which of two scented clay pots contained a buried reward. In context A, the clay pot with scent X would contain the reward, but in context B, the clay pot with scent Y would contain the reward. This study presented foundational evidence that individual neurons in the hippocampus coded for each stimulus-context pairing, allowing the animal to determine for which contexts a specific stimulus would result in reward (Komorowski et al., 2009). Further work indicated that the neural representations of context-dependent events differed along the dorsal-ventral axis of the hippocampus, with more dorsal regions coding for events occurring in specific locations, and more ventral regions generalizing coding of events

across locations (Komorowski et al., 2013). Recent work using a similar task in humans during fMRI scanning showed that implementation of higher order context-dependent rules is supported by more anterior regions of hippocampus (Brown et al., 2021).

Previous work suggests that communication between prefrontal cortex and the hippocampus facilitates the use of contextual information to guide behavior (for review, see H. Eichenbaum, 2017). Increased resting state functional connectivity between medial temporal regions and prefrontal networks is associated with better performance on a path integration task (Izen et al., 2018). Electrophysiological recordings from non-human primates during rule learning demonstrated that feedback-related signaling in the hippocampus is communicated to prefrontal cortex through frequency-dependent coupling (Brincat & Miller, 2015). Follow-up work showed that as rules were learned, neural representations in prefrontal cortex shifted from external sensory information to internal "top-down" processing, suggesting that rule representations were formed there (Brincat & Miller, 2016). Computational models have posited that context-dependent representations in hippocampus are passed to the prefrontal cortex to guide behavior (Hasselmo & Eichenbaum, 2005), and that sustained rule representations can be learned in prefrontal cortex with just transient encoding from the hippocampus (Liu et al., 2020).

In a spatial navigation task where human subjects had to disambiguate two routes that shared an overlapping hallway, researchers in our lab found that hippocampal and anterior prefrontal activity was greatest when navigating routes with shared hallways compared to routes that did not have shared paths (Brown et al., 2010). Additionally, they found that the hippocampus exhibited increased functional connectivity with orbitofrontal

cortex and the caudate nucleus in overlapping hallways, presumably to incorporate the present context during route planning (Brown et al., 2012). The hippocampus does not have direct anatomical connections to the caudate nucleus, but the two regions can communicate indirectly via orbitofrontal cortex (Barbas & Blatt, 1995; Cavada et al., 2000; Roberts et al., 2007). The hippocampus and striatum play separate but complementary roles in spatial navigation tasks, with the hippocampus implementing allocentric navigation strategies (e.g., go east at the fork), and the striatum being responsible for egocentric navigation strategies (e.g., turn right at the fork) (Packard & McGaugh, 1996). Recordings from non-human primates have demonstrated increases in functional connectivity between hippocampus and the basal ganglia during category learning (Antzoulatos & Miller, 2014). One theoretical framework suggests that the basal ganglia "trains" prefrontal cortex by pushing local areas of cortex into specific attractor states (Djurfeldt et al., 2001). Recent reviews of the literature on hippocampal-striatal interactions suggest that the two memory systems cooperate via prefrontal connections to support generalized learning of both spatial and non-spatial contexts (Freedberg et al., 2020; Goodroe et al., 2018).

Studies have demonstrated that spatial representations are organized along the dorsal-ventral axis of the hippocampus, with more dorsal regions having smaller place-fields and representing local spatial information, and more ventral regions having larger place fields and representing more global spatial information (Kjelstrup et al., 2008; Royer et al., 2010). Further evidence from fMRI studies provides evidence for this gradient along the analogous posterior-anterior hippocampal axis in humans (Brunec et al., 2018; Poppenk

et al., 2013). For a meta-analytical review of the human literature on this topic, see Grady, 2020.

Similarly, the prefrontal cortex also exhibits a hierarchical organization, with caudal regions supporting motor actions, mid-regions incorporating contextual information, and rostral regions drawing on learned schemas (Badre & D'Esposito, 2007; Badre & Nee, 2018; C. Kim et al., 2011; Taren et al., 2011). Similarly, researchers have proposed that the cerebral cortex is organized in a hierarchical topography of temporal receptive windows, with unimodal sensory regions processing more immediate information, and frontoparietal regions accumulating information over longer time scales (Hasson et al., 2015; Lerner et al., 2011). Recent work on spatial navigation in humans has shown that a hierarchical representation of space is also represented in PFC, with more anterior regions representing lengthier trajectories, and posterior regions representing immediate surroundings (Brunec et al., 2018; Brunec & Momennejad, 2021). Additional fMRI evidence suggests that more anterior regions of prefrontal cortex support rule learning at higher levels of abstraction (Badre et al., 2010). Because context-dependent rules require the brain to incorporate higher-order contextual information, we propose that interactions between anterior regions of the hippocampus and anterior regions of prefrontal cortex will support the acquisition and implementation of context-dependent rules.

In a recent rule learning study, our lab found evidence for an anterior-posterior gradient of organization in the medial temporal lobe on a hierarchical rule task. When the subject had to switch into a context at the highest rule-level, anterior regions of hippocampus became most active (Brown et al., 2021). Moreover, anterior regions of

hippocampus exhibited increased functional connectivity with frontal pole during highest order rule switches (Brown et al., 2021). The study posited that functional connectivity between the anterior hippocampus and anterior prefrontal cortex supports the retrieval of contextual cues. These results are supported by additional recent work examining the representation of abstract task structure in hippocampus and orbitofrontal cortex during a memory-guided decision-making task (Mızrak et al., 2021). Despite strong evidence that hippocampal-prefrontal interactions support context-dependent rule implementation, the question remains as to how these hippocampal-prefrontal interactions emerge as rules are learned.

In this study, we examined how functional connectivity with hippocampal regions changes as context-dependent rules are learned. Previously, we had conducted a dynamic network analysis of this dataset (Morin et al., 2021) and identified trends in resting state network connectivity that are altered during learning. For this study, we hypothesized that the context-dependent nature of the rules that were learned (and sometimes not learned) would result in a specific increase in functional connectivity between hippocampal head and anterior prefrontal cortex. Moreover, because the caudate is important for implementing motor actions, and there are indirect connections between hippocampus and caudate via the orbitofrontal cortex, we hypothesized increased functional connectivity with caudate as subjects learned the task. Overall, we found evidence for this connectivity pattern, as well as evidence that the hippocampal head becomes decoupled from the precuneus and mid-cingulate in successful learners. Finally, we found that (1) these functional connectivity changes are specific to hippocampal head (as opposed to

hippocampal body/tail), (2) they are specific to the cue period of the task (the time when context must be encoded/retrieved), and (3) they are related to individual learning rates with the greatest changes occurring in the fastest learners.

Methods

Full details regarding study participants, cognitive task, and MRI data acquisition were first reported by Morin et al., (2021).

Participants

Thirty-two healthy participants with normal or corrected to normal vision and no history or current diagnosis of neurological or psychiatric disorders were recruited from the Boston area for this study. Twenty-nine participants were included in the final analysis (mean age 22.78 years; SD 3.97 years; 14 females, 15 males). Three participants were excluded from the final analysis: one withdrew during scanning, one was excluded for undisclosed prior knowledge of the cognitive task, and one was excluded for excessive head motion (>3mm head displacement during two or more scanning runs). All participants gave written informed consent in accordance with Boston University's Institutional Review Board and were compensated for their time.

Cognitive Task

Before fMRI scanning, participants were not pre-trained or provided with task instructions. During scanning, subjects performed a cognitive task designed to test their ability to learn context-dependent associative rules (**Figure 4.1**). Our lab has previously

used this task for computational modeling, behavioral testing, and fMRI studies of context-dependent rule learning (Morin et al., 2021; Zhu et al., 2020). During the task, a cue image appeared on the screen (2.0s), followed by a delay (2.0s) and then an associate image (2.0s). Subjects were then allowed 2.0s to decide whether or not the cue image was correctly paired with the associate image. Subjects indicated their response (match or mismatch) by pressing the left or right button on a response-box, and were provided with feedback ("Correct," "Incorrect," or "No Response") for 0.5s. Between each trial, a fixation cross was displayed for 4.0s. There were four context-dependent cue-associate pairings that subjects encountered during the scan, and they are described in **Figure 4.1**. Scanning consisted of nine runs, with 32 trials per run.

Behavioral Data Analysis

To assess subject performance, we calculated accuracy during each scanning run and identified when (and if) subjects shifted from "learning" to "learned" phases. With the task set up in a 2-alternative forced choice format, we assumed that subjects who had not yet learned the context-dependent rules would achieve about 50% accuracy (16 correct responses per run) purely by chance. We set the threshold for above-chance performance to 26 correct responses out of 32 trials per scanning run (or 81.25% correct), which, using the binomial distribution, we determined would be the observed level of accuracy per run that would have a 0.1% likelihood of occurring by chance. If a subject achieved an accuracy of greater than or equal to 81.25% on a given run, then that run was classified as "learned." We classified subjects as "successful" learners if they achieved at least one "learned"

scanning run. Individual learning curves, as well as the mean learning curves for successful and unsuccessful learners are plotted in **Figure 4.2**.

MRI Data Acquisition

Scanning was conducted using a 3 Tesla Siemens TIM Trio magnetic resonance scanner and a 32-channel head coil at the Center for Brain Science at Harvard University in Cambridge, Massachusetts. High-resolution T1-weighted multi-planar rapidly acquired gradient echo (MP-RAGE) scans were acquired for each subject (TR = 2530 ms; TE = 1.64 ms; flip angle = 7º; slices = 176; resolution = 1 mm isotropic). T2*-weighted EPI (BOLD) images were acquired using a slice-accelerated EPI sequence that permitted simultaneous multi-slice acquisitions using the blipped-CAIPI technique (TR 2 s; TE 26 ms; flip angle 80º; 6/8 partial-fourier acquisition) (Setsompop et al., 2012). A total of 69 slices were acquired with a slice acceleration factor of 3 and no skip, covering the whole brain. Images were acquired at a nominal 2 mm isotropic spatial resolution (matrix size: 108 x 108).

fMRI Preprocessing

Structural and functional MRI data were preprocessed using a standard pipeline available through fMRIprep (v1.4.1) (Esteban et al., 2019). Preprocessing steps included skull-stripping, co-registration of each subject's functional data with their anatomical scan using boundary-based registration with 12-degrees of freedom, estimation of head-motion parameters, slice-time correction, and spatial normalization of the subject's anatomical and functional data to standard template space (MNI152NLin2009cAsym template from templateflow) (Ciric et al., 2021). Full details of the fMRIprep pipeline are outlined in the

Appendix. Nuisance regression was performed to denoise the data using standard procedures available in the NiBetaSeries BIDS-app (Kent & Herholz, 2019). In the denoising procedure, confound regressors included six head motion parameters and mean signal from CSF and white matter ROIs. The denoised data was high-pass filtered (0.008 Hz) to reduce the effect of signal drift.

Seed Regions and ROI Definition

Regions of interest (ROIs) included the left and right head, body, and tail of the hippocampus, which were anatomically determined and traced using ITK-SNAP (version 3.6.0; www.itksnap.org; Yushkevich et al., 2006) on each subject's T1-weighted anatomical scan according to criteria reported previously by our lab (Brown et al., 2012; Nauer et al., 2015, 2020). The boundary of the hippocampal head and body was marked by the disappearance/emergence of the uncal apex. The boundary of the hippocampal body and tail was delineated by the presence of the wing of the ambient cistern. (Daugherty et al., 2015; Pruessner et al., 2000). A combined bilateral ROI was created for each hippocampal subdivision: head, body, and tail, by adding together the ROIs from the left and right hemisphere.

Beta Series Correlation and Functional Connectivity Analysis

Functional connectivity was calculated using beta series correlation implemented using the least squares separate method in the BIDS-compatible app NiBetaSeries (Kent & Herholz, 2019; Mumford et al., 2012). With least squares separate beta-series correlation, univariate activity measures (betas) are calculated for each individual trial event separately

using a general linear model. For each trial event, a model was created with the following regressors: a regressor for the trial event of interest (e.g. the Cue period for a specific trial), a regressor for all other trial events of the same event type (e.g. all of the other Cue period events), a regressor for each of the other event types (e.g. a regressor for all Delay period events, a regressor for all Associate period events, etc.), and nuisance regressors for white matter, cerebrospinal fluid, and six degrees of head motion. Functional connectivity between two brain regions was calculated as the pairwise correlation of the series of beta estimates across events of the same type. The beta-series correlation method is useful for examining the changes in functional connectivity associated with specific sub-trial events. The least-squares separate method that we employed has been shown to decrease co-linearity between temporally adjacent trial events (Rissman et al., 2004; Turner et al., 2012). Using beta-series correlation, we examined event-related functional connectivity during the five events occurring during each trial: Cue, Delay, Associate, Response, and Feedback.

For each subject and scanning run, we calculated whole-brain seed-to-voxel beta-series correlation maps with seeds located in the hippocampal head, body, and tail (see above for details on hippocampal segmentation). For this analysis, we were interested in studying changes in connectivity associated with learning, so we examined all trials (correct and incorrect) and calculated the beta-series correlation measure separately for each of the nine scanning runs. This resulted in nine correlation maps for each subject, seed, and trial event.

Statistical Analysis of Connectivity Associated with Rule Learning

To test how functional connectivity differed between learning groups and changed throughout learning, we estimated a linear mixed effects model for each of the five trial events (Cue, Delay, Associate, Response, and Feedback). The model included fixed effects for learning group, time (scan run), and the interaction between learning group and time, as well as a random effect of subject. The model allowed the intercept to vary across subjects. Input to the model consisted of seed-to-voxel functional connectivity maps (Fisher-Z transformed Pearson correlation) for each of the three hippocampal seeds (head, body, and tail) and each of the nine scanning runs in individual subjects. We implemented the model using the AFNI command 3dLME (Cox, 1996). This resulted in seed-to-voxel group maps for the effects of learning group, time, and the interaction between learning group and time on the functional connectivity between each voxel and the hippocampal head, body, and tail seeds. Seed-to-voxel maps were FDR corrected for multiple comparisons and cluster corrected (> 25 voxels) (**see Figure 4.4**). In the text and in all tables, results are reported for clusters > 25 voxels. In figures, smaller clusters are also included for visualization purposes. Sub-threshold results are also plotted on the seed-to-voxel connectivity maps, with decreasing as results fall farther below the significance threshold.

Seed-to-Cluster Connectivity Post-hoc Analyses

To further investigate the direction and magnitude of interaction effects on functional connectivity during the Cue period, we conducted a post-hoc analysis on clusters of voxels that showed a significant effect of the interaction between learning group and

time on functional connectivity with the hippocampal head. Using the 3dclust command in AFNI (Cox, 1996), we created binary masks for each significant cluster. After combining clusters that were similar across the two brain hemispheres, we selected four clusters: caudate, lateral frontal pole, mid-cingulate, and precuneus. Using these four clusters, we performed a seed-to-seed functional connectivity analysis to determine the magnitude and direction of functional connectivity changes within each learning group over time. Mean beta-series were extracted from each cluster and the hippocampal head seed. The Fisher-Z transformed Pearson correlation was calculated between the hippocampal head beta series and the beta series from each cluster. The mean Cue-period functional connectivity is plotted in **Figure 4.6** for each learning group. We used the lme4 library in R to re-run the linear mixed effects model on the pairs of mean beta-series, and the *lstrends* command to conduct a post-hoc test examining the rate of change in functional connectivity for each learning group.

Individual Subject Analysis

To determine whether differences in Cue-period functional connectivity were strictly related to successful learning or whether they were related to individual differences in learning speed, we conducted an analysis in 29 individual subjects. First, we qualitatively examined the seed-to-voxel maps for each individual subject. Using group-effect masks, we mapped the Cue-period functional connectivity with hippocampal head for each scanning run. Maps for three representative subjects (an unsuccessful learner, a slow learner, and a fast learner) are displayed in **Figure 4.7** alongside the subjects' learning curves.

Next, we quantified whether individual learning-speed (measured by overall accuracy on the task) was associated with individual differences in Cue-period functional connectivity. Using the same four clusters as the group seed-to-cluster post-hoc connectivity analysis (caudate, lateral frontal pole, mid-cingulate, and precuneus), we fit a linear model to each subject's individual seed-to-cluster connectivity data (see **Figure 4.8a**). Then we plotted the linear model coefficient (the slope of a trendline fit to the functional connectivity data) for each subject vs. their overall accuracy on the task (see **Figure 4.8b**). We hypothesized that subjects who learned the context-dependent rules quickly would exhibit larger changes in Cue-period functional connectivity with the hippocampal head seed.

Results

Behavioral Results

Individual learning curves varied considerably across subjects (see **Figure 4.2**). While some subjects achieved ceiling-levels of accuracy after just two or three scanning runs, others remained at chance-levels throughout the entire scan. Based on their learning curve, each subject was classified as either a successful or unsuccessful learner. Subjects who achieved greater than chance levels of accuracy on at least one scanning run were classified as "successful" learners. Overall, twenty subjects met criteria to be classified as successful learners, and the remaining nine subjects were classified as unsuccessful learners. The variability in subject performance provided us with a natural control group for identifying functional connectivity differences associated with learning. In **Figure 4.2**,

we display each subject's individual learning curve, as well as the mean learning curve for the successful (blue) and unsuccessful (red) learning groups.

Seed-to-Voxel Connectivity Results

To identify changes in functional connectivity with hippocampal seed regions that were associated with learning, we performed a seed-to-voxel functional connectivity analysis using a linear mixed effects model. The model included fixed effects of learning group (successful vs. unsuccessful), time (scanning run), and the interaction of learning group and time. For each of the task periods (Cue, Delay, Associate, Response, and Feedback), we generated a group map where voxel clusters represented brain regions with a significant effect of the interaction between learning group and time on functional connectivity with a hippocampal seed. This means that for significant clusters, functional connectivity was changing over time differently in successful compared to unsuccessful learners.

The most widespread interaction effects were present during the 2.0s Cue period of the task. When considering functional connectivity with the hippocampal head as a seed region, we observed significant effects of the interaction between learning group and time in right superior frontal gyrus (right lateral frontal pole) ($F = 22.9$), left middle frontal gyrus ($F = 14.0$), left mid orbital gyrus (left lateral frontal pole) ($F = 18.4$), right caudate ($F = 13.2$), left caudate ($F = 12.7$), mid-cingulate ($F = 17.1$), and posterior cingulate/precuneus ($F = 12.5$). When considering the hippocampal body as a seed region, fewer regions showed a significant interaction effect. Significant clusters were located in the left inferior frontal gyrus ($F = 17.9$), right superior frontal gyrus ($F = 16.3$), and right anterior cingulate

(F = 18.2), mid-cingulate (F = 18.6), and posterior cingulate (F = 26.7). When considering the hippocampal tail, we found only one cluster with a significant interaction effect in the right middle frontal gyrus (F = 27.1). The full list of brain regions that showed a significant interaction effect with each hippocampal seed during the Cue period are recorded in **Table 4.1**. Seed-to-voxel maps for the Cue period are highlighted in **Figure 4.4**. Together, these results show that during the Cue period, the strongest learning-related changes in functional connectivity occurred in the hippocampal head, followed by slight changes in the body, and very limited changes in the tail.

During the 2.0s Delay period which immediately followed the Cue period, small clusters in the right posterior insula (F = 37.7) and left mid cingulate cortex (F = 24.0) showed a significant effect of the interaction between learning group and time on their functional connectivity with hippocampal head. There were no clusters showing a significant interaction effect with functional connectivity to hippocampal body or tail.

During the Associate period, clusters in the right precuneus (F = 32.4), left inferior frontal gyrus (F = 30.7), left inferior parietal lobule (F = 18.2), right inferior parietal lobule (F = 19.8), mid cingulate cortex (F = 20.5), right posterior insula (F = 29.9), and left insula (F = 22.2) showed a significant effect of the interaction between learning group and time on their functional connectivity with hippocampal head. There were no clusters showing a significant interaction effect with functional connectivity to hippocampal body or tail.

During the Response period of the task, small clusters in the inferior frontal gyrus (F = 23.2), left inferior frontal gyrus (F = 16.9), and right supramarginal gyrus (F = 21.6) showed a significant effect of the interaction between learning group and time on their

functional connectivity with hippocampal head. There were no clusters showing a significant interaction effect with functional connectivity to hippocampal body or tail.

During the Feedback period of the task, there were no clusters that showed a significant interaction effect with hippocampal head, body, or tail seeds.

Seed-to-voxel functional connectivity results for the hippocampal head seed are plotted for all task periods in **Figure 4.5**. For the hippocampal body and tail, we only show results from the Cue period (see **Figure 4.4**) because there were no clusters showing a significant interaction effect for the hippocampal body or tail during the other task periods.

Within each region that showed a significant interaction effect, functional connectivity could change in several ways. For example, functional connectivity between hippocampal head and another region could increase over time in successful learners but not in unsuccessful learners. Similarly, another region might show functional connectivity that decreases over time in successful learners. To visualize this, we constructed group difference maps where colored voxels show the mean difference in functional connectivity between successful and unsuccessful learners. These maps are statistically thresholded to only include voxels that showed a significant interaction effect between learning group and time (see **Figures 4.4** and **4.8**). The visualizations show that during the Cue period, functional connectivity between the hippocampal head and caudate is greater in successful learners compared to unsuccessful learners, and that this group difference increases over time as the successful learners achieve greater and greater accuracy. Similarly, successful learners exhibit greater functional connectivity between hippocampal head and lateral frontal pole compared to unsuccessful learners, and this group difference also increases

over time. Conversely, successful learners showed decreased functional connectivity between hippocampal head and precuneus compared to unsuccessful learners. Functional connectivity with hippocampal body exhibited similar group-level trends, but across smaller (and more caudal) clusters of prefrontal cortex. There were no significant voxel clusters for the hippocampal tail seed (see **Figure 4.4**).

Seed-to-Cluster Connectivity Post-Hoc Results

To visualize how Cue-period functional connectivity between the hippocampal head and significant clusters changed during learning, we plotted changes in functional connectivity for several clusters that showed a significant interaction effect in the linear mixed effects model. Four clusters were selected based on their size, symmetry across the left and right hemispheres, and *a priori* interest based on previous findings (Brown et al., 2010, 2012, 2021). The four clusters we examined were located in: caudate, lateral frontal pole, mid-cingulate, and precuneus. Results are plotted in **Figure 4.6**. Post-hoc analysis using the *lstrends* function in R demonstrated the following: Functional connectivity between the caudate and hippocampal head significantly decreased over time in unsuccessful learners (slope = -0.043; $T = -4.47$, $p < 0.01$) and significantly increased over time in successful learners (slope = 0.034; $T = 5.34$, $p < 0.01$). In the lateral frontal pole cluster, functional connectivity with hippocampal head significantly decreased over time in unsuccessful learners (slope = -0.048, $T = -5.51$, $p < 0.01$), and significantly increased over time in successful learners (slope = 0.013; $T = 2.18$, $p < 0.05$). In the precuneus cluster, functional connectivity with hippocampal head did not significantly change in unsuccessful learners (slope = 0.015; $T = 1.71$, $p = 0.089$), but significantly decreased in successful

learners (slope = -0.034; T = -5.67, $p < 0.01$). In the mid-cingulate cortex cluster, functional connectivity significantly increased in unsuccessful learners (slope = 0.029; T = 2.96, $p < 0.01$) and significantly decreased over time in successful learners (slope = -0.046, T = -7.02, $p < 0.01$). P-values for this post-hoc analysis were FDR-corrected for multiple comparisons.

Overall, this post hoc analysis demonstrated that the hippocampal head decreased its Cue-period functional connectivity with mid-cingulate and precuneus as subjects learned. Simultaneously the hippocampal head increased its Cue-period functional connectivity with the caudate and lateral frontal pole as learning occurred.

Single Subject Results

In addition to examining group-level differences in functional connectivity between successful and unsuccessful learners, we investigated the degree to which individual learning rates corresponded to changes in functional connectivity. We measured the individual functional changes in Cue period functional connectivity with the hippocampal head in individual subjects. **Figure 4.7** shows three example subjects: an unsuccessful learner, a "slow" learner (who did not show evidence of successful learning until run 6), and a "fast" learner (who reached ceiling levels of accuracy after just 2 scanning runs). For these three subjects, hippocampal head seed-to-voxel maps are presented. While the maps are noisier on the individual subject level compared to the group maps presented previously, several trends are visible. In the fast learner, functional connectivity with the caudate and lateral frontal pole increased quickly, while functional connectivity with the

precuneus and mid-cingulate cortex decreased quickly. In the unsuccessful learner there were inconsistent changes that do not appear to follow any sort of trend.

To further visualize the relationship between individual learning rates and functional connectivity patterns, we used a linear regression to fit trendlines to each subject's seed-to-cluster functional connectivity during the Cue period. Again, we examined Cue period functional connectivity between the hippocampal head and four clusters that exhibited a significant effect of the interaction between learning group and time according to the linear mixed effects model (caudate, lateral frontal pole, mid-cingulate, and precuneus). Trendlines are plotted for each subject in **Figure 4.8a**. If the fastest learners have the greatest changes in functional connectivity, then we would expect the slopes of these trendlines to be highest in subjects that achieved the highest accuracy. To test this, we calculated the correlation between functional connectivity trendline-slope and overall task accuracy for each of the four post-hoc ROIs (caudate, lateral frontal pole, mid-cingulate, and precuneus) (see **Figure 4.8b**).

We identified a positive correlation between overall task accuracy and the increase in functional connectivity between hippocampal head and both the caudate ($r = 0.55$) and lateral frontal pole ($r = 0.53$) clusters. Additionally, we identified a negative correlation between overall task accuracy and the change in functional connectivity between hippocampal head and both the precuneus ($r = -0.56$) and mid-cingulate cortex ($r = -0.58$) clusters. Because the four regions were selected from clusters showing a significant interaction effect between learning group and time, this follow-up analysis confirmed that

the linear mixed effects model identified regions where the changes in functional connectivity over time differed between successful and unsuccessful learners.

Together, our examination of individual subject functional connectivity trends indicated that the fastest learners showed the greatest increase in functional connectivity between the hippocampal head and both the caudate and lateral frontal pole. Similarly, the fastest learners showed the greatest decrease in functional connectivity between the hippocampal head and both the precuneus and mid-cingulate cortex.

Discussion

This study was designed to characterize the role of hippocampal-prefrontal functional connectivity during context-dependent rule learning. Our analysis identified several changes in functional connectivity with the hippocampus associated with successful learning, including increased functional connectivity with the lateral frontal pole and the caudate nucleus, and decreased functional connectivity with the precuneus and mid-cingulate. The greatest changes in functional connectivity occurred with the hippocampal head, followed by modest changes with the hippocampal body, and few changes with the hippocampal tail. This finding provides additional evidence that the hippocampus is organized along an anterior-posterior axis, with anterior regions representing higher order concepts such as the context-dependent rules on our task. Post-hoc analyses demonstrated that functional connectivity changes were greatest in the fastest learners. Overall, our study identifies a signature functional connectivity pattern between the hippocampus, caudate, and prefrontal cortex that emerges during learning.

Hippocampal and Prefrontal Hierarchies Support Context-Dependent Rule Learning

The prefrontal cortex is organized hierarchically with caudal regions supporting immediate motor actions and rostral regions involved in planning complex behaviors (Badre & D'Esposito, 2007; Badre & Nee, 2018). Similarly, the hippocampus exhibits an organization along the anterior-posterior axis when considering both spatial representations (Brunec et al., 2018; Brunec & Momennejad, 2021; Evensmoen et al., 2013; Izen et al., 2018; Kjelstrup et al., 2008), and conceptual behavior (Brown et al., 2021; Plachti et al., 2019; Theves et al., 2020). We demonstrated that context-dependent rule learning is associated with changes to the functional connectivity of hippocampal head more so than the hippocampal body or tail. This finding supports the framework that higher-order contexts are represented in more anterior regions of the hippocampus. Our findings are supported by previous work in our lab demonstrating that functional connectivity with the anterior hippocampus increased for the frontal pole and the caudate nucleus during the implementation of higher order rules (Brown et al., 2021). Notably, Brown et al. were unable to include the hippocampal head in their analyses due to signal dropout, and used a hippocampal body ROI to examine the anterior hippocampus (2021). Our findings extend this previous work by including results from the hippocampal head in addition to characterizing the emergence of the hippocampal-prefrontal functional connectivity during learning.

Anatomical Connections in Support of Observed Functional Connectivity

Functional connectivity measures (including the beta-series correlation method we used in this study) measure the correlation of BOLD signal across brain regions, and are

thought to represent communication or exchange of information between brain regions. However, functional connectivity measures are not necessarily indicative of direct anatomical connections between two brain regions. While we found evidence for increased functional connectivity between the hippocampus and caudate in successful learners, there is no direct anatomical connection between these two regions. There are, however, indirect connections via the orbitofrontal cortex, which receives input from the hippocampus and sends output to the caudate (Barbas & Blatt, 1995; Cavada et al., 2000; Roberts et al., 2007). Additionally, prefrontal cortex connects bidirectionally to the caudate through cortico-striatal loops ranging from associative loops in more anterior regions to motor loops in more posterior regions (Alexander et al., 1986; Haber, 2003; Parent & Hazrati, 1995). Through these connections, hippocampal representations of context-dependent rules can be passed to prefrontal cortex to guide behavior.

Considering our findings in posterior precuneus and mid-cingulate cortex, diffusion imaging studies in humans have shown that the precuneus is directly connected to the medial temporal lobe via the inferior longitudinal fascicle and that the mid-cingulate is indirectly connected through the cingulum bundle which projects to the precuneus (Horn et al., 2014). Tracer studies in rodents and non-human primates have identified that the retrosplenial cortex (a region commonly co-located with the ventral precuneus) receives and sends projections to the hippocampus (Kobayashi & Amaral, 2003, 2007). Functionally, the mid-cingulate and precuneus form posterior nodes of the default network, a group of cortical brain regions that are intrinsically connected at rest and exhibit decreased activity during tasks that require outwardly directed attention (Raichle, 2015).

While the hippocampus is typically functionally connected to the default network at rest (Laird et al., 2009; Raichle, 2015; Raichle et al., 2001; Utevsky et al., 2014), decoupling from the default network allows it to join "task-positive" regions engaged in rule learning. Additionally, the observed decoupling may reflect successful learners focusing on relevant task cues, while unsuccessful learners direct their attention inward for evaluating internal hypotheses and task strategies.

Functional Connectivity Changes Were Greatest When Retrieving Context

In our task, the Cue period was the task event that evoked the most widespread changes in learning-related functional connectivity. Once the context-dependent rules were learned, the Cue period became a critical time when context could be retrieved from memory. The stimulus context was dictated by the location where a cue stimulus was presented on the screen (Quadrants I/III, or II/IV) (see **Figure 4.1**). Once the learned context was retrieved, the subject could anticipate which associate-item would result in a match vs. a mismatch. When a subject learned the context-dependent rules, all possible trial outcomes could be anticipated quickly during the Cue period, with only a minor check necessary during the Associate period before making a correct response.

Learning-related changes in functional connectivity with the hippocampal head were primarily observed during the Cue period, with very few changes occurring during the Delay, Associate, Response, and Feedback periods. (see Results, and **Figure 4.5**). Because the strong hippocampal-prefrontal and hippocampal-caudate effects we saw in the Cue period were not present during other task periods, we have increased confidence that these functional connectivity results are related to the retrieval of context representations.

During the Feedback period of the task, we did not observe any significant learning-related changes in functional connectivity. We might have expected Feedback period functional connectivity between the hippocampus and reward-regions like medial prefrontal cortex and orbitofrontal cortex (regions known to respond strongly to predicted rewards) to change throughout learning as the context-dependent rule structure was learned (Carlson et al., 2011; Kahnt, 2018; Knutson & Cooper, 2005). However, the Feedback period on our task was quite short (only 0.5s) compared to the other task periods (2.0s each). As has been documented previously, our ability to detect context-related changes in functional connectivity with beta series may have been limited by the short duration of the Feedback period (Cisler et al., 2014).

The current task design leaves us with some uncertainty about whether the functional connectivity changes we identified are associated with learning in general, or whether they are specifically associated with learning context-dependent rules. With the current task design, we were unable to make a direct comparison in the brain representations of context-dependent and context-independent rules. In support of our interpretation, previous work has compared functional connectivity during context-dependent cognition with context-independent controls (Brown et al., 2010, 2012, 2021). Moreover, the fact that our results were strongest during the Cue period does suggest that the information being manipulated during the Cue period (which we believe is the stimulus-context pairing) is being transferred between hippocampus and caudate. An additional concern is whether the functional connectivity changes we observed were strictly associated with learning, or whether they were associated with reduced mental effort as the

task became more automatic for successful learners. With additional participants, it would be possible to compare fast learners to slow learners. We would expect fast learners to show learning-related changes in functional connectivity early, followed by later changes associated with automaticity and reduced mental effort as they became true task-experts. These results could be compared to slow learners, who would presumably show more gradual learning-related changes in functional connectivity.

Hippocampal Segmentation

Evidence from studies of anatomical connectivity, functional connectivity, gene expression, and electrophysiological recordings provide conflicting yet complementary evidence about how we can best divide the hippocampus along its long axis (Grady, 2020; Poppenk et al., 2013; Strange et al., 2014). We chose to segment the hippocampus into head, body, and tail ROIs using anatomical landmarks to match previous literature (Brown et al., 2010, 2012, 2021; Nauer et al., 2015, 2020; Pruessner et al., 2000). While previous studies have reported increased noise in the hippocampal head (e.g., Brown et al., 2021), we found robust, statistically significant results in functional connectivity with the hippocampal head. This is perhaps because our functional data were acquired with different scanning parameters compared to previous studies. Notably, our study was acquired at a slightly higher spatial resolution, resulting in more voxels per hippocampal ROI compared to previous studies (2x2x2mm^3 voxel size in our study compared to 3x3x4mm^3 in Brown et al., 2021).

Functional Connectivity Between Hippocampus, Basal Ganglia, and Prefrontal Cortex Supports Context-Dependent Cognition

Recent reviews of the literature suggest that hippocampal and striatal memory systems cooperate via prefrontal connections to retrieve and utilize contextual information during rule-guided behavior (Freedberg et al., 2020; Goodroe et al., 2018). Computational models suggest context-dependent rule representations could be passed from the hippocampus to prefrontal cortex (Hasselmo & Eichenbaum, 2005; Liu et al., 2020), and the caudate can select rule representations to guide behavior (Djurfeldt et al., 2001). An fMRI study of motor sequence learning conducted in our lab suggested that the hippocampus may quickly learn stimulus associations that are later utilized by fronto-striatal circuits (Schendan et al., 2003). Results from our study demonstrated that as context-dependent rules are successfully learned, functional connectivity of the hippocampal head increases with the lateral frontal pole and the caudate nucleus. These results are supported by previous work showing increased functional connectivity in these regions during the implementation of higher order rules (Brown et al., 2021), the disambiguation of overlapping spatial routes (Brown et al., 2012), and the disambiguation of overlapping sequences of visual stimuli (Ross et al., 2011). Together with prior literature, our results suggest that the hippocampus may be representing context-dependent rules, providing fronto-striatal circuits with a set of criteria for implementing rule-guided behavior.

Conclusion

This study demonstrates that increased functional connectivity between hippocampal head and the lateral frontal pole/caudate supports the retrieval of successfully learned contexts when implementing context-dependent rules. We show that this connectivity pattern emerges in successful learners as they learn, but not in a natural control group of unsuccessful learners. We suggest that the hippocampal head is uniquely positioned to represent higher-order rules and contexts through a gradient organization that mirrors the hierarchical organization of the prefrontal cortex.

Tables

Seed	No. Voxels	Max X (mm)	Max Y (mm)	Max Z (mm)	F-Stat	Region
Hippocampal Head	1260	-36	-16	-26	27.3	L Fusiform Gyrus
	674	40	0	-16	51.6	R Post. Insula
	587	0	-14	32	17.1	Middle Cingulate
	519	16	54	10	22.9	R Sup Frontal/Mid Orbital Gyri (Frontal Pole)
	261	0	-40	22	12.5	Posterior Cingulate/Precuneus
	212	62	-52	12	17.5	R Middle Temporal Gyrus
	208	18	26	12	13.2	R Caudate
	187	-12	-20	78	15.3	L Precentral Gyrus
	96	26	-42	-8	12.3	R Lingual Gyrus
	88	-14	-20	-32	22.0	Brain Stem
	88	44	6	-30	14.3	R Middle Temporal Gyrus
	78	-36	54	-8	18.4	L Mid Orbital Gyrus (Frontal Pole)
	74	-40	-52	-12	23.9	L Fusiform/Inf. Temp. Gyrus
	70	8	-16	-28	14.6	Brain Stem
	67	-22	30	2	12.7	L Caudate/Insula
	61	-4	-20	0	17.9	L Thalamus
	55	-14	18	18	18.1	L Cerebral WM/Caudate
	48	-4	54	-40	12.8	R Cerebellum
	42	36	-62	6	14.0	L Middle Frontal Gyrus
	41	22	90	-22	11.1	L Cerebellum
	40	-4	4	10	17.7	R Thalamus
	27	-26	24	2	13.4	R Thalamus
	26	4	-18	-20	16.1	L Gyrus Rectus
Hippocampal Body	233	-2	-48	22	26.7	Posterior Cingulate
	145	-64	-18	-14	25.7	L Middle Temporal Gyrus
	136	34	8	-24	30.2	R Temporal Pole
	130	-54	-6	-32	21.0	L Inferior Temporal Gyrus
	115	40	-40	-22	13.3	R Fusiform Gyrus
	99	40	-8	-34	25.4	R Fusiform Gyrus
	75	8	-12	36	18.6	Middle Cingulate
	57	-26	-2	28	26.6	L Cerebral White Matter
	52	-50	14	4	17.9	L Inferior Frontal Gyrus
	47	30	-20	-2	17.2	R Putamen/Insula
	45	-44	-58	18	17.7	L Middle Temporal Gyrus
	38	24	64	6	16.3	R Superior Frontal Gyrus
	29	18	46	16	18.2	R Anterior Cingulate
	27	-6	-30	38	16.5	Middle Cingulate
Hippocampal Tail	35	42	30	38	27.1	R Middle Frontal Gyrus

Table 4.1 Clusters of Significant Learning-Group-by-Time Interaction Effect on Cue Period Hippocampal Functional Connectivity

This table presents the coordinates of peak F-statistics for clusters showing a significant interaction effect between learning group and time on functional connectivity with the hippocampus during the Cue Period of the task. We analyzed functional connectivity with three hippocampal seeds: head, body, and tail (see **Figure 4.3**). Clusters exhibited a significant interaction effect if changes in functional connectivity over time differed between successful and unsuccessful learners according to a linear mixed effects model. Coordinates are in MNI space (LPI orientation). Coordinates of peak F-statistics were used to determine region names, as defined by the Eickoff-Zilles Macrolabel atlas available in AFNI. F-statistics are presented for the peak voxel of each cluster that showed a significant interaction effect. Voxelwise FDR correction was performed on the brain maps. Cluster size > 25 voxels are shown in this table. Corresponding brain maps are displayed in **Figure 4.4**.

Figures

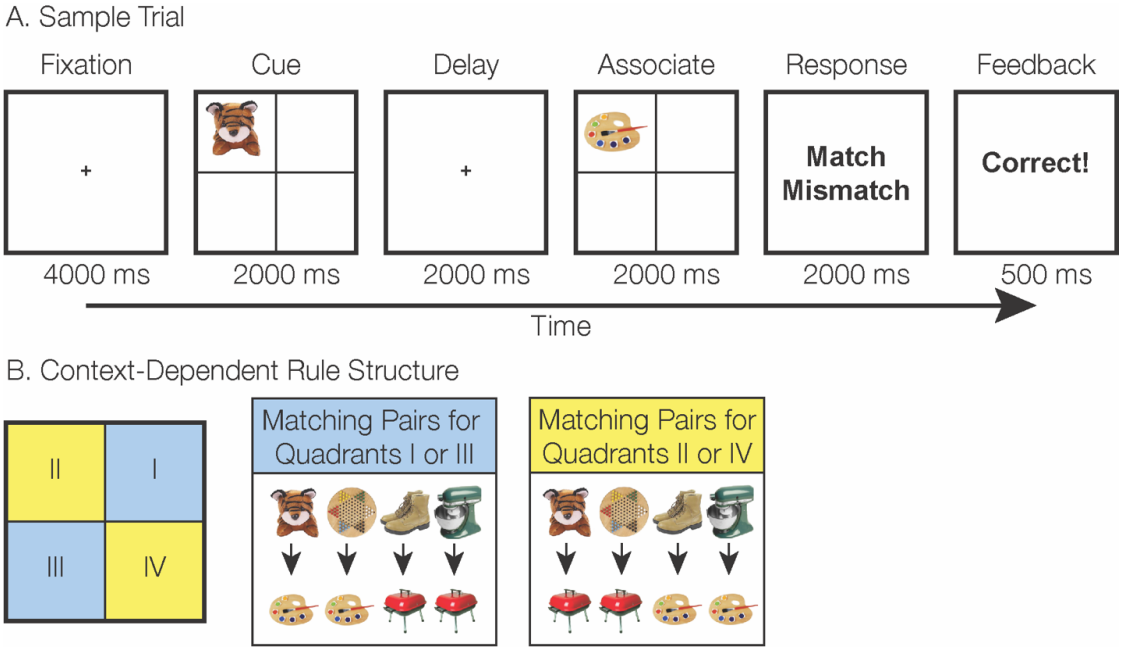

Figure 4.1 Context-Dependent Rule Learning Task

(A) During each trial, the subject saw a fixation (4000ms), followed by a cue stimulus (2000ms), delay (2000ms), and an associate stimulus (2000ms). Then, the subject was given 2000ms to decide whether or not the cue image was correctly paired with the associate image. Subjects indicated their response by pressing the left or right button on a response box. The trial ended with 500ms of feedback ("Correct," "Incorrect," or "No Response"). **(B)** Subjects were naïve to the fact that a context-dependent rule structure dictated whether cue and associate stimuli were correctly paired. If the cue and associate appeared in Quadrant I or III (highlighted here in blue for emphasis), they obeyed one set of rules (e.g., the tiger and paint-palette are a pair). If instead the cue and associate appeared in Quadrant II or IV (yellow), they obeyed an alternate set of rules (e.g., the tiger and grill are now a match). Subjects were tasked with learning these context-dependent pairings over the course of nine scanning runs. Each scanning run consisted of 32 trials of the task.

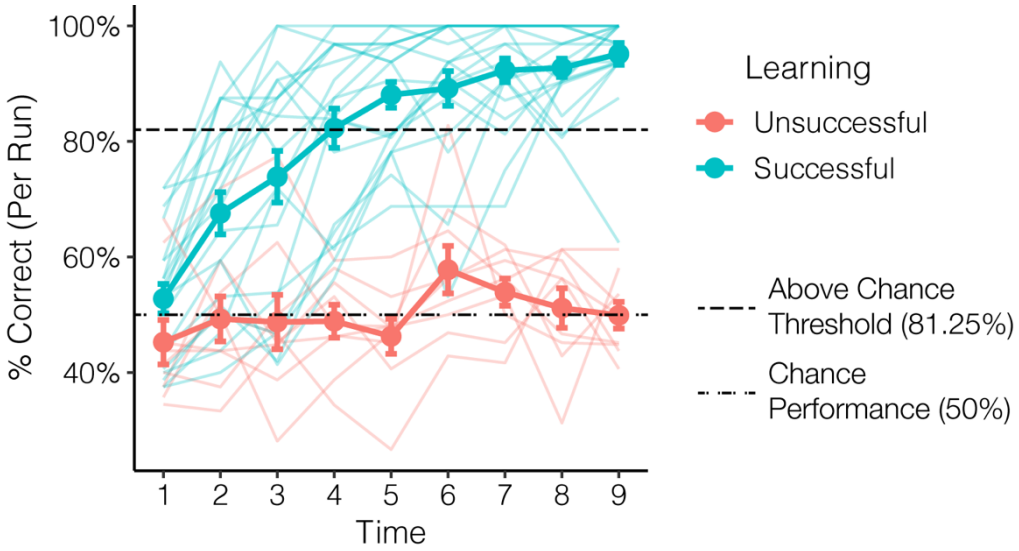

Figure 4.2 Behavioral Results

Subject accuracy plotted over time. Time points represent each of the 9 scanning runs (32 trials per run). Thin lines represent learning curves for individual subjects. Thick lines represent group averages for successful learners in blue (n=20) and unsuccessful learners in red (n=9). Error bars represent standard error.

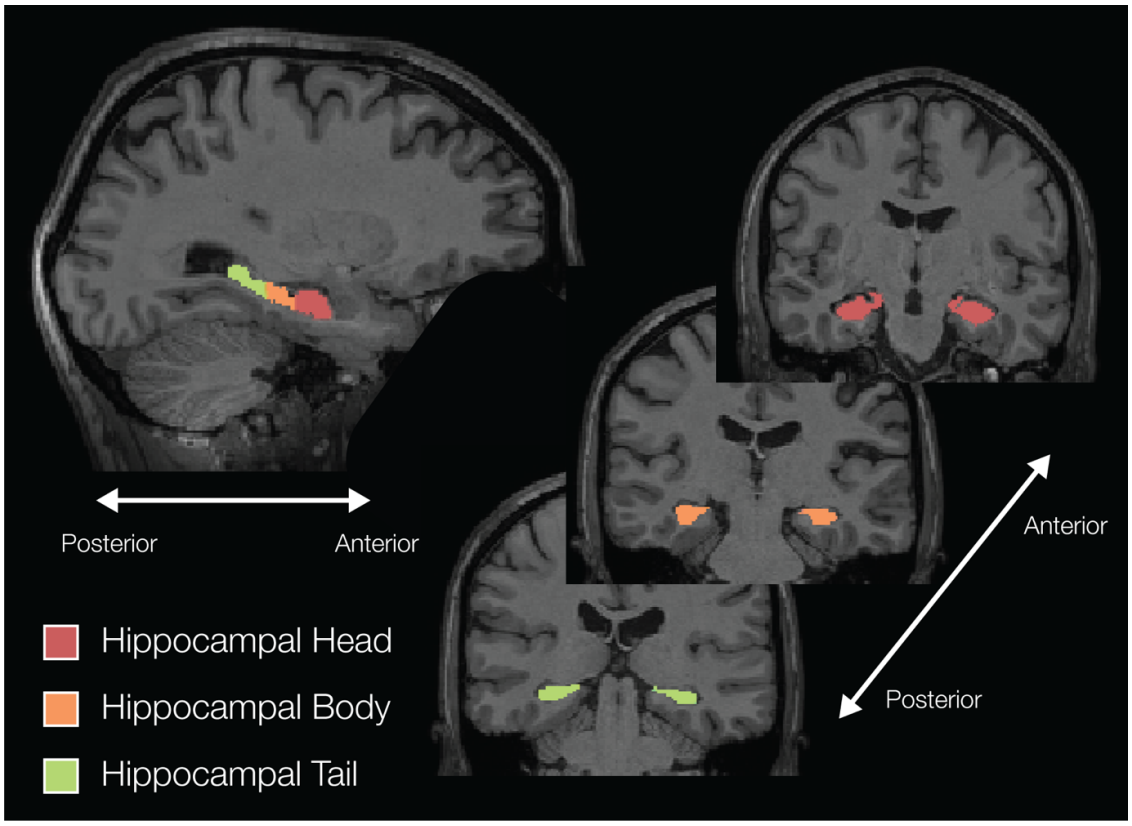

Figure 4.3 Hippocampal Regions of Interest

Hippocampal segmentation for a single subject is shown. The hippocampus was hand-traced from each subject's T1-w anatomical scan following established protocols. Two subregions were identified for each subject: hippocampal head (red), hippocampal body (orange), and hippocampal tail (green). ROIs were traced individually in each hemisphere and then combined to form bilateral regions.

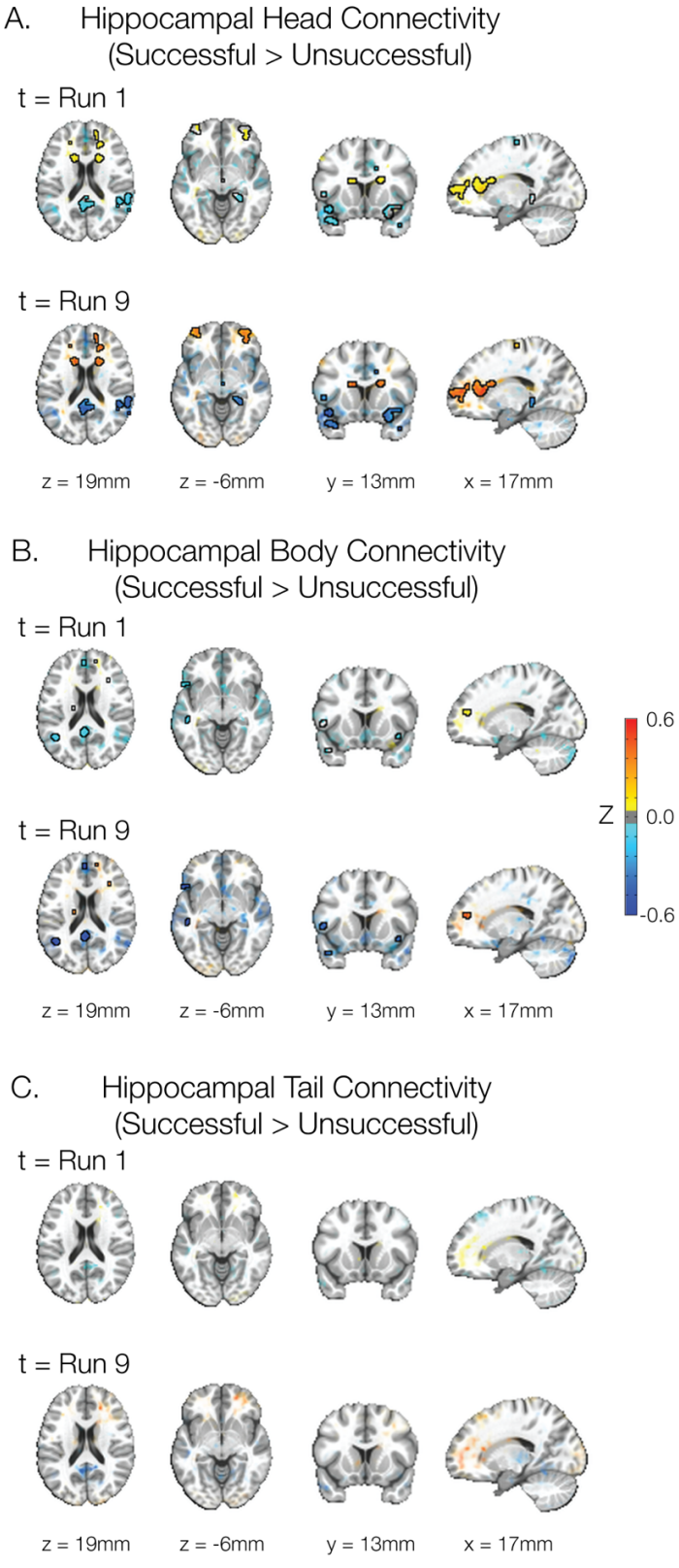
A. Hippocampal Head Connectivity
(Successful > Unsuccessful)
t = Run 1
t = Run 9
z = 19mm
z = -6mm
y = 13mm
x = 17mm
B. Hippocampal Body Connectivity
(Successful > Unsuccessful)
t = Run 1
t = Run 9
z = 19mm
z = -6mm
y = 13mm
x = 17mm
Z
0.6
0.0
-0.6
C. Hippocampal Tail Connectivity
(Successful > Unsuccessful)
t = Run 1
t = Run 9
z = 19mm
z = -6mm
y = 13mm
x = 17mm

Figure 4.4 Cue-Period Learning-Related Hippocampal Functional Connectivity

Results from a linear mixed effects model of seed-to-voxel functional connectivity during the Cue period are plotted here. Clusters outlined in black showed a significant effect of the interaction between learning group and time on seed-based functional connectivity. Color represents the difference in functional connectivity (Fisher's Z transformed Pearson correlation) between successful and unsuccessful learners during the first scan run (top row) and the last scan run (bottom row). Voxel opacity is solid for voxels that surpassed the threshold ($p < 0.05$, FDR corrected). Opacity decreases as voxels fell farther and farther below the significance threshold. Results are plotted for the hippocampal head (A), hippocampal body (B), and hippocampal tail (C) seeds.

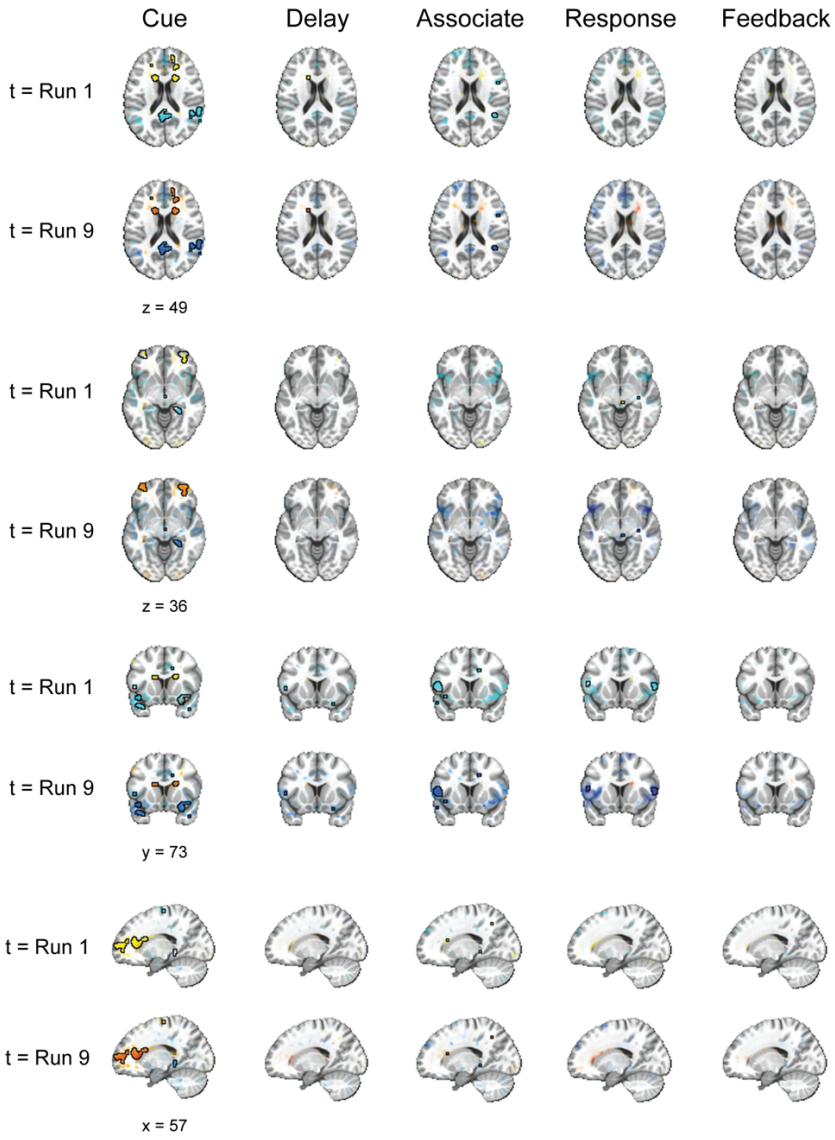

Figure 4.5 Learning-Related Functional Connectivity with Hippocampal Head

Results from a linear mixed effects model of seed-to-voxel functional connectivity during each task period are plotted here. Clusters outlined in black showed a significant effect of the interaction between learning group and time on seed-based functional connectivity. Color represents the difference in functional connectivity (Fisher's Z transformed Pearson correlation) between successful and unsuccessful learners during the first scan run (t = Run 1) and the last scan run (t = Run 9). Voxel opacity is solid for voxels that surpassed the threshold ($p < 0.05$, FDR corrected). Opacity decreases as voxels fell farther below the significance threshold. Results are plotted for the hippocampal head seed.

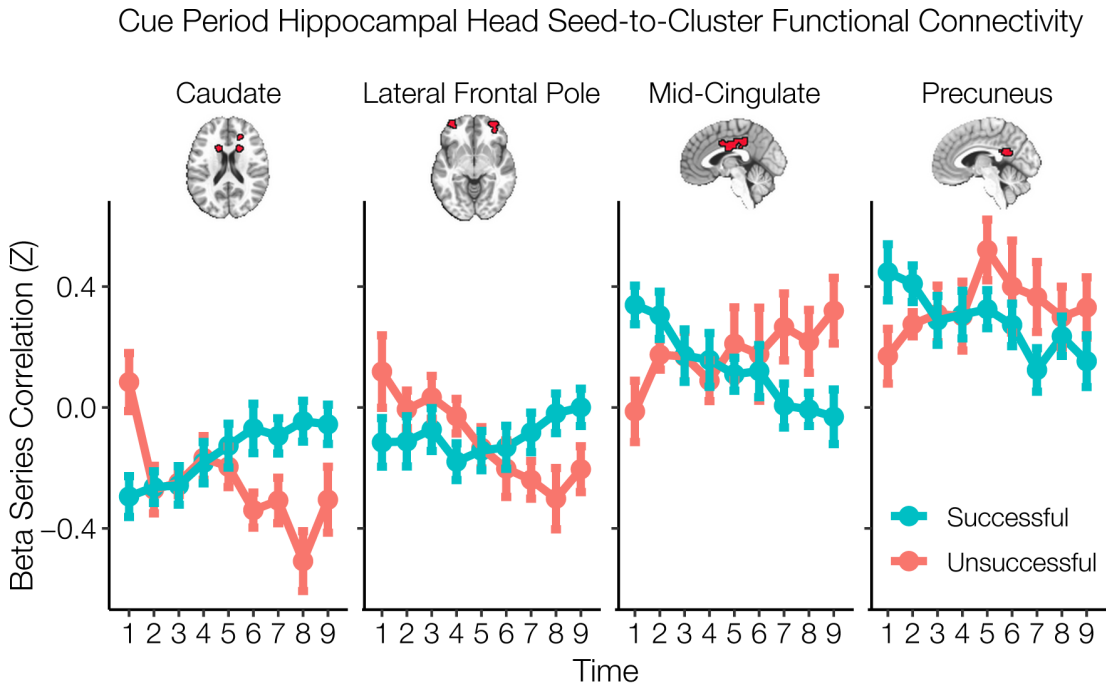

Figure 4.6 Cue-Period Post-hoc Analysis: Hippocampal Head Seed-to-Cluster Functional Connectivity

Functional connectivity (Fisher's Z-transformed Pearson correlation) with the hippocampal head is plotted for four cluster ROIs (caudate, lateral frontal pole, mid-cingulate, and precuneus; mapped on the brain in red) that showed a significant effect of the interaction between learning and time on functional connectivity during the Cue period of the task. Cluster ROIs were chosen from the results of a seed-to-voxel linear mixed effects model (see **Figure 4.4**) to visualize how changes in functional connectivity with the hippocampal head differed between learning groups. Lines represent mean connectivity within each learning group (successful = blue; unsuccessful = red). Time points represent the nine scanning runs. Error bars represent standard error.

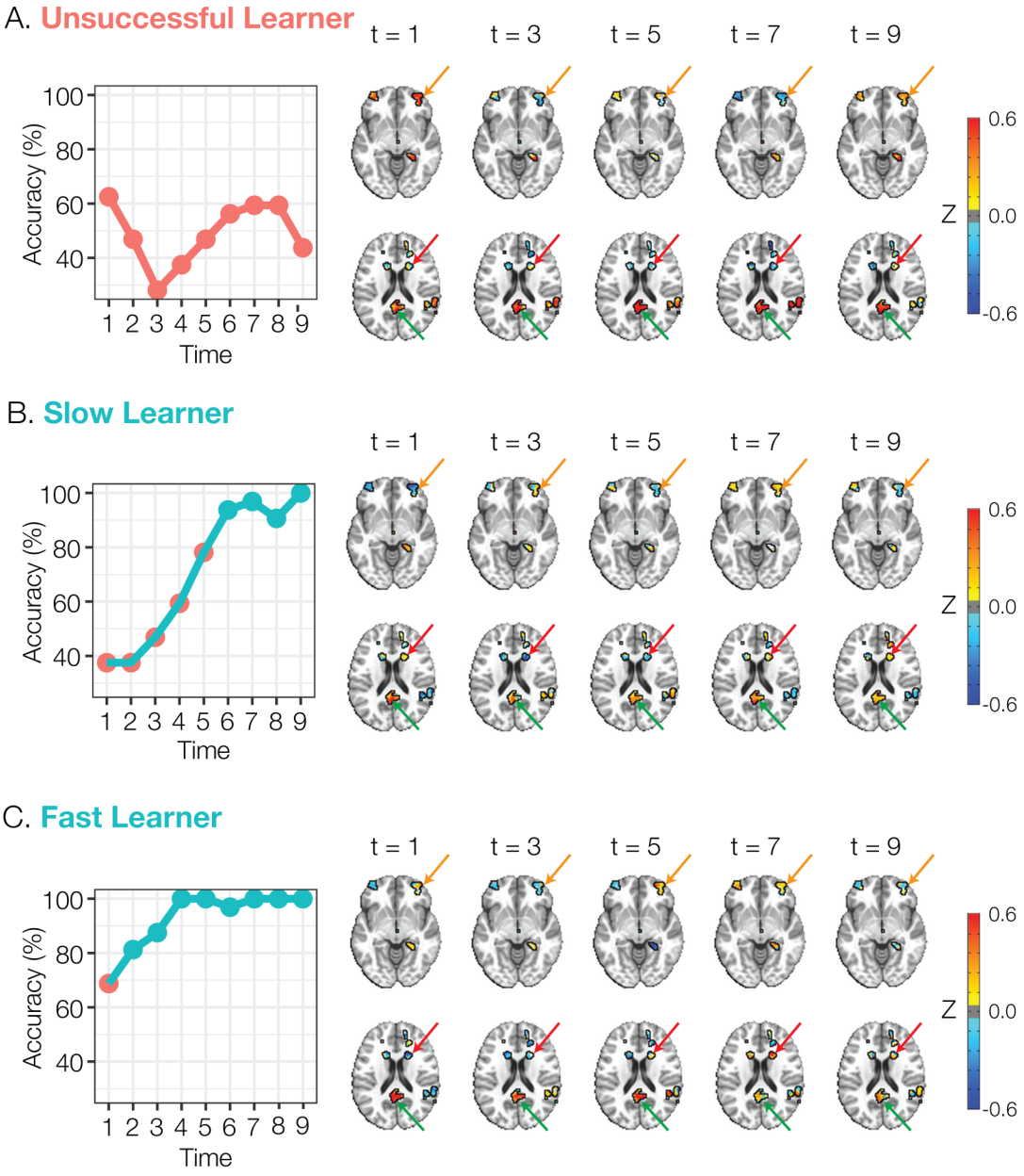

Figure 4.7 Cue-Period Functional Connectivity with Hippocampal Head in Individual Subjects

Functional connectivity patterns are plotted for three representative subjects: an unsuccessful learner (A), a slow learner (B), and a fast learner (C). Left: learning curves are plotted. Red points denote the accuracy on unlearned runs and blue points denote the accuracy on learned runs. Line color is red for the unsuccessful subject (A) and blue for successful subjects (B and C). Right: hippocampal head seed-to-voxel functional connectivity (Fisher's Z-transformed Pearson correlation) maps are plotted. Maps are

presented for five time points (Scanning runs 1, 3, 5, 7, and 9). Maps are thresholded for clusters that showed significant effect of an interaction between learning group and time according to a linear mixed effects model on the group data (FDR corrected; cluster size > 25 voxels). Orange arrows point to the right lateral frontal pole and red arrows point to the right caudate nucleus – two regions where functional connectivity generally increased over time in the successful learners, but not in unsuccessful learners. Green arrows point to the mid cingulate, a region where functional connectivity generally decreased over time in successful learners, but not in unsuccessful learners.

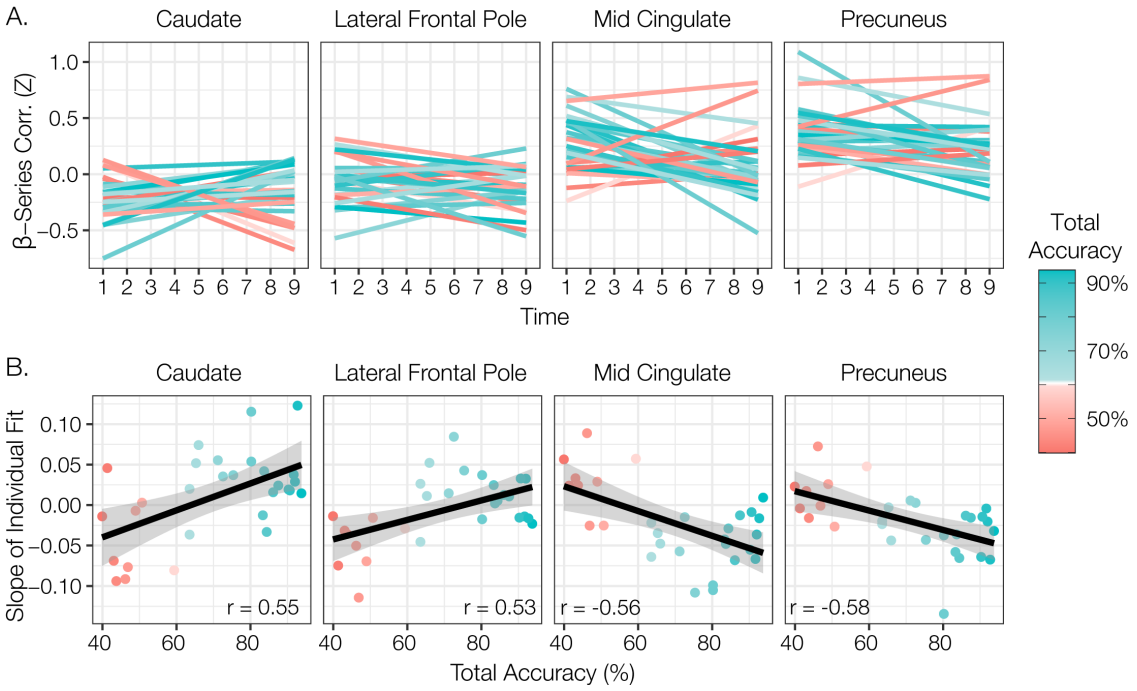

Figure 4.8 Individual Trends in Cue-Period Functional Connectivity Correlate with Overall Accuracy

(A) For each subject, a linear model was fit to the cue-period functional connectivity between the hippocampal head and four ROIs. Trendlines for each subject's linear model fit are plotted. Color represents overall accuracy on the task with successful learners plotted on a blue gradient and unsuccessful learners plotted on a red gradient. (B) The slope of each subject's trendline is plotted against their overall accuracy. The correlation between slopes and overall accuracy is plotted in black. ROIs were chosen from *a priori* hypotheses and comprised clusters that showed a significant effect of the interaction between learning group and time on functional connectivity.

CHAPTER FIVE: SUMMARY AND DISCUSSION

Restatement of Original Goals

The primary objective of this dissertation was to characterize the dynamic brain network states that support abstract reasoning and context-dependent rule learning. Through three experiments presented across Chapters Two, Three, and Four, I investigated how differences in functional brain network stability and flexibility support both abstract reasoning and context-dependent rule learning. The first study, presented in Chapter Two, investigated regionally specific brain network stability to determine which regions of cortex remained stable or flexibly reconfigured to support abstract reasoning. Chapter Three investigated how the stability and flexibility of cortical functional networks supported individual differences in context-dependent rule learning. Chapter Four examined whether increased functional connectivity between the hippocampus and anterior prefrontal cortex supported context-dependent rule learning, focusing also on individual differences in learning rates.

Summary of Findings

The first experiment, described in Chapter Two, sought to determine whether functional connectivity flexibly shifted or remained stable in response to shifting task demands during abstract reasoning. A simplified version of the Raven's Progressive Matrices task (Raven, 1941) was used to measure brain activity and functional connectivity during two types of reasoning: symbolic and perceptual. Twenty-seven subjects performed at ceiling levels of accuracy on the task, and response times were similar across all

conditions. A univariate analysis demonstrated consistent activation of the frontoparietal control network during both types of reasoning, with increased activation in prefrontal cortex during symbolic reasoning, and increased activation in inferior temporal cortex during perceptual reasoning (see **Figure 2.3**). Despite these significant differences in activation patterns between perceptual and symbolic reasoning, a dynamic network analysis demonstrated that a stable community architecture was consistent across all task conditions. Additionally, regionally specific changes in functional connectivity between task and rest were also observed. During rest, frontoparietal regions formed many small, loosely connected functional communities. During the task, these regions joined together with visual regions to form one large community (see **Figure 2.5**). This agglomerative frontoparietal-visual community was positively activated for each task (see **Figure 2.6**). Together, these results showed that a stable functional community architecture supports both symbolic and perceptual reasoning, and that activity within a task-specific community can be dialed up and down to meet the unique demands of each reasoning condition. This experiment suggested that the stable community architecture acts as a cognitive control mechanism, creating a "ready" brain state that is prepared to process reasoning-based information via small changes to the brain activity within these stable communities.

Chapter Three examined the relative contributions of stable and flexible brain networks to context-dependent rule learning. Twenty-nine naïve participants were tasked with learning a set of context-dependent rules through trial and error over the course of an fMRI scanning session. Subject performance on the task varied considerably, with some subjects learning the context-dependent rules within the first two scan runs, and others

remaining at chance-levels of accuracy throughout the entire scan. This design resulted in a group of successful learners and a natural control group of unsuccessful learners. A dynamic network analysis demonstrated that the regionally specific flexible switching of brain network nodes between network communities was associated with overall accuracy on the rule learning task. Specifically, results demonstrated that increased stability in ventral attention and somatomotor regions was associated with higher overall accuracy on the task (see **Figure 3.4**). Conversely, a (non-significant) trend was observed suggesting that increased flexibility in frontoparietal control regions was also associated with higher overall accuracy (see **Figure 3.4**). Additional analyses demonstrated that the assortativity (the ratio of how strongly connected a node is to its own community compared to another community) of the cognitive control network increased over time in successful learners, but decreased over time in unsuccessful learners (see **Figure 3.5**). Finally, an analysis of inter-community edge strength (which measures the degree to which two communities were interconnected) showed that over time, functional connectivity between the ventral attention and cognitive control communities increased in successful learners, but not in unsuccessful learners (see **Figure 3.6**). Altogether, results from this analysis suggested that a stable ventral attention community and more flexible cognitive control community support rule learning (see **Figures 3.4**, **3.5**, and **3.6**). As a working hypothesis, I suggested that the cognitive control community showed increased flexibility because functional connectivity dynamically shifted as context-dependent rule representations were formed in these regions. Meanwhile, stability within the ventral attention community supported sustained directed attention to relevant task features as rule representations were learned

and implemented. Overall, successful subjects exhibited greater brain network stability during the task because they formed neural representations of the context-dependent rules quickly and maintained these representations throughout the entire scanning session.

Chapter Four presented a follow-up analysis of the context-dependent rule learning experiment focused specifically on the hippocampal and prefrontal hierarchies that support context-dependent rule learning. Using the same dataset as Chapter Three, the hippocampus was manually segmented for each subject into head, body, and tail regions of interest. A beta-series correlation analysis was conducted to calculate seed-to-voxel functional connectivity maps for each of the nine scanning runs. Using a linear mixed-effects model, voxel clusters were identified that exhibited a significant interaction effect between learning group (successful vs. unsuccessful) and time (scanning run). A gradient of learning-related changes in functional connectivity were observed during the Cue period of the task: hippocampal head showed increased functional connectivity with lateral frontal pole and the caudate; hippocampal body showed increased functional connectivity with middle regions of prefrontal cortex, and the hippocampal tail showed increased functional connectivity with dorsolateral prefrontal cortex (see **Figure 4.4**). Additionally, during the Cue period, the hippocampal head showed decreased functional connectivity with the precuneus and mid-cingulate over time in successful but not in unsuccessful learners (see **Figure. 4.4**). Results demonstrated that individual differences in functional connectivity were associated with individual learning rates, as measured by overall accuracy on the task (see **Figure 4.8**). Overall, these results provided evidence for a working hypothesis that

functional connectivity between the hippocampus and fronto-striatal circuits supports the retrieval and implementation of higher-order context during rule-guided behavior.

Discussion

The studies I have presented in this dissertation demonstrated that regionally specific network stability coupled with flexibility of functional connectivity support abstract reasoning and context-dependent rule learning. While a stable network core was maintained in default and somatomotor regions, results also demonstrated flexible reconfiguration of frontoparietal cortex during both reasoning and rule learning. From the experimental results I propose that flexible reconfiguration of frontoparietal control regions is beneficial for higher order cognition. Additionally, stability within somatomotor, default, and ventral attention regions is beneficial for higher order cognition. These networks remained stable across all reasoning conditions and were largely maintained during the transition from rest to reasoning and they exhibited greater stability in successful rule learners. These conclusions are supported by prior work suggesting that rest-to-task reconfiguration is characterized by a stable network core and a more flexible associative cortex (Krienen et al., 2014).

Engagement of the Frontoparietal Control Network Supports Higher Order Cognition

A key result from this dissertation was that the frontoparietal control network was flexibly reconfigured to support higher order cognitive tasks such as reasoning and rule learning. While this network was only loosely connected at rest (exhibiting a fractured community structure), it became much more highly interconnected with itself when

engaged by reasoning tasks (Chapter 2). Chapter 3 demonstrated a similar pattern of higher frontoparietal interconnectivity when examining assortativity in successful rule learners: as subjects successfully learned, their frontoparietal control network became more highly interconnected to itself (Chapter 3). Finally, the lateral frontal pole, which became more highly connected with anterior hippocampus in successful learners during rule learning, was anatomically co-located with atlas-defined frontoparietal control network regions (Chapter 4).

These results are supported by prior literature demonstrating that frontoparietal control network regions are flexibly reconfigured to support cognitive control, abstract reasoning, working memory, and implicit motor sequence learning (Bassett et al., 2011; Braun et al., 2015; Hearne et al., 2017; Ray et al., 2020). Additional studies have demonstrated that the functional connectivity of the frontoparietal control network flexibly adapts to meet task demands (M. W. Cole et al., 2013). The rule learning task in Chapter Three demonstrated increased functional connectivity between frontoparietal control and ventral attention networks in successful learners. This result is supported by previous work (using analogous networks from the Power atlas) indicating that frontoparietal and cingulo-opercular networks become more highly activated and integrated in hierarchical rule tasks (Cocchi et al., 2014; A. Eichenbaum et al., 2020). The frontoparietal network is thought to implement trial-by-trial task control, with the cingulo-opercular network maintaining task-sets (Dosenbach et al., 2007, 2008). This framework was also supported by results from Chapters Two and Three demonstrating increased frontoparietal control flexibility and ventral attention stability during rule learning and abstract reasoning.

Frontoparietal Network Theories of General Cognitive Ability

More broadly, there are several conceptual and theoretical frameworks suggesting that the frontoparietal control network is essential for fluid intelligence and general cognitive ability. Matrix reasoning tasks like the Raven's Progressive Matrices task were originally developed to measure fluid intelligence (Raven, 1941; Ward et al., 2012), and elicit increased activity in frontoparietal cortex during fMRI scanning (Christoff et al., 2001; Golde et al., 2010; Melrose et al., 2007, 2018; Prabhakaran et al., 1997; Shin & Jeon, 2021). Through literature review and meta-analyses researchers have outlined the parieto-frontal integration theory of intelligence (PFIT), proposing that human intelligence is linked to the structural and functional properties of frontoparietal brain regions (Fraenz et al., 2021; Jung & Haier, 2007; Vakhtin et al., 2014). Another body of research views frontoparietal cortex as a multiple demand network implicated in domain-general processing (Duncan, 2010). Like PFIT, the multiple demand framework proposes that frontoparietal cortical activity is associated with fluid intelligence and general cognitive ability (Assem et al., 2020; Tschentscher et al., 2017). A third framework based on a review of the network neuroscience literature is known as the network neuroscience theory of human intelligence (Barbey, 2018; Girn et al., 2019). According to this theoretical framework, human intelligence is largely supported by the brain's ability to flexibly reconfigure its functional community architecture to meet task demands. Based on prior work using network control theory, Barbey proposes that fluid intelligence is supported by the ability of cognitive control networks to drive the brain into difficult-to-reach activity states (Barbey, 2018; Gu et al., 2015). Using network-based approaches, the results from

this dissertation provided additional evidence for the network neuroscience theory of intelligence, demonstrating that the activation and functional reconfiguration of frontoparietal cortex supports higher order cognition.

Decoupling of Attention and Default Networks Supports Higher Order Cognition

Another common theme across the studies described in this dissertation is the decoupling of attention networks from default network during reasoning and rule learning. The default network was first defined as a set of task-negative regions; brain regions that exhibited decreased activation during an externally-directed attention task, and increased activation and metabolic rate during resting state (Fox et al., 2005; Raichle, 2015). In the study on reasoning (Chapter 2), the default network was deactivated during all four conditions of the reasoning task. Default regions also maintained a stable community structure segregated from attention networks. In the study of rule learning (Chapters 3 and 4), the default network was more highly decoupled from attention networks in successful learners compared to unsuccessful learners. Additionally, the mid-cingulate and precuneus, prominent nodes in the default network, became more strongly decoupled from the hippocampus in successful learners during rule learning. These results are supported by previous work demonstrating that the degree to which default and attention regions are decoupled is associated with working memory scores (J. B. Keller et al., 2015) and indicative of task state (Dixon et al., 2017, 2018). It is hypothesized that the frontoparietal control network (Spreng et al., 2013) and salience network (Seeley et al., 2007) regulate this decoupling. Moreover, previous work suggests that the frontoparietal control network integrates external and internal information via weak connections with both the dorsal

attention network and the default network (Dixon et al., 2017, 2018; Spreng et al., 2013). Combined with results from prior work, this dissertation supports the framework that while the default network is decoupled from attention networks, information from internal schemas and long-term memory can still be incorporated via connections with the frontoparietal control network.

Hierarchical Organization of Functional Brain Networks Supports Complex Cognition

Foundational studies of higher order cognition have delineated a rostro-caudal axis of organization in lateral prefrontal cortex, with rostral regions activating for more abstract task demands, and caudal regions responding to more immediate motor demands (Badre & D'Esposito, 2007, 2009; Badre & Nee, 2018). During abstract reasoning, increased relational integration elicits stronger activity in anterior regions of prefrontal cortex (Badre et al., 2010; Bunge et al., 2009; Christoff et al., 2001). Chapter Two demonstrated that activation of anterior prefrontal cortex was greater during reasoning compared to matching conditions (especially during symbolic reasoning). Functional networks differentially contribute to this hierarchy. Sensorimotor and dorsal attention networks are located more caudally in prefrontal cortex and process information related to immediate task demands (Badre & Nee, 2018; Choi et al., 2018; Nee, 2021). The frontoparietal control network (which may be split into multiple networks) is located more anteriorly in prefrontal cortex and is activated by tasks that require the brain to integrate higher-order rules and contexts (Badre & Nee, 2018; Choi et al., 2018; Nee, 2021).

The rostro-caudal functional organization of prefrontal cortex is supported by anatomical studies demonstrating that prefrontal connections with striatum are organized

in a series of parallel loops (Alexander et al., 1986; Haber, 2003). These fronto-striatal loops are hierarchically organized into motor (posterior), associative (central), and limbic (anterior) circuits (Jahanshahi et al., 2015; Lawrence et al., 1998; Obeso et al., 2008). A study of resting state functional connectivity demonstrated that the basal ganglia exhibit an intrinsic functional network structure that corresponds to the anatomy of fronto-striatal loops (Choi et al., 2012). Chapter Three demonstrated that as subjects learned context-dependent rules, functional connectivity increased between the anterior hippocampus and functionally linked regions of anterior prefrontal cortex and the caudate nucleus. Specifically, the prefrontal and caudate regions that showed increased functional connectivity in Chapter Three also co-localize with frontoparietal control network regions (Choi et al., 2012; Schaefer et al., 2018; Yeo et al., 2011). These results suggested that hippocampal functional connectivity increased with more rostral/abstract regions of the fronto-striatal hierarchy when learning context-dependent rules.

Anatomical and functional evidence suggests that lateral parietal cortex exhibits a hierarchical organization that mirrors that of lateral prefrontal cortex (Choi et al., 2018). Recent work has proposed that the rostro-caudal organization of prefrontal cortex is actually part of a broader frontoparietal network organization based on distance from sensorimotor cortex (Choi et al., 2018; Nee, 2021). By considering whole-brain functional networks, this dissertation is able to examine the dynamic, parallel contributions of lateral prefrontal and parietal cortices during higher order cognitive tasks. Chapters 2 and 3 demonstrated that regions within the frontoparietal control network flexibly reconfigured and became more strongly connected to each other during reasoning and rule learning.

These results supported the framework that the frontoparietal control network is composed of several subnetworks (Dixon et al., 2018; Nee, 2021; Yeo et al., 2011) that flexibly reconfigure and synchronize to support cognitive control processes (Cocchi et al., 2014; M. W. Cole et al., 2013; Nee, 2021).

Limitations

The cognitive tasks presented in this dissertation were meant to operationalize higher order cognitive skills that humans use every day: namely, reasoning and context-dependent rule learning. When designing a task for use in a well-controlled neuroimaging experiment, external validity (the extent to which results can be generalized to real-world situations) is limited. Some recent approaches to study functional brain networks have attempted to do so with more naturalistic tasks. Rather than displaying hundreds of repeated trials of abstract tasks, recent studies have conducted brain scans during movie watching (Cooper et al., 2021; Finn & Bandettini, 2021; Nishimoto et al., 2011; Silva et al., 2019; Visconti di Oleggio Castello et al., 2020), natural language/narrative processing (Baldassano et al., 2017; Huth et al., 2016), or simulated real-world navigation (Brunec et al., 2018; Howard et al., 2014). These naturalistic tasks more accurately mimic the continuous flow of information our brains are confronted with every day, rather than the tightly controlled, discretized tasks we present in this dissertation. Future studies of rule learning and reasoning might aim to do so in more naturalistic and continuous task paradigms. The dynamic network analyses employed in this dissertation may be particularly well-suited to analyzing continuous streams of data.

In this dissertation, I used group network atlases to define network regions, but significant recent work has investigated individual differences in functional brain network architecture. While the dynamic network metrics (e.g., Louvain community detection) used in this dissertation account for individual differences in functional network connectivity, the labels assigned to each node by *a priori* group atlases (e.g., dorsal attention, frontoparietal control, etc.) might not be the most accurate network labels for each individual participant. Recent work has made strides in characterizing individual differences in the default network (Braga & Buckner, 2017; Laumann et al., 2015; Toro-Serey et al., 2020), as well as whole-brain network parcellations (Gordon et al., 2017; Kong et al., 2019; Laumann et al., 2015; Wang et al., 2015). Future work may benefit from using individualized functional network parcellations prior to calculating network statistics.

Additionally, this dissertation focused primarily on neocortical brain networks, but recent work has extended brain network atlases into subcortical areas. For example, the Yeo7 and Yeo17 parcellations have been extended to include the cerebellum (Buckner et al., 2011) and the basal ganglia (Choi et al., 2012), and the Power atlas has been extended into subcortical regions (Ji et al., 2019). Recent foundational work has established that in the cerebellum, functional connectivity networks show task-related activation, suggesting that cerebellar regions contribute to higher order cognitive processing (e.g., the dorsal and ventral attention regions of the cerebellum are activated by top-down attention and working memory tasks) (Brissenden et al., 2016; Brissenden & Somers, 2019) .

Finally, even in group network atlases there is no agreement for the precise topography and best practices for network labeling. Encouragingly, the network

neuroscience community has made a concerted effort to build a consensus on the topography and taxonomy of cortical functional networks (Uddin et al., 2019, 2021). In addition to consensus efforts for discrete labelling of cortical networks, others have proposed that network labels could be overlapping: one brain region could belong to multiple networks at the same time (Cookson & Esposito, 2021; Najafi et al., 2016). From this perspective, a brain region could belong to different networks depending on the other regions it co-activates with. Another perspective removes the discrete network labels entirely, instead focusing on cortical gradients: axes along which functional connectivity patterns gradually shift (e.g., each region of cortex is labelled with the degree to which it is unimodal vs. associative) (Huntenburg et al., 2018; Margulies et al., 2016). With so much exciting research emerging from this field, the network labels we used in this dissertation may be substantially different from accepted labelling schemes as these efforts advance.

Future Directions

In network neuroscience, the theoretical framework known as network control theory is rapidly gaining popularity and applications. Network control theory is a mathematical framework that allows researchers to build the structure of a network, and then study the way that activity "flows" through that structure by "injecting" activation at specific nodes through computational simulations (Betzel et al., 2016; Cornblath et al., 2020; Gu et al., 2015; Scheid et al., 2021). Given a specific connectivity pattern (defined using structural images or DTI scans), a researcher could identify the amount of "activation energy" required to reach a specific activity state (defined using functional MRI). One

potential follow-up to our study on abstract reasoning could measure the activation energy required to reach a reasoning activation state. Using network control theory, we could simulate the activation energy required for a brain network in a resting state configuration compared to a task configuration. Results from Chapter Two demonstrated that the frontoparietal control network had stronger functional connectivity during the task compared to resting state. Hypothetically, in a network control theory model of the task, less activation energy might be required to reach a reasoning activation state if the frontoparietal control network was in a task-based network configuration compared to a resting-state network configuration. As a working hypothesis, I propose that the underlying task-related functional connectivity primes the network to more easily reach reasoning-based activation states. Network control theory methods could help to quantify the amount of energy saved or expended by reconfiguring functional network topology when transitioning from resting to task states.

Another avenue of future exploration is in multi-sensory task paradigms. This dissertation only used visually-presented tasks, but recent work has demonstrated that prefrontal cortex exhibits sensory-biased functional topography during working memory and attention tasks. In prefrontal cortex, interleaved regions are activated for visual, auditory, and tactile attention and working memory (Michalka et al., 2015; Tobyne, 2019; Tobyne et al., 2017). Using an auditory reasoning or rule learning task, one might expect to see functional network changes centered around auditory-biased prefrontal regions and/or primary auditory cortex. Results from Chapter Two showed that during the simplified Raven's Progressive Matrices task (a visually presented task), there was

increased coupling between frontoparietal cortex and primary visual cortex. On an auditory version of the task, functional connectivity might instead increase between frontoparietal and auditory cortices.

Another interesting follow-up would be to investigate the neurotransmitter systems involved in flexibly reconfiguring functional brain network connectivity. Previous work has shown that cortico-subcortical network connectivity is dopamine-dependent (D. M. Cole, Beckmann, et al., 2013; D. M. Cole, Oei, et al., 2013). Another study used simultaneous MR/PET to demonstrate that network coupling/decoupling is associated with cortical and striatal dopamine D1 receptor density (Roffman et al., 2017). Additional work showed that the increased production of dopamine in older adults is related to cognitive resilience, particularly when considering higher order cognitive skills like cognitive flexibility (Berry et al., 2018; Ciampa et al., 2021, 2022). The widespread innervation of neuromodulatory substances such as dopamine, serotonin, norepinephrine, and acetylcholine positions these molecules to have large-scale modulatory effects on the entirety of neocortex, including functional network organization. Disentangling the potential role of these neurotransmitter systems in the regulation of brain network coupling, integration, and flexibility is a fascinating topic of research and a potential application of emerging simultaneous MR/PET technology.

Conclusion

The work in this dissertation demonstrated that abstract reasoning and rule learning capitalize on flexible reconfiguration of the frontoparietal control network alongside

stability of the somatomotor and ventral attention networks. Three experiments demonstrated that the regionally specific dynamic reconfiguration (and stability) of functional brain networks plays an essential role in supporting higher order cognition.

APPENDIX: SUPPLEMENTARY METHODS

Preprocessing in fMRIprep

The following is a boilerplate statement output by the fMRIprep preprocessing pipeline that we used for our fMRI scans:

Anatomical T1-weighted (T1w) images were corrected for intensity non-uniformity (INU) with `N4BiasFieldCorrection` (Tustison et al., 2010), distributed with ANTs 2.3.1 (Avants et al., 2008), and used as T1w-reference throughout the workflow. The T1w-reference was then skull-stripped with a Nipype implementation of the `antsBrainExtraction.sh` workflow (from ANTs), using OASIS30ANTs as target template. Brain tissue segmentation of cerebrospinal fluid (CSF), white-matter (WM), and gray-matter (GM) was performed on the brain-extracted T1w using `fast` [FSL 6.0.1] (Y. Zhang et al., 2001). Brain surfaces were reconstructed using `recon-all` [FreeSurfer 6.0.0] (Dale et al., 1999), and the brain mask estimated previously was refined with a custom variation of the method to reconcile ANTs-derived and FreeSurfer-derived segmentations of the cortical gray-matter of Mindboggle (Klein et al., 2017). Volume-based spatial normalization to one standard space (MNI152NLin2009cAsym) was performed through nonlinear registration with `antsRegistration` (ANTs 2.3.1), using brain-extracted versions of both T1w reference and the T1w template. The following template was selected for spatial normalization: ICBM 152 Nonlinear Asymmetrical template version 2009c (Fonov et al., 2009).

The following preprocessing steps were performed on the resting-state and task BOLD scans for each subject. First, a reference volume and its skull-stripped version were

generated using a custom methodology of fMRIPrep. A deformation field to correct for susceptibility distortions was estimated based on two echo-planar imaging (EPI) references with opposing phase-encoding directions, using `3dQwarp` (AFNI 2019.01.00) (Cox & Hyde, 1997). Based on the estimated susceptibility distortion, an unwarped BOLD reference was calculated for a more accurate co-registration with the anatomical reference. The BOLD reference was then co-registered to the T1w reference using `bbregister` (FreeSurfer) which implements boundary-based registration (Greve & Fischl, 2009). Co-registration was configured with nine degrees of freedom to account for distortions remaining in the BOLD reference. Head-motion parameters with respect to the BOLD reference (transformation matrices, and six corresponding rotation and translation parameters) are estimated before any spatiotemporal filtering using `mcflirt` [FSL 6.0.1] (Jenkinson et al., 2002). BOLD runs were slice-time corrected using `3dTshift` from AFNI 2019.01.00 (Cox & Hyde, 1997). The BOLD time-series, were resampled to surfaces on the following spaces: fsaverage. The BOLD time-series (including slice-timing correction when applied) were resampled onto their original, native space by applying a single, composite transform to correct for head-motion and susceptibility distortions. These resampled BOLD time-series will be referred to as preprocessed BOLD in original space, or just preprocessed BOLD. The BOLD time-series were resampled into standard space, generating a preprocessed BOLD run in 'MNI152NLin2009cAsym' space. First, a reference volume and its skull-stripped version were generated using a custom methodology of fMRIPrep. Several confounding time-series were calculated based on the preprocessed BOLD: framewise displacement (FD), DVARS and three region-wise global

signals. FD and DVARS are calculated for each functional run, both using their implementations in Nipype [following the definitions by (Power et al., 2014)]. The three global signals are extracted within the CSF, the WM, and the whole-brain masks. The head-motion estimates calculated in the correction step were placed within the corresponding confounds file. The confound time series derived from head motion estimates and global signals were expanded with the inclusion of temporal derivatives and quadratic terms for each (Satterthwaite et al., 2013). Frames that exceeded a threshold of 0.5 mm FD or 1.5 standardised DVARS were annotated as motion outliers.

All resamplings can be performed with a single interpolation step by composing all the pertinent transformations (i.e., head-motion transform matrices, susceptibility distortion correction when available, and co-registrations to anatomical and output spaces). Gridded (volumetric) resamplings were performed using `antsApplyTransforms` (ANTs), configured with Lanczos interpolation to minimize the smoothing effects of other kernels (Lanczos, 1964). Non-gridded (surface) resamplings were performed using `mri_vol2surf` (FreeSurfer). Many internal operations of fMRIPrep use Nilearn 0.5.2 (Abraham et al., 2014), mostly within the functional processing workflow. For more details of the pipeline, see the section corresponding to workflows in fMRIPrep's documentation (https://fmriprep.readthedocs.io/en/latest/workflows.html).

BIBLIOGRAPHY

Abraham, A., Pedregosa, F., Eickenberg, M., Gervais, P., Mueller, A., Kossaifi, J., Gramfort, A., Thirion, B., & Varoquaux, G. (2014). Machine learning for neuroimaging with scikit-learn. *Frontiers in Neuroinformatics*, *8*. https://doi.org/10.3389/fninf.2014.00014

Alexander, G. E., Delong, M. R., & Strick, P. L. (1986). Parallel organization of functionally segregated circuits linking basal ganglia and cortex. *Annual Reviews in Neuroscience*, *9*, 357–381. www.annualreviews.org

Ansari, D., Fugelsang, J. A., Dhital, B., & Venkatraman, V. (2006). Dissociating response conflict from numerical magnitude processing in the brain: An event-related fMRI study. *NeuroImage*, *32*(2), 799–805. https://doi.org/10.1016/J.NEUROIMAGE.2006.04.184

Antzoulatos, E. G., & Miller, E. K. (2014). Increases in Functional Connectivity between Prefrontal Cortex and Striatum during Category Learning. *Neuron*, *83*(1), 216–225. https://doi.org/10.1016/J.NEURON.2014.05.005

Arbabshirani, M. R., Havlicek, M., Kiehl, K. A., Pearlson, G. D., & Calhoun, V. D. (2013). Functional network connectivity during rest and task conditions: A comparative study. *Human Brain Mapping*, *34*(11), 2959–2971. https://doi.org/10.1002/HBM.22118

Assem, M., Blank, I. A., Mineroff, Z., Ademoglu, A., & Fedorenko, E. (2020). Activity in the Fronto-Parietal Multiple-Demand Network is Robustly Associated with Individual Differences in Working Memory and Fluid Intelligence. *Cortex*. https://doi.org/10.1016/j.cortex.2020.06.013

Avants, B. B., Epstein, C. L., Grossman, M., & Gee, J. C. (2008). Symmetric diffeomorphic image registration with cross-correlation: Evaluating automated labeling of elderly and neurodegenerative brain. *Medical Image Analysis*, *12*(1), 26–41. https://doi.org/10.1016/j.media.2007.06.004

Avena-Koenigsberger, A., Misic, B., & Sporns, O. (2017). Communication dynamics in complex brain networks. *Nature Reviews Neuroscience 2017 19:1*, *19*(1), 17–33. https://doi.org/10.1038/nrn.2017.149

Badre, D., & D'Esposito, M. (2007). Functional Magnetic Resonance Imaging Evidence for a Hierarchical Organization of the Prefrontal Cortex. *Journal of Cognitive Neuroscience*, *19*(12), 2082–2099. https://doi.org/10.1162/jocn.2007.19.12.2082

Badre, D., & D'Esposito, M. (2009). Is the rostro-caudal axis of the frontal lobe hierarchical? *Nature Reviews. Neuroscience*, *10*(9), 659–669. https://doi.org/10.1038/nrn2667

Badre, D., Kayser, A. S., & D'Esposito, M. (2010). Frontal Cortex and the Discovery of Abstract Action Rules. *Neuron*, *66*(2), 315–326. https://doi.org/10.1016/J.NEURON.2010.03.025

Badre, D., & Nee, D. E. (2018). Frontal Cortex and the Hierarchical Control of Behavior. *Trends in Cognitive Sciences*, *22*(2), 170–188. https://doi.org/10.1016/j.tics.2017.11.005

Badre, D., & Wagner, A. D. (2007). Left ventrolateral prefrontal cortex and the cognitive control of memory. *Neuropsychologia*, *45*(13), 2883–2901. https://doi.org/10.1016/j.neuropsychologia.2007.06.015

Baldassano, C., Chen, J., Zadbood, A., Pillow, J. W., Hasson, U., & Norman, K. A. (2017). Discovering Event Structure in Continuous Narrative Perception and Memory. *Neuron*, *95*(3), 709-721.e5. https://doi.org/10.1016/J.NEURON.2017.06.041

Barbas, H., & Blatt, G. J. (1995). Topographically specific hippocampal projections target functionally distinct prefrontal areas in the rhesus monkey. *Hippocampus*, *5*(6), 511–533. https://doi.org/10.1002/HIPO.450050604

Barbey, A. K. (2018). Network Neuroscience Theory of Human Intelligence. *Trends in Cognitive Sciences*, *22*(1), 8–20. https://doi.org/10.1016/J.TICS.2017.10.001

Bassett, D. S., & Mattar, M. G. (2017). A Network Neuroscience of Human Learning: Potential to Inform Quantitative Theories of Brain and Behavior. *Trends in Cognitive Sciences*, *21*(4), 250–264. https://doi.org/10.1016/J.TICS.2017.01.010

Bassett, D. S., Wymbs, N. F., Porter, M. A., Mucha, P. J., Carlson, J. M., & Grafton, S. T. (2011). Dynamic reconfiguration of human brain networks during learning. *Proceedings of the National Academy of Sciences*, *108*(18), 7641–7646. https://doi.org/10.1073/pnas.1018985108

Bassett, D. S., Yang, M., Wymbs, N. F., & Grafton, S. T. (2015). Learning-induced autonomy of sensorimotor systems. *Nature Neuroscience*, *18*(5), 744–751. https://doi.org/10.1038/nn.3993

Benjamini, Y., & Hochberg, Y. (1995). Controlling the False Discovery Rate: A Practical and Powerful Approach to Multiple Testing. *Journal of the Royal Statistical Society: Series B (Methodological)*, *57*(1), 289–300. https://doi.org/10.1111/j.2517-6161.1995.tb02031.x

Berry, A. S., Shah, V. D., & Jagust, W. J. (2018). The Influence of Dopamine on Cognitive Flexibility Is Mediated by Functional Connectivity in Young but Not Older Adults. *Journal of Cognitive Neuroscience*, *30*(9), 1330–1344. https://doi.org/10.1162/JOCN_A_01286

Betzel, R. F. (2022). Network neuroscience and the connectomics revolution. *Connectomic Deep Brain Stimulation*, 25–58. https://doi.org/10.1016/B978-0-12-821861-7.00002-6

Betzel, R. F., Gu, S., Medaglia, J. D., Pasqualetti, F., & Bassett, D. S. (2016). Optimally controlling the human connectome: the role of network topology. *Scientific Reports 2016 6:1*, *6*(1), 1–14. https://doi.org/10.1038/srep30770

Betzel, R. F., Satterthwaite, T. D., Gold, J. I., & Bassett, D. S. (2017). Positive affect, surprise, and fatigue are correlates of network flexibility. *Scientific Reports*, *7*(1), 1–10. https://doi.org/10.1038/s41598-017-00425-z

Bisley, J. W., & Goldberg, M. E. (2003). Neuronal Activity in the Lateral Intraparietal Area and Spatial Attention. *Science*, *299*(5603), 81–86. https://doi.org/10.1126/science.1077395

Braga, R. M., & Buckner, R. L. (2017). Parallel Interdigitated Distributed Networks within the Individual Estimated by Intrinsic Functional Connectivity. *Neuron*, *95*(2), 457-471.e5. https://doi.org/10.1016/J.NEURON.2017.06.038

Braun, U., Schäfer, A., Walter, H., Erk, S., Romanczuk-Seiferth, N., Haddad, L., Schweiger, J. I., Grimm, O., Heinz, A., Tost, H., Meyer-Lindenberg, A., & Bassett, D. S. (2015). Dynamic reconfiguration of frontal brain networks during executive cognition in humans. *Proceedings of the National Academy of Sciences*, *112*(37), 11678–11683. https://doi.org/10.1073/pnas.1422487112

Bray, S., Arnold, A. E. G. F., Levy, R. M., & Iaria, G. (2015). Spatial and temporal functional connectivity changes between resting and attentive states. *Human Brain Mapping*, *36*(2), 549–565. https://doi.org/10.1002/HBM.22646

Brincat, S. L., & Miller, E. K. (2015). Frequency-specific hippocampal-prefrontal interactions during associative learning. *Nature Publishing Group*, *18*. https://doi.org/10.1038/nn.3954

Brincat, S. L., & Miller, E. K. (2016). Prefrontal Cortex Networks Shift from External to Internal Modes during Learning. *Journal of Neuroscience*, *36*(37), 9739–9754. https://doi.org/10.1523/JNEUROSCI.0274-16.2016

Brissenden, J. A., Levin, E. J., Osher, D. E., Halko, M. A., & Somers, D. C. (2016). Functional Evidence for a Cerebellar Node of the Dorsal Attention Network.

Journal of Neuroscience, *36*(22), 6083–6096. https://doi.org/10.1523/JNEUROSCI.0344-16.2016

Brissenden, J. A., & Somers, D. C. (2019). Cortico–cerebellar networks for visual attention and working memory. *Current Opinion in Psychology*, *29*, 239–247. https://doi.org/10.1016/J.COPSYC.2019.05.003

Brown, T. I., He, Q., Aselcioglu, I., & Stern, C. E. (2021). Evidence for a gradient within the medial temporal lobes for flexible retrieval under hierarchical task rules. *Hippocampus*, *31*(9), 1003–1019. https://doi.org/10.1002/HIPO.23365

Brown, T. I., Ross, R. S., Keller, J. B., Hasselmo, M. E., & Stern, C. E. (2010). Which Way Was I Going? Contextual Retrieval Supports the Disambiguation of Well Learned Overlapping Navigational Routes. *Journal of Neuroscience*, *30*(21), 7414–7422. https://doi.org/10.1523/JNEUROSCI.6021-09.2010

Brown, T. I., Ross, R. S., Tobyne, S. M., & Stern, C. E. (2012). Cooperative interactions between hippocampal and striatal systems support flexible navigation. *NeuroImage*, *60*(2), 1316–1330. https://doi.org/10.1016/j.neuroimage.2012.01.046

Brunec, I. K., Bellana, B., Ozubko, J. D., Man, V., Robin, J., Liu, Z. X., Grady, C., Rosenbaum, R. S., Winocur, G., Barense, M. D., & Moscovitch, M. (2018). Multiple Scales of Representation along the Hippocampal Anteroposterior Axis in Humans. *Current Biology*, *28*(13), 2129-2135.e6. https://doi.org/10.1016/J.CUB.2018.05.016

Brunec, I. K., & Momennejad, I. (2021). Predictive Representations in Hippocampal and Prefrontal Hierarchies. *Journal of Neuroscience*, JN-RM-1327-21. https://doi.org/10.1523/JNEUROSCI.1327-21.2021

Buckner, R. L., Krienen, F. M., Castellanos, A., Diaz, J. C., & Thomas Yeo, B. T. (2011). The organization of the human cerebellum estimated by intrinsic functional connectivity. *Journal of Neurophysiology*, *106*(5), 2322. https://doi.org/10.1152/JN.00339.2011

Bulkin, D. A., Law, L. M., & Smith, D. M. (2016). Placing memories in context: Hippocampal representations promote retrieval of appropriate memories. *Hippocampus*, *26*(7), 958–971. https://doi.org/10.1002/HIPO.22579

Bullmore, E., Fadili, J., Maxim, V., Şendur, L., Whitcher, B., Suckling, J., Brammer, M., & Breakspear, M. (2004). Wavelets and functional magnetic resonance imaging of the human brain. *NeuroImage*, *23*(SUPPL. 1), S234–S249. https://doi.org/10.1016/j.neuroimage.2004.07.012

Bunge, S. A., Helskog, E. H., & Wendelken, C. (2009). Left, but not right, rostrolateral prefrontal cortex meets a stringent test of the relational integration hypothesis.

NeuroImage, *46*(1), 338–342. https://doi.org/10.1016/J.NEUROIMAGE.2009.01.064

Bunge, S. A., Wendelken, C., Badre, D., & Wagner, A. D. (2005). Analogical reasoning and prefrontal cortex: Evidence for separable retrieval and integration mechanisms. *Cerebral Cortex*, *15*(3), 239–249. https://doi.org/10.1093/cercor/bhh126

Carlson, J. M., Foti, D., Mujica-Parodi, L. R., Harmon-Jones, E., & Hajcak, G. (2011). Ventral striatal and medial prefrontal BOLD activation is correlated with reward-related electrocortical activity: A combined ERP and fMRI study. *NeuroImage*, *57*(4), 1608–1616. https://doi.org/10.1016/J.NEUROIMAGE.2011.05.037

Carp, J. (2013). Optimizing the order of operations for movement scrubbing: Comment on Power et al. *NeuroImage*, *76*, 436–438. https://doi.org/10.1016/j.neuroimage.2011.12.061

Cavada, C., Compañy, T., Tejedor, J., Cruz-Rizzolo, R. J., & Reinoso-Suárez, F. (2000). The anatomical connections of the macaque monkey orbitofrontal cortex. A review. *Cerebral Cortex*, *10*(3), 220–242. https://doi.org/10.1093/CERCOR/10.3.220

Chai, X. J., Castañón, A. N., Öngür, D., & Whitfield-Gabrieli, S. (2012). Anticorrelations in resting state networks without global signal regression. *NeuroImage*, *59*(2), 1420. https://doi.org/10.1016/J.NEUROIMAGE.2011.08.048

Chai, X. J., Whitfield-Gabrieli, S., Shinn, A. K., Gabrieli, J. D. E., Nieto Castãón, A., McCarthy, J. M., Cohen, B. M., & Öngür, D. (2011). Abnormal Medial Prefrontal Cortex Resting-State Connectivity in Bipolar Disorder and Schizophrenia. *Neuropsychopharmacology 2011 36:10*, *36*(10), 2009–2017. https://doi.org/10.1038/npp.2011.88

Choi, E. Y., Drayna, G. K., & Badre, D. (2018). Evidence for a functional hierarchy of association networks. *Journal of Cognitive Neuroscience*, *30*(5), 722–736. https://doi.org/10.1162/JOCN_A_01229

Choi, E. Y., Thomas Yeo, B. T., & Buckner, R. L. (2012). The organization of the human striatum estimated by intrinsic functional connectivity. *Journal of Neurophysiology*, *108*(8), 2242–2263. https://doi.org/10.1152/JN.00270.2012

Christoff, K., Prabhakaran, V., Dorfman, J., Zhao, Z., Kroger, J. K., Holyoak, K. J., & Gabrieli, J. D. E. (2001). Rostrolateral Prefrontal Cortex Involvement in Relational Integration during Reasoning. *NeuroImage*, *14*(5), 1136–1149. https://doi.org/10.1006/nimg.2001.0922

Ciampa, C. J., Parent, J. H., Harrison, T. M., Fain, R. M., Betts, M. J., Maass, A., Winer, J. R., Baker, S. L., Janabi, M., Furman, D. J., D'Esposito, M., Jagust, W. J., &

Berry, A. S. (2022). Associations among locus coeruleus catecholamines, tau pathology, and memory in aging. *Neuropsychopharmacology 2022*, 1–8. https://doi.org/10.1038/s41386-022-01269-6

Ciampa, C. J., Parent, J. H., Lapoint, M. R., Swinnerton, K. N., Taylor, M. M., Tennant, V. R., Whitman, A. J., Jagust, W. J., & Berry, A. S. (2021). Elevated Dopamine Synthesis as a Mechanism of Cognitive Resilience in Aging. *Cerebral Cortex*. https://doi.org/10.1093/CERCOR/BHAB379

Ciric, R., Thompson, W. H., Lorenz, R., Goncalves, M., MacNicol, E., Markiewicz, C. J., Halchenko, Y. O., Ghosh, S. S., Gorgolewski, K. J., Poldrack, R. A., & Esteban, O. (2021). TemplateFlow: FAIR-sharing of multi-scale, multi-species brain models. *BioRxiv*, 2021.02.10.430678. https://doi.org/10.1101/2021.02.10.430678

Cisler, J. M., Bush, K., & Steele, J. S. (2014). A comparison of statistical methods for detecting context-modulated functional connectivity in fMRI. *NeuroImage*, *84*, 1042–1052. https://doi.org/10.1016/J.NEUROIMAGE.2013.09.018

Cocchi, L., Halford, G. S., Zalesky, A., Harding, I. H., Ramm, B. J., Cutmore, T., Shum, D. H. K., & Mattingley, J. B. (2014). Complexity in Relational Processing Predicts Changes in Functional Brain Network Dynamics. *Cerebral Cortex*, *24*(9), 2283–2296. https://doi.org/10.1093/CERCOR/BHT075

Cohen, J. E., Ross, R. S., & Stern, C. E. (2018). Predictability matters: role of the hippocampus and prefrontal cortex in disambiguation of overlapping sequences. *Learning & Memory*, *25*(8), 335–346. https://doi.org/10.1101/LM.047175.117

Cohen, Y., Schneidman, E., & Paz, R. (2021). The geometry of neuronal representations during rule learning reveals complementary roles of cingulate cortex and putamen. *Neuron*, *109*(5), 839-851.e9. https://doi.org/10.1016/j.neuron.2020.12.027

Cole, D. M., Beckmann, C. F., Oei, N. Y. L., Both, S., van Gerven, J. M. A., & Rombouts, S. A. R. B. (2013). Differential and distributed effects of dopamine neuromodulations on resting-state network connectivity. *NeuroImage*, *78*, 59–67. https://doi.org/10.1016/J.NEUROIMAGE.2013.04.034

Cole, D. M., Oei, N. Y. L., Soeter, R. P., Both, S., van Gerven, J. M. A., Rombouts, S. A. R. B., & Beckmann, C. F. (2013). Dopamine-Dependent Architecture of Cortico-Subcortical Network Connectivity. *Cerebral Cortex*, *23*(7), 1509–1516. https://doi.org/10.1093/CERCOR/BHS136

Cole, M. W., Bassett, D. S., Power, J. D., Braver, T. S., & Petersen, S. E. (2014). Intrinsic and Task-Evoked Network Architectures of the Human Brain. *Neuron*, *83*(1), 238–251. https://doi.org/10.1016/J.NEURON.2014.05.014

Cole, M. W., Ito, T., Bassett, D. S., & Schultz, D. H. (2016). Activity flow over resting-state networks shapes cognitive task activations. *Nature Neuroscience*, *19*(12), 1718. https://doi.org/10.1038/NN.4406

Cole, M. W., Ito, T., Cocuzza, C., & Sanchez-Romero, R. (2021). The Functional Relevance of Task-State Functional Connectivity. *Journal of Neuroscience*, *41*(12), 2684–2702. https://doi.org/10.1523/JNEUROSCI.1713-20.2021

Cole, M. W., Reynolds, J. R., Power, J. D., Repovs, G., Anticevic, A., & Braver, T. S. (2013). Multi-task connectivity reveals flexible hubs for adaptive task control. *Nature Neuroscience 2013 16:9*, *16*(9), 1348–1355. https://doi.org/10.1038/nn.3470

Cole, M. W., & Schneider, W. (2007). The cognitive control network: Integrated cortical regions with dissociable functions. *NeuroImage*, *37*(1), 343–360. https://doi.org/10.1016/j.neuroimage.2007.03.071

Cole, M. W., Yarkoni, T., Repovš, G., Anticevic, A., & Braver, T. S. (2012). Global connectivity of prefrontal cortex predicts cognitive control and intelligence. *Journal of Neuroscience*, *32*(26), 8988–8999. https://doi.org/10.1523/JNEUROSCI.0536-12.2012

Collins, A. G. E., & Frank, M. J. (2013). Cognitive control over learning: Creating, clustering, and generalizing task-set structure. *Psychological Review*, *120*(1), 190–229. https://doi.org/10.1037/a0030852

Cookson, S. L., & Esposito, M. D. ’. (2021). Evaluating the reliability, validity, and utility of overlapping networks: Implications for cognitive control. *BioRxiv*, 2021.09.28.462232. https://doi.org/10.1101/2021.09.28.462232

Cooper, R. A., Kurkela, K. A., Davis, S. W., & Ritchey, M. (2021). Mapping the organization and dynamics of the posterior medial network during movie watching. *NeuroImage*, *236*, 118075. https://doi.org/10.1016/J.NEUROIMAGE.2021.118075

Corbetta, M., & Shulman, G. L. (2002). Control of goal-directed and stimulus-driven attention in the brain. *Nature Reviews Neuroscience*, *3*(3), 201–215. https://doi.org/10.1038/nrn755

Cornblath, E. J., Ashourvan, A., Kim, J. Z., Betzel, R. F., Ciric, R., Adebimpe, A., Baum, G. L., He, X., Ruparel, K., Moore, T. M., Gur, R. C., Gur, R. E., Shinohara, R. T., Roalf, D. R., Satterthwaite, T. D., & Bassett, D. S. (2020). Temporal sequences of brain activity at rest are constrained by white matter structure and modulated by cognitive demands. *Communications Biology 2020 3:1*, *3*(1), 1–12. https://doi.org/10.1038/s42003-020-0961-x

Cox, R. W. (1996). AFNI: software for analysis and visualization of functional magnetic resonance neuroimages. *Computers and Biomedical Research, an International Journal*, *29*(3), 162–173. http://www.ncbi.nlm.nih.gov/pubmed/8812068

Cox, R. W. (2019). Equitable Thresholding and Clustering: A Novel Method for Functional Magnetic Resonance Imaging Clustering in AFNI. *Brain Connectivity*, *9*(7), 529–538. https://doi.org/10.1089/brain.2019.0666

Cox, R. W., & Hyde, J. S. (1997). Software tools for analysis and visualization of fMRI data. *NMR in Biomedicine*, *10*(4–5), 171–178. https://doi.org/10.1002/(SICI)1099-1492(199706/08)10:4/5<171::AID-NBM453>3.0.CO;2-L

Crittenden, B. M., Mitchell, D. J., & Duncan, X. J. (2016). Task Encoding across the Multiple Demand Cortex Is Consistent with a Frontoparietal and Cingulo-Opercular Dual Networks Distinction. *Journal of Neuroscience*, *36*(23), 6147–6155. https://doi.org/10.1523/JNEUROSCI.4590-15.2016

Cromer, J. A., Machon, M., & Miller, E. K. (2011). Rapid association learning in the primate prefrontal cortex in the absence of behavioral reversals. *Journal of Cognitive Neuroscience*, *23*(7), 1823–1828. https://doi.org/10.1162/jocn.2010.21555

Crone, E. A., Donohue, S. E., Honomichl, R., Wendelken, C., & Bunge, S. A. (2006). Brain Regions Mediating Flexible Rule Use during Development. *Journal of Neuroscience*, *26*(43), 11239–11247. https://doi.org/10.1523/JNEUROSCI.2165-06.2006

Crone, E. A., Wendelken, C., Donohue, S. E., & Bunge, S. A. (2006). Neural Evidence for Dissociable Components of Task-switching. *Cerebral Cortex*, *16*(4), 475–486. https://doi.org/10.1093/cercor/bhi127

Dale, A. M., Fischl, B., & Sereno, M. I. (1999). Cortical Surface-Based Analysis: I. Segmentation and Surface Reconstruction. *NeuroImage*, *9*(2), 179–194. https://doi.org/10.1006/nimg.1998.0395

Daugherty, A. M., Yu, Q., Flinn, R., & Ofen, N. (2015). A reliable and valid method for manual demarcation of hippocampal head, body, and tail. *International Journal of Developmental Neuroscience : The Official Journal of the International Society for Developmental Neuroscience*, *41*, 115–122. https://doi.org/10.1016/J.IJDEVNEU.2015.02.001

Dixon, M. L., Andrews-Hanna, J. R., Spreng, R. N., Irving, Z. C., Mills, C., Girn, M., & Christoff, K. (2017). Interactions between the default network and dorsal attention network vary across default subsystems, time, and cognitive states. *NeuroImage*, *147*, 632–649. https://doi.org/10.1016/J.NEUROIMAGE.2016.12.073

Dixon, M. L., Vega, A. D. la, Mills, C., Andrews-Hanna, J., Spreng, R. N., Cole, M. W., & Christoff, K. (2018). Heterogeneity within the frontoparietal control network and its relationship to the default and dorsal attention networks. *Proceedings of the National Academy of Sciences*, *115*(7), E1598–E1607. https://doi.org/10.1073/PNAS.1715766115

Djurfeldt, M., Ekeberg, Ö., & Graybiel, A. M. (2001). Cortex–basal ganglia interaction and attractor states. *Neurocomputing*, *38–40*, 573–579. https://doi.org/10.1016/S0925-2312(01)00413-1

Dosenbach, N. U. F., Fair, D. A., Cohen, A. L., Schlaggar, B. L., & Petersen, S. E. (2008). A dual-networks architecture of top-down control. *Trends in Cognitive Sciences*, *12*(3), 99–105. https://doi.org/10.1016/J.TICS.2008.01.001

Dosenbach, N. U. F., Fair, D. A., Miezin, F. M., Cohen, A. L., Wenger, K. K., Dosenbach, R. A. T., Fox, M. D., Snyder, A. Z., Vincent, J. L., Raichle, M. E., Schlaggar, B. L., & Petersen, S. E. (2007). Distinct brain networks for adaptive and stable task control in humans. *Proceedings of the National Academy of Sciences of the United States of America*, *104*(26), 11073–11078. https://doi.org/10.1073/pnas.0704320104

Duncan, J. (2010). The multiple-demand (MD) system of the primate brain: mental programs for intelligent behaviour. *Trends in Cognitive Sciences*, *14*(4), 172–179. https://doi.org/10.1016/J.TICS.2010.01.004

Eichenbaum, A., Scimeca, J. M., & D'Esposito, M. (2020). Dissociable Neural Systems Support the Learning and Transfer of Hierarchical Control Structure. *Journal of Neuroscience*, *40*(34), 6624–6637. https://doi.org/10.1523/JNEUROSCI.0847-20.2020

Eichenbaum, H. (2017). Prefrontal–hippocampal interactions in episodic memory. *Nature Reviews Neuroscience 2017 18:9*, *18*(9), 547–558. https://doi.org/10.1038/nrn.2017.74

Esteban, O., Markiewicz, C. J., Blair, R. W., Moodie, C. A., Isik, A. I., Erramuzpe, A., Kent, J. D., Goncalves, M., DuPre, E., Snyder, M., Oya, H., Ghosh, S. S., Wright, J., Durnez, J., Poldrack, R. A., & Gorgolewski, K. J. (2019). fMRIPrep: a robust preprocessing pipeline for functional MRI. *Nature Methods*, *16*(1), 111–116. https://doi.org/10.1038/s41592-018-0235-4

Evensmoen, H. R., Lehn, H., Xu, J., Witter, M. P., Nadel, L., & Håberg, A. K. (2013). The Anterior Hippocampus Supports a Coarse, Global Environmental Representation and the Posterior Hippocampus Supports Fine-grained, Local Environmental Representations. *Journal of Cognitive Neuroscience*, *25*(11), 1908–1925. https://doi.org/10.1162/JOCN_A_00436

Fatima, Z., Kovacevic, N., Misic, B., & McIntosh, A. R. (2016). Dynamic functional connectivity shapes individual differences in associative learning. *Human Brain Mapping*, *37*(11), 3911–3928. https://doi.org/10.1002/hbm.23285

Ferguson, M. A., Anderson, J. S., & Spreng, R. N. (2017). Fluid and flexible minds: Intelligence reflects synchrony in the brain's intrinsic network architecture. *Network Neuroscience*, *1*(2), 192–207. https://doi.org/10.1162/netn_a_00010

Finc, K., Bonna, K., He, X., Lydon-Staley, D. M., Kühn, S., Duch, W., & Bassett, D. S. (2020). Dynamic reconfiguration of functional brain networks during working memory training. *Nature Communications 2020 11:1*, *11*(1), 1–15. https://doi.org/10.1038/s41467-020-15631-z

Finn, E. S., & Bandettini, P. A. (2021). Movie-watching outperforms rest for functional connectivity-based prediction of behavior. *NeuroImage*, *235*, 117963. https://doi.org/10.1016/J.NEUROIMAGE.2021.117963

Fischl, B. (2012). FreeSurfer. *NeuroImage*, *62*(2), 774–781. https://doi.org/10.1016/j.neuroimage.2012.01.021

Fonov, V. S., Evans, A. C., McKinstry, R. C., Almli, C. R., & Collins, D. L. (2009). Unbiased nonlinear average age-appropriate brain templates from birth to adulthood. *NeuroImage*, *47, Supple*, S102. https://doi.org/10.1016/S1053-8119(09)70884-5

Fornito, A., Zalesky, A., & Breakspear, M. (2015). The connectomics of brain disorders. *Nature Reviews Neuroscience*, *16*(3), 159–172. https://doi.org/10.1038/nrn3901

Fortunato, S. (2010). Community detection in graphs. *Physics Reports*, *486*(3–5), 75–174. https://doi.org/10.1016/J.PHYSREP.2009.11.002

Fox, M. D., Snyder, A. Z., Vincent, J. L., Corbetta, M., van Essen, D. C., & Raichle, M. E. (2005). The human brain is intrinsically organized into dynamic, anticorrelated functional networks. *Proceedings of the National Academy of Sciences*, *5*, 9673–9678. www.pnas.orgcgidoi10.1073pnas.0504136102

Fraenz, C., Schlüter, C., Friedrich, P., Jung, R. E., Güntürkün, O., & Genç, E. (2021). Interindividual differences in matrix reasoning are linked to functional connectivity between brain regions nominated by Parieto-Frontal Integration Theory. *Intelligence*, *87*, 101545. https://doi.org/10.1016/J.INTELL.2021.101545

Freedberg, M., Toader, A. C., Wassermann, E. M., & Voss, J. L. (2020). Competitive and cooperative interactions between medial temporal and striatal learning systems. *Neuropsychologia*, *136*, 107257. https://doi.org/10.1016/J.NEUROPSYCHOLOGIA.2019.107257

Freeman, L. C. (1978). Centrality in social networks conceptual clarification. *Social Networks*, *1*(3), 215–239. https://doi.org/10.1016/0378-8733(78)90021-7

Garrison, K. A., Scheinost, D., Finn, E. S., Shen, X., & Constable, R. T. (2015). The (in)stability of functional brain network measures across thresholds. *NeuroImage*, *118*, 651–661. https://doi.org/10.1016/J.NEUROIMAGE.2015.05.046

Gerraty, R. T., Davidow, J. Y., Foerde, K., Galvan, A., Bassett, D. S., & Shohamy, D. (2018). Dynamic flexibility in striatal-cortical circuits supports reinforcement learning. *Journal of Neuroscience*, *38*(10), 2442–2453. https://doi.org/10.1523/JNEUROSCI.2084-17.2018

Girn, M., Mills, C., & Christoff, K. (2019). Linking brain network reconfiguration and intelligence: Are we there yet? *Trends in Neuroscience and Education*, *15*, 62–70. https://doi.org/10.1016/J.TINE.2019.04.001

Girvan, M., & Newman, M. E. J. (2002). Community structure in social and biological networks. *Proceedings of the National Academy of Sciences*, *99*(12), 7821–7826. https://doi.org/10.1073/pnas.122653799

Golde, M., Cramon, D. Y. von, & Schubotz, R. I. (2010). Differential role of anterior prefrontal and premotor cortex in the processing of relational information. *Neuroimage*, *49*, 2890–2900. https://ac.els-cdn.com/S1053811909009884/1-s2.0-S1053811909009884-main.pdf?_tid=97aed7e8-d9ef-11e7-a3e2-00000aacb361&acdnat=1512501052_d09f4fc9870e53ff7fcf531f3e7547f0

Goni, J., van den Heuvel, M. P., Avena-Koenigsberger, A., de Mendizabal, N. V., Betzel, R. F., Griffa, A., Hagmann, P., Corominas-Murtra, B., Thiran, J. P., & Sporns, O. (2014). Resting-brain functional connectivity predicted by analytic measures of network communication. *Proceedings of the National Academy of Sciences of the United States of America*, *111*(2), 833–838. https://doi.org/10.1073/PNAS.1315529111

Gonzalez-Castillo, J., & Bandettini, P. A. (2018). Task-based dynamic functional connectivity: Recent findings and open questions. *NeuroImage*, *180*, 526–533. https://doi.org/10.1016/J.NEUROIMAGE.2017.08.006

Gonzalez-Castillo, J., Handwerker, D. A., Robinson, M. E., Hoy, C. W., Buchanan, L. C., Saad, Z. S., & Bandettini, P. A. (2014). The spatial structure of resting state connectivity stability on the scale of minutes. *Frontiers in Neuroscience*, *0*(8 JUN), 138. https://doi.org/10.3389/FNINS.2014.00138/ABSTRACT

Goodroe, S. C., Starnes, J., & Brown, T. I. (2018). The Complex Nature of Hippocampal-Striatal Interactions in Spatial Navigation. *Frontiers in Human Neuroscience*, *12*, 250. https://doi.org/10.3389/FNHUM.2018.00250/BIBTEX

Gordon, E. M., Laumann, T. O., Gilmore, A. W., Newbold, D. J., Greene, D. J., Berg, J. J., Ortega, M., Hoyt-Drazen, C., Gratton, C., Sun, H., Hampton, J. M., Coalson, R. S., Nguyen, A. L., McDermott, K. B., Shimony, J. S., Snyder, A. Z., Schlaggar, B. L., Petersen, S. E., Nelson, S. M., & Dosenbach, N. U. F. (2017). Precision Functional Mapping of Individual Human Brains. *Neuron*, *95*(4), 791-807.e7. https://doi.org/10.1016/J.NEURON.2017.07.011

Gordon, E. M., Lynch, C. J., Gratton, C., Petersen, S. E., Dosenbach, N. U. F., & Nelson Correspondence, S. M. (2018). Three Distinct Sets of Connector Hubs Integrate Human Brain Function. *Cell Reports*, *24*, 1687–1695. https://doi.org/10.1016/j.celrep.2018.07.050

Goulas, A., Uylings, H. B. M., & Stiers, P. (2014). Mapping the Hierarchical Layout of the Structural Network of the Macaque Prefrontal Cortex. *Cerebral Cortex*, *24*(5), 1178–1194. https://doi.org/10.1093/CERCOR/BHS399

Grady, C. L. (2020). Meta-analytic and functional connectivity evidence from functional magnetic resonance imaging for an anterior to posterior gradient of function along the hippocampal axis. *Hippocampus*, *30*(5), 456–471. https://doi.org/10.1002/HIPO.23164

Gratton, C., Laumann, T. O., Gordon, E. M., Adeyemo, B., & Petersen, S. E. (2016). Evidence for Two Independent Factors that Modify Brain Networks to Meet Task Goals. *Cell Reports*, *17*(5), 1276–1288. https://doi.org/10.1016/j.celrep.2016.10.002

Gratton, C., Laumann, T. O., Nielsen, A. N., Greene, D. J., Gordon, E. M., Gilmore, A. W., Nelson, S. M., Coalson, R. S., Snyder, A. Z., Schlaggar, B. L., Dosenbach, N. U. F., & Petersen, S. E. (2018). Functional Brain Networks Are Dominated by Stable Group and Individual Factors, Not Cognitive or Daily Variation. *Neuron*, *98*(2), 439-452.e5. https://doi.org/10.1016/J.NEURON.2018.03.035

Gratton, C., Sun, H., & Petersen, S. E. (2018). Control networks and hubs. *Psychophysiology*, *55*(3). https://doi.org/10.1111/psyp.13032

Gratton, G., Cooper, P., Fabiani, M., Carter, C. S., & Karayanidis, F. (2018). Dynamics of cognitive control: Theoretical bases, paradigms, and a view for the future. *Psychophysiology*, *55*(3). https://doi.org/10.1111/psyp.13016

Green, A. E., Kraemer, D. J. M., Fugelsang, J. A., Gray, J. R., & Dunbar, K. N. (2010). Connecting Long Distance: Semantic Distance in Analogical Reasoning Modulates Frontopolar Cortex Activity. *Cerebral Cortex*, *20*(1), 70–76. https://doi.org/10.1093/cercor/bhp081

Greene, A. S., Gao, S., Scheinost, D., & Constable, R. T. (2018). Task-induced brain state manipulation improves prediction of individual traits. *Nature Communications 2018 9:1*, *9*(1), 1–13. https://doi.org/10.1038/s41467-018-04920-3

Greve, D. N., & Fischl, B. (2009). Accurate and robust brain image alignment using boundary-based registration. *NeuroImage*, *48*(1), 63–72. https://doi.org/10.1016/j.neuroimage.2009.06.060

Gu, S., Pasqualetti, F., Cieslak, M., Telesford, Q. K., Yu, A. B., Kahn, A. E., Medaglia, J. D., Vettel, J. M., Miller, M. B., Grafton, S. T., & Bassett, D. S. (2015). Controllability of structural brain networks. *Nature Communications*, *6*(1), 1–10. https://doi.org/10.1038/ncomms9414

Haber, S. N. (2003). The primate basal ganglia: parallel and integrative networks. *Journal of Chemical Neuroanatomy*, *26*(4), 317–330. https://doi.org/10.1016/J.JCHEMNEU.2003.10.003

Hasselmo, M. E., & Eichenbaum, H. (2005). Hippocampal mechanisms for the context-dependent retrieval of episodes. *Neural Networks*, *18*(9), 1172–1190. https://doi.org/10.1016/J.NEUNET.2005.08.007

Hasselmo, M. E., & Stern, C. E. (2018). A network model of behavioural performance in a rule learning task. *Philosophical Transactions of the Royal Society B: Biological Sciences*, *373*(1744). https://doi.org/10.1098/RSTB.2017.0275

Hasson, U., Chen, J., & Honey, C. J. (2015). Hierarchical process memory: memory as an integral component of information processing. *Trends in Cognitive Sciences*, *19*(6), 304–313. https://doi.org/10.1016/J.TICS.2015.04.006

Hearne, L. J., Cocchi, L., Zalesky, A., & Mattingley, J. B. (2015). Interactions between default mode and control networks as a function of increasing cognitive reasoning complexity. *Human Brain Mapping*, *36*(7), 2719–2731. https://doi.org/10.1002/hbm.22802

Hearne, L. J., Cocchi, L., Zalesky, A., & Mattingley, J. B. (2017). Reconfiguration of brain network architectures between resting-state and complexity-dependent cognitive reasoning. *Journal of Neuroscience*, *37*(35), 8399–8411. https://doi.org/10.1523/JNEUROSCI.0485-17.2017

Hilger, K., Fukushima, M., Sporns, O., & Fiebach, C. J. (2020). Temporal stability of functional brain modules associated with human intelligence. *Human Brain Mapping*, *41*(2), 362–372. https://doi.org/10.1002/HBM.24807

Holloway, I. D., Price, G. R., & Ansari, D. (2010). Common and segregated neural pathways for the processing of symbolic and nonsymbolic numerical magnitude: An

fMRI study. *NeuroImage*, *49*(1), 1006–1017. https://doi.org/10.1016/J.NEUROIMAGE.2009.07.071

Horn, A., Ostwald, D., Reisert, M., & Blankenburg, F. (2014). The structural–functional connectome and the default mode network of the human brain. *NeuroImage*, *102*(P1), 142–151. https://doi.org/10.1016/J.NEUROIMAGE.2013.09.069

Hoshi, E., Shima, K., & Tanji, J. (2000). Neuronal activity in the primate prefrontal cortex in the process of motor selection based on two behavioral rules. *Journal of Neurophysiology*, *83*(4), 2355–2373. https://doi.org/10.1152/jn.2000.83.4.2355

Howard, L. R., Javadi, A. H., Yu, Y., Mill, R. D., Morrison, L. C., Knight, R., Loftus, M. M., Staskute, L., & Spiers, H. J. (2014). The Hippocampus and Entorhinal Cortex Encode the Path and Euclidean Distances to Goals during Navigation. *Current Biology*, *24*(12), 1331–1340. https://doi.org/10.1016/J.CUB.2014.05.001

Huntenburg, J. M., Bazin, P. L., & Margulies, D. S. (2018). Large-Scale Gradients in Human Cortical Organization. *Trends in Cognitive Sciences*, *22*(1), 21–31. https://doi.org/10.1016/J.TICS.2017.11.002

Huth, A. G., de Heer, W. A., Griffiths, T. L., Theunissen, F. E., & Gallant, J. L. (2016). Natural speech reveals the semantic maps that tile human cerebral cortex. *Nature 2016 532:7600*, *532*(7600), 453–458. https://doi.org/10.1038/nature17637

Izen, S. C., Chrastil, E. R., & Stern, C. E. (2018). Resting state connectivity between medial temporal lobe regions and intrinsic cortical networks predicts performance in a path integration task. *Frontiers in Human Neuroscience*, *12*, 415. https://doi.org/10.3389/FNHUM.2018.00415/BIBTEX

Jahanshahi, M., Obeso, I., Rothwell, J. C., & Obeso, J. A. (2015). A fronto–striato–subthalamic–pallidal network for goal-directed and habitual inhibition. *Nature Reviews Neuroscience 2015 16:12*, *16*(12), 719–732. https://doi.org/10.1038/nrn4038

Jarbo, K., & Verstynen, T. D. (2015). Converging Structural and Functional Connectivity of Orbitofrontal, Dorsolateral Prefrontal, and Posterior Parietal Cortex in the Human Striatum. *Journal of Neuroscience*, *35*(9), 3865–3878. https://doi.org/10.1523/JNEUROSCI.2636-14.2015

Jenkinson, M., Bannister, P., Brady, M., & Smith, S. (2002). Improved Optimization for the Robust and Accurate Linear Registration and Motion Correction of Brain Images. *NeuroImage*, *17*(2), 825–841. https://doi.org/10.1006/nimg.2002.1132

Ji, J. L., Spronk, M., Kulkarni, K., Repovš, G., Anticevic, A., & Cole, M. W. (2019). Mapping the human brain's cortical-subcortical functional network organization. *NeuroImage*, *185*, 35–57. https://doi.org/10.1016/J.NEUROIMAGE.2018.10.006

Jung, R. E., & Haier, R. J. (2007). The Parieto-Frontal Integration Theory (P-FIT) of intelligence: converging neuroimaging evidence. *The Behavioral and Brain Sciences*, *30*(2), 135–154. https://doi.org/10.1017/S0140525X07001185

Kahnt, T. (2018). A decade of decoding reward-related fMRI signals and where we go from here. *NeuroImage*, *180*, 324–333. https://doi.org/10.1016/J.NEUROIMAGE.2017.03.067

Kaiser, R. H., Whitfield-Gabrieli, S., Dillon, D. G., Goer, F., Beltzer, M., Minkel, J., Smoski, M., Dichter, G., & Pizzagalli, D. A. (2015). Dynamic Resting-State Functional Connectivity in Major Depression. *Neuropsychopharmacology 2016 41:7*, *41*(7), 1822–1830. https://doi.org/10.1038/npp.2015.352

Keller, C. J., Bickel, S., Honey, C. J., Groppe, D. M., Entz, L., Craddock, R. C., Lado, F. A., Kelly, C., Milham, M., & Mehta, A. D. (2013). Neurophysiological investigation of spontaneous correlated and anticorrelated fluctuations of the BOLD signal. *Journal of Neuroscience*, *33*(15), 6333–6342. https://doi.org/10.1523/JNEUROSCI.4837-12.2013

Keller, J. B., Hedden, T., Thompson, T. W., Anteraper, S. A., Gabrieli, J. D. E., & Whitfield-Gabrieli, S. (2015). Resting-state anticorrelations between medial and lateral prefrontal cortex: Association with working memory, aging, and individual differences. *Cortex*, *64*, 271–280. https://doi.org/10.1016/j.cortex.2014.12.001

Kent, J. D., & Herholz, P. (2019). *NiBetaSeries: task related correlations in fMRI Software • Review • Repository • Archive*. https://doi.org/10.21105/joss.01295

Kim, C., Johnson, N. F., Cilles, S. E., & Gold, B. T. (2011). Common and Distinct Mechanisms of Cognitive Flexibility in Prefrontal Cortex. *Journal of Neuroscience*, *31*(13), 4771–4779. https://doi.org/10.1523/JNEUROSCI.5923-10.2011

Kim, H. (2014). Involvement of the dorsal and ventral attention networks in oddball stimulus processing: A meta-analysis. *Human Brain Mapping*, *35*(5), 2265–2284. https://doi.org/10.1002/hbm.22326

Kjelstrup, K. B., Solstad, T., Brun, V. H., Hafting, T., Leutgeb, S., Witter, M. P., Moser, E. I., & Moser, M. B. (2008). Finite scale of spatial representation in the hippocampus. *Science*, *321*(5885), 140–143. https://doi.org/10.1126/SCIENCE.1157086/SUPPL_FILE/KJELSTRUP.SOM.PDF

Klein, A., Ghosh, S. S., Bao, F. S., Giard, J., Häme, Y., Stavsky, E., Lee, N., Rossa, B., Reuter, M., Neto, E. C., & Keshavan, A. (2017). Mindboggling morphometry of human brains. *PLOS Computational Biology*, *13*(2), e1005350. https://doi.org/10.1371/journal.pcbi.1005350

Knutson, B., & Cooper, J. C. (2005). Functional magnetic resonance imaging of reward prediction. *Current Opinion in Neurology*, *18*(4), 411–417. https://doi.org/10.1097/01.WCO.0000173463.24758.F6

Kobayashi, Y., & Amaral, D. G. (2003). Macaque monkey retrosplenial cortex: II. Cortical afferents. *The Journal of Comparative Neurology*, *466*(1), 48–79. https://doi.org/10.1002/CNE.10883

Kobayashi, Y., & Amaral, D. G. (2007). Macaque monkey retrosplenial cortex: III. Cortical efferents. *Journal of Comparative Neurology*, *502*(5), 810–833. https://doi.org/10.1002/cne.21346

Koechlin, E., Ody, C., & Kouneiher, F. (2003). The Architecture of Cognitive Control in the Human Prefrontal Cortex. *Science*, *302*(5648), 1181–1185. https://doi.org/10.1126/SCIENCE.1088545/SUPPL_FILE/KOECHLIN.SOM.PDF

Kolaczyk, E. (2009). Statistical analysis of network data - Methods and models. In *Springer series in Statistics*. https://doi.org/10.1007/978-0-387-88146-1

Komorowski, R. W., Garcia, C. G., Wilson, A., Hattori, S., Howard, M. W., & Eichenbaum, H. (2013). *Behavioral/Cognitive Ventral Hippocampal Neurons Are Shaped by Experience to Represent Behaviorally Relevant Contexts*. https://doi.org/10.1523/JNEUROSCI.5458-12.2013

Komorowski, R. W., Manns, J. R., & Eichenbaum, H. (2009). Robust conjunctive item-place coding by hippocampal neurons parallels learning what happens where. *Journal of Neuroscience*, *29*(32), 9918–9929. https://doi.org/10.1523/JNEUROSCI.1378-09.2009

Kong, R., Li, J., Orban, C., Sabuncu, M. R., Liu, H., Schaefer, A., Sun, N., Zuo, X. N., Holmes, A. J., Eickhoff, S. B., & Yeo, B. T. T. (2019). Spatial Topography of Individual-Specific Cortical Networks Predicts Human Cognition, Personality, and Emotion. *Cerebral Cortex*, *29*(6), 2533–2551. https://doi.org/10.1093/CERCOR/BHY123

Kraus, B. T., Perez, D., Ladwig, Z., Seitzman, B. A., Dworetsky, A., Petersen, S. E., & Gratton, C. (2021). Network variants are similar between task and rest states. *NeuroImage*, *229*, 117743. https://doi.org/10.1016/J.NEUROIMAGE.2021.117743

Krienen, F. M., Thomas Yeo, B. T., & Buckner, R. L. (2014). Reconfigurable task-dependent functional coupling modes cluster around a core functional architecture. *Philosophical Transactions of the Royal Society B: Biological Sciences*, *369*(1653). https://doi.org/10.1098/RSTB.2013.0526

Kringelbach, M. L. (2005). The human orbitofrontal cortex: linking reward to hedonic experience. *Nature Reviews Neuroscience 2005 6:9*, *6*(9), 691–702. https://doi.org/10.1038/nrn1747

Kroger, J., Sabb, F., Fales, C., Bookheimer, S., Cohen, M., & Holyoak, K. (2002). Recruitment of Anterior Dorsolateral Prefrontal Cortex in Human Reasoning: a Parametric Study of Relational Complexity. *Cerebral Cortex*, *12*(5), 477–485.

Laird, A. R., Eickhoff, S. B., Li, K., Robin, D. A., Glahn, D. C., & Fox, P. T. (2009). Investigating the Functional Heterogeneity of the Default Mode Network Using Coordinate-Based Meta-Analytic Modeling. *Journal of Neuroscience*, *29*(46), 14496–14505. https://doi.org/10.1523/JNEUROSCI.4004-09.2009

Lancichinetti, A., & Fortunato, S. (2009). Community detection algorithms: A comparative analysis. *Physical Review E - Statistical, Nonlinear, and Soft Matter Physics*, *80*(5), 056117. https://doi.org/10.1103/PHYSREVE.80.056117/FIGURES/8/MEDIUM

Lanczos, C. (1964). Evaluation of Noisy Data. *Journal of the Society for Industrial and Applied Mathematics Series B Numerical Analysis*, *1*(1), 76–85. https://doi.org/10.1137/0701007

Lashkari, D., Vul, E., Kanwisher, N., & Golland, P. (2010). Discovering structure in the space of fMRI selectivity profiles. *NeuroImage*, *50*(3), 1085–1098. https://doi.org/10.1016/J.NEUROIMAGE.2009.12.106

Laumann, T. O., Gordon, E. M., Adeyemo, B., Snyder, A. Z., Joo, S. J., Chen, M. Y., Gilmore, A. W., McDermott, K. B., Nelson, S. M., Dosenbach, N. U. F., Schlaggar, B. L., Mumford, J. A., Poldrack, R. A., & Petersen, S. E. (2015). Functional System and Areal Organization of a Highly Sampled Individual Human Brain. *Neuron*, *87*(3), 657–670. https://doi.org/10.1016/J.NEURON.2015.06.037

Lawrence, A. D., Sahakian, B. J., & Robbins, T. W. (1998). Cognitive functions and corticostriatal circuits: insights from Huntington's disease. *Trends in Cognitive Sciences*, *2*(10), 379–388. https://doi.org/10.1016/S1364-6613(98)01231-5

Lerner, Y., Honey, C. J., Silbert, L. J., & Hasson, U. (2011). Topographic Mapping of a Hierarchy of Temporal Receptive Windows Using a Narrated Story. *Journal of Neuroscience*, *31*(8), 2906–2915. https://doi.org/10.1523/JNEUROSCI.3684-10.2011

Liu, Y., Brincat, S. L., Miller, E. K., & Hasselmo, M. E. (2020). A Geometric Characterization of Population Coding in the Prefrontal Cortex and Hippocampus during a Paired-Associate Learning Task. *Journal of Cognitive Neuroscience*, *32*(8), 1455–1465. https://doi.org/10.1162/JOCN_A_01569

Maloney, E. A., Risko, E. F., Preston, F., Ansari, D., & Fugelsang, J. (2010). Challenging the reliability and validity of cognitive measures: The case of the numerical distance effect. *Acta Psychologica*, *134*(2), 154–161. https://doi.org/10.1016/J.ACTPSY.2010.01.006

Manns, J. R., & Eichenbaum, H. (2009). A cognitive map for object memory in the hippocampus. *Learning & Memory*, *16*(10), 616–624. https://doi.org/10.1101/LM.1484509

Mansouri, F. A., Freedman, D. J., & Buckley, M. J. (2020). Emergence of abstract rules in the primate brain. *Nature Reviews Neuroscience*, *21*(11), 595–610. https://doi.org/10.1038/s41583-020-0364-5

Mantini, D., Corbetta, M., Perrucci, M. G., Romani, G. L., & Del Gratta, C. (2009). Large-scale brain networks account for sustained and transient activity during target detection. *NeuroImage*, *44*(1), 265–274. https://doi.org/10.1016/j.neuroimage.2008.08.019

Margulies, D. S., Ghosh, S. S., Goulas, A., Falkiewicz, M., Huntenburg, J. M., Langs, G., Bezgin, G., Eickhoff, S. B., Castellanos, F. X., Petrides, M., Jefferies, E., & Smallwood, J. (2016). Situating the default-mode network along a principal gradient of macroscale cortical organization. *Proceedings of the National Academy of Sciences of the United States of America*, *113*(44), 12574–12579. https://doi.org/10.1073/PNAS.1608282113/-/DCSUPPLEMENTAL

Meilă, M. (2007). Comparing clusterings—an information based distance. *Journal of Multivariate Analysis*, *98*(5), 873–895. https://doi.org/10.1016/J.JMVA.2006.11.013

Melrose, R. J., Jimenez, A. M., Riskin-Jones, H., Weissberger, G., Veliz, J., Hasratian, A. S., Wilkins, S., & Sultzer, D. L. (2018). Alterations to task positive and task negative networks during executive functioning in Mild Cognitive Impairment. *NeuroImage : Clinical*, *19*, 970. https://doi.org/10.1016/J.NICL.2018.06.014

Melrose, R. J., Poulin, R. M., & Stern, C. E. (2007). An fMRI investigation of the role of the basal ganglia in reasoning. *Brain Research*, *1142*, 146–158. https://doi.org/10.1016/j.brainres.2007.01.060

Menon, V., & D'Esposito, M. (2021). The role of PFC networks in cognitive control and executive function. *Neuropsychopharmacology 2021 47:1*, *47*(1), 90–103. https://doi.org/10.1038/s41386-021-01152-w

Menon, V., & Uddin, L. Q. (2010). Saliency, switching, attention and control: a network model of insula function. *Brain Structure & Function*, *214*(5–6), 655–667. https://doi.org/10.1007/s00429-010-0262-0

Mesulam, M.-M., Jackson, H., & Bullard, F. (1990). Large-scale neurocognitive networks and distributed processing for attention, language, and memory. *Annals of Neurology*, *28*(5), 597–613. https://doi.org/10.1002/ANA.410280502

Michalka, S. W., Kong, L., Rosen, M. L., Shinn-Cunningham, B. G., & Somers, D. C. (2015). Short-Term Memory for Space and Time Flexibly Recruit Complementary Sensory-Biased Frontal Lobe Attention Networks. *Neuron*, *87*(4), 882–892. https://doi.org/10.1016/J.NEURON.2015.07.028

Miller, E. K., & Buschman, T. J. (2014). Neural Mechanisms for the Executive Control of Attention. In A. Nobre & S. Kastner (Eds.), *The Oxford Handbook of Attention* (Issue January). https://doi.org/10.1093/oxfordhb/9780199675111.013.017

Mızrak, E., Bouffard, N. R., Libby, L. A., Boorman, E. D., & Ranganath, C. (2021). The hippocampus and orbitofrontal cortex jointly represent task structure during memory-guided decision making. *Cell Reports*, *37*(9), 110065. https://doi.org/10.1016/J.CELREP.2021.110065

Morin, T. M., Chang, A. E., Ma, W., McGuire, J. T., & Stern, C. E. (2021). Dynamic Network Analysis Demonstrates the Formation of Stable Functional Networks During Rule Learning. *Cerebral Cortex*. https://doi.org/10.1093/CERCOR/BHAB175

Mucha, P. J., Richardson, T., Macon, K., Porter, M. A., & Onnela, J. P. (2010). Community structure in time-dependent, multiscale, and multiplex networks. *Science*, *328*(5980), 876–878. https://doi.org/10.1126/science.1184819

Mueller, S., Wang, D., Fox, M. D., Yeo, B. T. T., Sepulcre, J., Sabuncu, M. R., Shafee, R., Lu, J., & Liu, H. (2013). Individual Variability in Functional Connectivity Architecture of the Human Brain. *Neuron*, *77*(3), 586–595. https://doi.org/10.1016/J.NEURON.2012.12.028

Mumford, J. A., Turner, B. O., Ashby, F. G., & Poldrack, R. A. (2012). Deconvolving BOLD activation in event-related designs for multivoxel pattern classification analyses. *NeuroImage*, *59*(3), 2636–2643. https://doi.org/10.1016/J.NEUROIMAGE.2011.08.076

Najafi, M., McMenamin, B. W., Simon, J. Z., & Pessoa, L. (2016). Overlapping communities reveal rich structure in large-scale brain networks during rest and task conditions. *NeuroImage*, *135*, 92–106. https://doi.org/10.1016/J.NEUROIMAGE.2016.04.054

Nauer, R. K., Dunne, M. F., Stern, C. E., Storer, T. W., & Schon, K. (2020). Improving fitness increases dentate gyrus/CA3 volume in the hippocampal head and enhances memory in young adults. *Hippocampus*, *30*(5), 488–504. https://doi.org/10.1002/HIPO.23166

Nauer, R. K., Whiteman, A. S., Dunne, M. F., Stern, C. E., & Schon, K. (2015). Hippocampal subfield and medial temporal cortical persistent activity during working memory reflects ongoing encoding. *Frontiers in Systems Neuroscience*, *9*(MAR), 30. https://doi.org/10.3389/FNSYS.2015.00030/BIBTEX

Nee, D. E. (2021). Integrative frontal-parietal dynamics supporting cognitive control. *ELife*, *10*. https://doi.org/10.7554/ELIFE.57244

Newman, M. E. J. (2003). Mixing patterns in networks. *Physical Review E - Statistical Physics, Plasmas, Fluids, and Related Interdisciplinary Topics*, *67*(2), 13. https://doi.org/10.1103/PhysRevE.67.026126

Newman, M. E. J., & Girvan, M. (2004). Finding and evaluating community structure in networks. *Physical Review E*, *69*(026113). https://doi.org/10.1103/PhysRevE.69.026113

Nishimoto, S., Vu, A. T., Naselaris, T., Benjamini, Y., Yu, B., & Gallant, J. L. (2011). Reconstructing Visual Experiences from Brain Activity Evoked by Natural Movies. *Current Biology*, *21*(19), 1641–1646. https://doi.org/10.1016/J.CUB.2011.08.031

Nyhus, E., & Barceló, F. (2009). The Wisconsin Card Sorting Test and the cognitive assessment of prefrontal executive functions: A critical update. *Brain and Cognition*, *71*(3), 437–451. https://doi.org/10.1016/J.BANDC.2009.03.005

Obeso, J. A., Rodríguez-Oroz, M. C., Benitez-Temino, B., Blesa, F. J., Guridi, J., Marin, C., & Rodriguez, M. (2008). Functional organization of the basal ganglia: Therapeutic implications for Parkinson's disease. *Movement Disorders*, *23*(S3), S548–S559. https://doi.org/10.1002/MDS.22062

Osher, D. E., Brissenden, J. A., & Somers, D. C. (2019). Predicting an individual's dorsal attention network activity from functional connectivity fingerprints. *Journal of Neurophysiology*, *122*(1), 232–240. https://doi.org/10.1152/JN.00174.2019

Packard, M. G., & McGaugh, J. L. (1996). Inactivation of Hippocampus or Caudate Nucleus with Lidocaine Differentially Affects Expression of Place and Response Learning. *Neurobiology of Learning and Memory*, *65*(1), 65–72. https://doi.org/10.1006/NLME.1996.0007

Palla, G., Barabási, A. L., & Vicsek, T. (2007). Quantifying social group evolution. *Nature 2007 446:7136*, *446*(7136), 664–667. https://doi.org/10.1038/nature05670

Parent, A., & Hazrati, L. N. (1995). Functional anatomy of the basal ganglia. I. The cortico-basal ganglia-thalamo-cortical loop. *Brain Research Reviews*, *20*(1), 91–127. https://doi.org/10.1016/0165-0173(94)00007-C

Parks, E. L., & Madden, D. J. (2013). Brain Connectivity and Visual Attention. *Https://Home.Liebertpub.Com/Brain*, *3*(4), 317–338. https://doi.org/10.1089/BRAIN.2012.0139

Passingham, R. E., Stephan, K. E., & Kötter, R. (2002). The anatomical basis of functional localization in the cortex. *Nature Reviews Neuroscience 2002 3:8*, *3*(8), 606–616. https://doi.org/10.1038/nrn893

Passingham, R. E., Toni, I., & Rushworth, M. F. S. (2000). Specialisation within the prefrontal cortex: The ventral prefrontal cortex and associative learning. In *Experimental Brain Research* (Vol. 133, Issue 1, pp. 103–113). Exp Brain Res. https://doi.org/10.1007/s002210000405

Pasupathy, A., & Miller, E. K. (2005). Different time courses of learning-related activity in the prefrontal cortex and striatum. *Nature*, *433*(7028), 873–876. https://doi.org/10.1038/nature03287

Peirce, J. W. (2007). PsychoPy—Psychophysics software in Python. *Journal of Neuroscience Methods*, *162*(1–2), 8–13. https://doi.org/10.1016/j.jneumeth.2006.11.017

Peirce, J. W. (2008). Generating stimuli for neuroscience using PsychoPy. *Frontiers in Neuroinformatics*, *2*. https://doi.org/10.3389/neuro.11.010.2008

Plachti, A., Eickhoff, S. B., Hoffstaedter, F., Patil, K. R., Laird, A. R., Fox, P. T., Amunts, K., & Genon, S. (2019). Multimodal Parcellations and Extensive Behavioral Profiling Tackling the Hippocampus Gradient. *Cerebral Cortex*, *29*(11), 4595–4612. https://doi.org/10.1093/CERCOR/BHY336

Poldrack, R. A., Laumann, T. O., Koyejo, O., Gregory, B., Hover, A., Chen, M. Y., Gorgolewski, K. J., Luci, J., Joo, S. J., Boyd, R. L., Hunicke-Smith, S., Simpson, Z. B., Caven, T., Sochat, V., Shine, J. M., Gordon, E., Snyder, A. Z., Adeyemo, B., Petersen, S. E., … Mumford, J. A. (2015). Long-term neural and physiological phenotyping of a single human. *Nature Communications 2015 6:1*, *6*(1), 1–15. https://doi.org/10.1038/ncomms9885

Poppenk, J., Evensmoen, H. R., Moscovitch, M., & Nadel, L. (2013). Long-axis specialization of the human hippocampus. *Trends in Cognitive Sciences*, *17*(5), 230–240. https://doi.org/10.1016/J.TICS.2013.03.005

Porter, A., Nielsen, A., Gratton, C., St Louis, in, & Louis, S. (2021). Masked features of task states found in individual brain networks. *BioRxiv*, 2021.06.12.448198. https://doi.org/10.1101/2021.06.12.448198

Porter, M. A., Onnela, J.-P., & Mucha, P. J. (2009). Communities in Networks. *Notices of the American Mathematical Society*, *56*(9), 1082–1097.

Power, J. D., Barnes, K. A., Snyder, A. Z., Schlaggar, B. L., & Petersen, S. E. (2012). Spurious but systematic correlations in functional connectivity MRI networks arise from subject motion. *NeuroImage*, *59*(3), 2142–2154. https://doi.org/10.1016/j.neuroimage.2011.10.018

Power, J. D., Cohen, A. L., Nelson, S. M., Wig, G. S., Barnes, K. A., Church, J. A., Vogel, A. C., Laumann, T. O., Miezin, F. M., Schlaggar, B. L., & Petersen, S. E. (2011). Functional Network Organization of the Human Brain. *Neuron*, *72*(4), 665–678. https://doi.org/10.1016/J.NEURON.2011.09.006

Power, J. D., Mitra, A., Laumann, T. O., Snyder, A. Z., Schlaggar, B. L., & Petersen, S. E. (2014). Methods to detect, characterize, and remove motion artifact in resting state fMRI. *NeuroImage*, *84*(Supplement C), 320–341. https://doi.org/10.1016/j.neuroimage.2013.08.048

Prabhakaran, V., Smith, J. A. L., Desmond, J. E., Glover, G. H., & Gabrieli, J. D. E. (1997). Neural Substrates of Fluid Reasoning: An fMRI Study of Neocortical Activation during Performance of the Raven's Progressive Matrices Test. *Cognitive Psychology*, *33*(1), 43–63. https://doi.org/10.1006/cogp.1997.0659

Pruessner, J. C., Li, L. M., Serles, W., Pruessner, M., Collins, D. L., Kabani, N., Lupien, S., & Evans, A. C. (2000). Volumetry of Hippocampus and Amygdala with High-resolution MRI and Three-dimensional Analysis Software: Minimizing the Discrepancies between Laboratories. *Cerebral Cortex*, *10*(4), 433–442. https://doi.org/10.1093/CERCOR/10.4.433

Raichle, M. E. (2015). The Brain's Default Mode Network. *Http://Dx.Doi.Org/10.1146/Annurev-Neuro-071013-014030*, *38*, 433–447. https://doi.org/10.1146/ANNUREV-NEURO-071013-014030

Raichle, M. E., MacLeod, A. M., Snyder, A. Z., Powers, W. J., Gusnard, D. A., & Shulman, G. L. (2001). A default mode of brain function. *Proceedings of the National Academy of Sciences*, *98*(2), 676–682. https://doi.org/10.1073/PNAS.98.2.676

Raven, J. C. (1941). Standardization of progressive matrices. *British Journal of Medical Psychology*, *19*(1), 137–150. https://doi.org/10.1111/j.2044-8341.1941.tb00316.x

Ray, K. L., Ragland, J. D., MacDonald, A. W., Gold, J. M., Silverstein, S. M., Barch, D. M., & Carter, C. S. (2020). Dynamic reorganization of the frontal parietal network during cognitive control and episodic memory. *Cognitive, Affective and Behavioral Neuroscience*, *20*(1), 76–90. https://doi.org/10.3758/S13415-019-00753-9/FIGURES/6

Rissman, J., Gazzaley, A., & D'Esposito, M. (2004). Measuring functional connectivity during distinct stages of a cognitive task. *NeuroImage*, *23*(2), 752–763. https://doi.org/10.1016/j.neuroimage.2004.06.035

Roberts, A. C., Tomic, D. L., Parkinson, C. H., Roeling, T. A., Cutter, D. J., Robbins, T. W., & Everitt, B. J. (2007). Forebrain connectivity of the prefrontal cortex in the marmoset monkey (Callithrix jacchus): An anterograde and retrograde tract-tracing study. *Journal of Comparative Neurology*, *502*(1), 86–112. https://doi.org/10.1002/CNE.21300

Roffman, J. L., Tanner, A. S., Eryilmaz, H., Rodriguez-Thompson, A., Silverstein, N. J., Ho, N. F., Nitenson, A. Z., Chonde, D. B., Greve, D. N., Abi-Dargham, A., Buckner, R. L., Manoach, D. S., Rosen, B. R., Hooker, J. M., & Catana, C. (2017). Dopamine D 1 signaling organizes network dynamics underlying working memory. *Scientific Advances*, *2*(6). https://doi.org/10.1126/sciadv.1501672

Rosen, M. L., Stern, C. E., Michalka, S. W., Devaney, K. J., & Somers, D. C. (2016). Cognitive Control Network Contributions to Memory-Guided Visual Attention. *Cerebral Cortex*, *26*(5), 2059–2073. https://doi.org/10.1093/cercor/bhv028

Ross, R. S., Sherrill, K. R., & Stern, C. E. (2011). The hippocampus is functionally connected to the striatum and orbitofrontal cortex during context dependent decision making. *Brain Research*, *1423*, 53–66. https://doi.org/10.1016/J.BRAINRES.2011.09.038

Rosvall, M., & Bergstrom, C. T. (2010). Mapping Change in Large Networks. *PLOS ONE*, *5*(1), e8694. https://doi.org/10.1371/JOURNAL.PONE.0008694

Royer, S., Sirota, A., Patel, J., & Buzsáki, G. (2010). Distinct Representations and Theta Dynamics in Dorsal and Ventral Hippocampus. *Journal of Neuroscience*, *30*(5), 1777–1787. https://doi.org/10.1523/JNEUROSCI.4681-09.2010

Rubinov, M., & Sporns, O. (2010). Complex network measures of brain connectivity: Uses and interpretations. *NeuroImage*, *52*(3), 1059–1069. https://doi.org/10.1016/J.NEUROIMAGE.2009.10.003

Rubinov, M., & Sporns, O. (2011). Weight-conserving characterization of complex functional brain networks. *NeuroImage*, *56*(4), 2068–2079. https://doi.org/10.1016/j.neuroimage.2011.03.069

Saad, Z. S., & Reynolds, R. C. (2012). SUMA. *Neuroimage*, *62*(2), 768. https://doi.org/10.1016/J.NEUROIMAGE.2011.09.016

Sadtler, P. T., Quick, K. M., Golub, M. D., Chase, S. M., Ryu, S. I., Tyler-Kabara, E. C., Yu, B. M., & Batista, A. P. (2014). Neural constraints on learning. *Nature*, *512*(7515), 423–426. https://doi.org/10.1038/nature13665

Sahyoun, C. P., Belliveau, J. W., Soulières, I., Schwartz, S., & Mody, M. (2010). Neuroimaging of the functional and structural networks underlying visuospatial vs. linguistic reasoning in high-functioning autism. *Neuropsychologia*, *48*(1), 86–95. https://doi.org/10.1016/j.neuropsychologia.2009.08.013

Salehi, M., Karbasi, A., Barron, D. S., Scheinost, D., & Constable, R. T. (2020). Individualized functional networks reconfigure with cognitive state. *NeuroImage*, *206*, 116233. https://doi.org/10.1016/J.NEUROIMAGE.2019.116233

Salvo, J. J., Holubecki, A. M., & Braga, R. M. (2021). Correspondence between functional connectivity and task-related activity patterns within the individual. *Current Opinion in Behavioral Sciences*, *40*, 178–188. https://doi.org/10.1016/J.COBEHA.2021.05.003

Satterthwaite, T. D., Elliott, M. A., Gerraty, R. T., Ruparel, K., Loughead, J., Calkins, M. E., Eickhoff, S. B., Hakonarson, H., Gur, R. C., Gur, R. E., & Wolf, D. H. (2013). An improved framework for confound regression and filtering for control of motion artifact in the preprocessing of resting-state functional connectivity data. *NeuroImage*, *64*(1), 240–256. https://doi.org/10.1016/j.neuroimage.2012.08.052

Schaefer, A., Kong, R., Gordon, E. M., Laumann, T. O., Zuo, X.-N., Holmes, A. J., Eickhoff, S. B., & Yeo, B. T. T. (2018). Local-Global Parcellation of the Human Cerebral Cortex from Intrinsic Functional Connectivity MRI. *Cerebral Cortex*, *28*(9), 3095–3114. https://doi.org/10.1093/cercor/bhx179

Scheid, B. H., Ashourvan, A., Stiso, J., Davis, K. A., Mikhail, F., Pasqualetti, F., Litt, B., & Bassett, D. S. (2021). Time-evolving controllability of effective connectivity networks during seizure progression. *Proceedings of the National Academy of Sciences of the United States of America*, *118*(5), 2006436118. https://doi.org/10.1073/PNAS.2006436118/-/DCSUPPLEMENTAL

Schendan, H. E., Searl, M. M., Melrose, R. J., & Stern, C. E. (2003). An FMRI study of the role of the medial temporal lobe in implicit and explicit sequence learning. *Neuron*, *37*(6), 1013–1025. https://doi.org/10.1016/S0896-6273(03)00123-5

Schendan, H. E., & Stern, C. E. (2007). Mental rotation and object categorization share a common network of prefrontal and dorsal and ventral regions of posterior cortex.

NeuroImage, *35*(3), 1264–1277. https://doi.org/10.1016/J.NEUROIMAGE.2007.01.012

Schendan, H. E., & Stern, C. E. (2008). Where Vision Meets Memory: Prefrontal–Posterior Networks for Visual Object Constancy during Categorization and Recognition. *Cerebral Cortex*, *18*(7), 1695–1711. https://doi.org/10.1093/cercor/bhm197

Schnider, A., Treyer, V., & Buck, A. (2005). The human orbitofrontal cortex monitors outcomes even when no reward is at stake. *Neuropsychologia*, *43*(3), 316–323. https://doi.org/10.1016/J.NEUROPSYCHOLOGIA.2004.07.003

Schultz, D. H., & Cole, X. W. (2016). Higher Intelligence Is Associated with Less Task-Related Brain Network Reconfiguration. *The Journal of Neuroscience*, *36*(33), 8551–8561. https://doi.org/10.1523/JNEUROSCI.0358-16.2016

Schwarz, A. J., & McGonigle, J. (2011). Negative edges and soft thresholding in complex network analysis of resting state functional connectivity data. *NeuroImage*, *55*(3), 1132–1146. https://doi.org/10.1016/j.neuroimage.2010.12.047

Seeley, W. W., Menon, V., Schatzberg, A. F., Keller, J., Glover, G. H., Kenna, H., Reiss, A. L., & Greicius, M. D. (2007). Dissociable intrinsic connectivity networks for salience processing and executive control. *Journal of Neuroscience*, *27*(9), 2349–2356. https://doi.org/10.1523/JNEUROSCI.5587-06.2007

Setsompop, K., Gagoski, B. A., Polimeni, J. R., Witzel, T., Wedeen, V. J., & Wald, L. L. (2012). Blipped-controlled aliasing in parallel imaging for simultaneous multislice echo planar imaging with reduced g-factor penalty. *Magnetic Resonance in Medicine*, *67*(5), 1210–1224. https://doi.org/10.1002/mrm.23097

Shin, M., & Jeon, H.-A. (2021). A Cortical Surface-Based Meta-Analysis of Human Reasoning. *Cerebral Cortex*. https://doi.org/10.1093/CERCOR/BHAB174

Silva, M., Baldassano, C., & Fuentemilla, L. (2019). Rapid Memory Reactivation at Movie Event Boundaries Promotes Episodic Encoding. *Journal of Neuroscience*, *39*(43), 8538–8548. https://doi.org/10.1523/JNEUROSCI.0360-19.2019

Sokolowski, H. M., Fias, W., Mousa, A., & Ansari, D. (2017). Common and distinct brain regions in both parietal and frontal cortex support symbolic and nonsymbolic number processing in humans: A functional neuroimaging meta-analysis. *NeuroImage*, *146*, 376–394. https://doi.org/10.1016/J.NEUROIMAGE.2016.10.028

Spreng, R. N., Sepulcre, J., Turner, G. R., Stevens, W. D., & Schacter, D. L. (2013). Intrinsic architecture underlying the relations among the default, dorsal attention,

and frontoparietal control networks of the human brain. *Journal of Cognitive Neuroscience*, *25*(1), 74–86. https://doi.org/10.1162/jocn_a_00281

Sridharan, D., Levitin, D. J., & Menon, V. (2008). A critical role for the right fronto-insular cortex in switching between central-executive and default-mode networks. *Proceedings of the National Academy of Sciences of the United States of America*, *105*(34), 12569–12574. https://doi.org/10.1073/pnas.0800005105

Strange, B. A., Witter, M. P., Lein, E. S., & Moser, E. I. (2014). Functional organization of the hippocampal longitudinal axis. *Nature Reviews Neuroscience 2014 15:10*, *15*(10), 655–669. https://doi.org/10.1038/nrn3785

Taren, A. A., Venkatraman, V., & Huettel, S. A. (2011). A Parallel Functional Topography between Medial and Lateral Prefrontal Cortex: Evidence and Implications for Cognitive Control. *Journal of Neuroscience*, *31*(13), 5026–5031. https://doi.org/10.1523/JNEUROSCI.5762-10.2011

Theves, S., Fernández, G., & Doeller, C. F. (2020). The Hippocampus Maps Concept Space, Not Feature Space. *Journal of Neuroscience*, *40*(38), 7318–7325. https://doi.org/10.1523/JNEUROSCI.0494-20.2020

Thiele, J. A., Faskowitz, J., Sporns, O., & Hilger, K. (2021). Multitask Brain Network Reconfiguration Is Inversely Associated with Human Intelligence. *Cerebral Cortex*. https://doi.org/10.1093/CERCOR/BHAB473

Tobyne, S. M. (2019). *Network Organization of Sensory-Biased and Multi-Sensory Working Memory and Attention in Human Cortex with fMRI - ProQuest*. https://www.proquest.com/docview/2247931963?pq-origsite=gscholar&fromopenview=true

Tobyne, S. M., Osher, D. E., Michalka, S. W., & Somers, D. C. (2017). Sensory-biased attention networks in human lateral frontal cortex revealed by intrinsic functional connectivity. *NeuroImage*, *162*, 362–372. https://doi.org/10.1016/J.NEUROIMAGE.2017.08.020

Tobyne, S. M., Somers, D. C., Brissenden, J. A., Michalka, S. W., Noyce, A. L., & Osher, D. E. (2018). Prediction of individualized task activation in sensory modality-selective frontal cortex with "connectome fingerprinting." *NeuroImage*, *183*, 173–185. https://doi.org/10.1016/j.neuroimage.2018.08.007

Tomasi, D., & Volkow, N. D. (2019). Association Between Brain Activation and Functional Connectivity. *Cerebral Cortex*, *29*(5), 1984–1996. https://doi.org/10.1093/CERCOR/BHY077

Toro-Serey, C., Tobyne, S. M., & McGuire, J. T. (2020). Spectral partitioning identifies individual heterogeneity in the functional network topography of ventral and anterior medial prefrontal cortex. *NeuroImage*, *205*, 116305. https://doi.org/10.1016/J.NEUROIMAGE.2019.116305

Tschentscher, N., Mitchell, D., & Duncan, J. (2017). Fluid Intelligence Predicts Novel Rule Implementation in a Distributed Frontoparietal Control Network. *Journal of Neuroscience*, *37*(18), 4841–4847. https://doi.org/10.1523/JNEUROSCI.2478-16.2017

Turner, B. O., Mumford, J. A., Poldrack, R. A., & Ashby, F. G. (2012). Spatiotemporal activity estimation for multivoxel pattern analysis with rapid event-related designs. *NeuroImage*, *62*(3), 1429–1438. https://doi.org/10.1016/J.NEUROIMAGE.2012.05.057

Tustison, N. J., Avants, B. B., Cook, P. A., Zheng, Y., Egan, A., Yushkevich, P. A., & Gee, J. C. (2010). N4ITK: Improved N3 Bias Correction. *IEEE Transactions on Medical Imaging*, *29*(6), 1310–1320. https://doi.org/10.1109/TMI.2010.2046908

Uddin, L., Betzel, R., Cohen, J., Damoiseaux, J., de Brigard, F., Eickhoff, S., Fornito, A., Gratton, C., Gordon, E., Laird, A., Larson-Prior, L., McIntosh, A., Nickerson, L., Pessoa, L., Luísa Pino, A., Poldrack, R., Razi, A., Sadaghiani, S., Shine, J., … Spreng, N. (2021). Update from WHATNET: Workgroup for HArmonized Taxonomy of NETworks. *Organization for Human Brain Mapping*.

Uddin, L. Q., Betzel, R. F., Cohen, J. R., Damoiseaux, J. S., Brigard, F. de, Eickhoff, S. B., Fornito, A., Gratton, C., Gordon, E. M., Laird, A., Larson-Prior, L. J., McIntosh, A. R., Nickerson, L. D., Pessoa, L., Pinho, A. L., Poldrack, R., Razi, A., Sadaghiani, S., Shine, J. M., … Spreng, R. N. (2022). Controversies and current progress on large-scale brain network nomenclature from OHBM WHATNET: Workgroup for HArmonized Taxonomy of NETworks. *Open Science Framework Preprints*. https://doi.org/10.31219/OSF.IO/25ZA6

Uddin, L. Q., Yeo, B. T. T., & Spreng, R. N. (2019). Towards a universal taxonomy of macro-scale functional human brain networks. *Brain Topography*, *32*(6), 926. https://doi.org/10.1007/S10548-019-00744-6

Utevsky, A. v., Smith, D. v., & Huettel, S. A. (2014). Precuneus Is a Functional Core of the Default-Mode Network. *Journal of Neuroscience*, *34*(3), 932–940. https://doi.org/10.1523/JNEUROSCI.4227-13.2014

Vakhtin, A. A., Ryman, S. G., Flores, R. A., & Jung, R. E. (2014). Functional brain networks contributing to the Parieto-Frontal Integration Theory of Intelligence. *NeuroImage*, *103*, 349–354. https://doi.org/10.1016/J.NEUROIMAGE.2014.09.055

van den Heuvel, M. P., & Sporns, O. (2011). Rich-Club Organization of the Human Connectome. *Journal of Neuroscience*, *31*(44), 15775–15786. https://doi.org/10.1523/JNEUROSCI.3539-11.2011

Van Dijk, K. R. A., Hedden, T., Venkataraman, A., Evans, K. C., Lazar, S. W., & Buckner, R. L. (2010). Intrinsic functional connectivity as a tool for human connectomics: Theory, properties, and optimization. *Journal of Neurophysiology*, *103*(1), 297–321. https://doi.org/10.1152/jn.00783.2009

Van Opstal, F., & Verguts, T. (2013). Is there a generalized magnitude system in the brain? Behavioral, neuroimaging, and computational evidence. *Frontiers in Psychology*, *4*, 435. https://doi.org/10.3389/fpsyg.2013.00435

Vincent, J. L., Kahn, I., Snyder, A. Z., Raichle, M. E., & Buckner, R. L. (2008). Evidence for a Frontoparietal Control System Revealed by Intrinsic Functional Connectivity. *Journal of Neurophysiology*, *100*(6), 3328–3342. https://doi.org/10.1152/jn.90355.2008

Visconti di Oleggio Castello, M., Chauhan, V., Jiahui, G., & Gobbini, M. I. (2020). An fMRI dataset in response to "The Grand Budapest Hotel", a socially-rich, naturalistic movie. *Scientific Data 2020 7:1*, *7*(1), 1–9. https://doi.org/10.1038/s41597-020-00735-4

Wallis, J. D., Anderson, K. C., & Miller, E. K. (2001). Single neurons in prefrontal cortex encode abstract rules. *Nature*, *411*(6840), 953–956. https://doi.org/10.1038/35082081

Walsh, V. (2003). A theory of magnitude: common cortical metrics of time, space and quantity. *Trends in Cognitive Sciences*, *7*(11), 483–488. https://doi.org/10.1016/J.TICS.2003.09.002

Wang, D., Buckner, R. L., Fox, M. D., Holt, D. J., Holmes, A. J., Stoecklein, S., Langs, G., Pan, R., Qian, T., Li, K., Baker, J. T., Stufflebeam, S. M., Wang, K., Wang, X., Hong, B., & Liu, H. (2015). Parcellating cortical functional networks in individuals. *Nature Neuroscience*, *18*(12), 1853–1860. https://doi.org/10.1038/nn.4164

Ward, L. C., Bergman, M. A., & Hebert, K. R. (2012). WAIS-IV subtest covariance structure: Conceptual and statistical considerations. *Psychological Assessment*, *24*(2), 328–340. https://doi.org/10.1037/A0025614

Watson, C. E., & Chatterjee, A. (2012). A bilateral frontoparietal network underlies visuospatial analogical reasoning. *NeuroImage*, *59*(3), 2831–2838. https://doi.org/10.1016/J.NEUROIMAGE.2011.09.030

Wendelken, C., Chung, D., & Bunge, S. A. (2012). Rostrolateral prefrontal cortex: Domain-general or domain-sensitive? *Human Brain Mapping*, *33*(8), 1952–1963. https://doi.org/10.1002/hbm.21336

Whitfield-Gabrieli, S., & Nieto-Castanon, A. (2012). Conn: A Functional Connectivity Toolbox for Correlated and Anticorrelated Brain Networks. *Https://Home.Liebertpub.Com/Brain*, *2*(3), 125–141. https://doi.org/10.1089/BRAIN.2012.0073

Wotruba, D., Michels, L., Buechler, R., Metzler, S., Theodoridou, A., Gerstenberg, M., Walitza, S., Kollias, S., Rössler, W., & Heekeren, K. (2014). Aberrant Coupling Within and Across the Default Mode, Task-Positive, and Salience Network in Subjects at Risk for Psychosis. *Schizophrenia Bulletin*, *40*(5), 1095–1104. https://doi.org/10.1093/SCHBUL/SBT161

Yeo, B. T. T., Krienen, F. M., Sepulcre, J., Sabuncu, M. R., Lashkari, D., Hollinshead, M., Roffman, J. L., Smoller, J. W., Zöllei, L., Polimeni, J. R., Fischl, B., Liu, H., & Buckner, R. L. (2011). The organization of the human cerebral cortex estimated by intrinsic functional connectivity. *Journal of Neurophysiology*, *106*(3), 1125–1165. https://doi.org/10.1152/jn.00338.2011

Yushkevich, P. A., Piven, J., Hazlett, H. C., Smith, R. G., Ho, S., Gee, J. C., & Gerig, G. (2006). User-guided 3D active contour segmentation of anatomical structures: Significantly improved efficiency and reliability. *NeuroImage*, *31*(3), 1116–1128. https://doi.org/10.1016/J.NEUROIMAGE.2006.01.015

Zhang, Y., Brady, M., & Smith, S. (2001). Segmentation of brain {MR} images through a hidden Markov random field model and the expectation-maximization algorithm. *IEEE Transactions on Medical Imaging*, *20*(1), 45–57. https://doi.org/10.1109/42.906424

Zhang, Z., Telesford, Q. K., Giusti, C., Lim, K. O., & Bassett, D. S. (2016). Choosing wavelet methods, filters, and lengths for functional brain network construction. *PLoS ONE*, *11*(6), e0157243. https://doi.org/10.1371/journal.pone.0157243

Zhu, H., Paschalidis, I. Ch., Chang, A., Stern, C. E., & Hasselmo, M. E. (2020). A neural circuit model for a contextual association task inspired by recommender systems. *Hippocampus*, *30*(4), 384–395. https://doi.org/10.1002/hipo.23194

CURRICULUM VITAE

THOMAS M. MORIN

www.tmmorin.com
tommorin@bu.edu
@ThomasMorin1

EDUCATION

2017 – 2022 *(anticipated)*
Boston University
PhD Candidate, Computational Neuroscience
Dissertation: *Dynamic Brain Network Reconfiguration Supports Abstract Reasoning and Rule Learning*

2013 – 2017
Tufts University
B.S., *magna cum laude*, Thesis Honors
Cognitive & Brain Science, Computer Science
Senior Honors Thesis: *Optimizing fPET-FDG*

TRAINING

2017 – 2022
Department of Psychological & Brain Sciences, Boston University
Cognitive Neuroimaging Lab
PhD Student Researcher
Mentor: Chantal Stern, DPhil

Spring 2020
MIT IMPACT Program
Fellow

2017 – 2018
Department of Psychological & Brain Sciences, Boston University
Attention & Perception Neuroimaging Lab
Lab Rotation & Collaborating PhD Student
Mentor: David Somers, PhD

2015 – 2017
A. A. Martinos Center for Biomedical Imaging, Massachusetts General Hospital, Harvard Medical School
Hooker Research Group
Research Intern
Mentors: Hsiao-Ying Wey, PhD, and Jacob Hooker, PhD

2014 – 2015 **Department of Psychology, Tufts University**
Memory and Cognition Lab
Undergraduate Research Assistant, May 2014 - May 2015
Mentor: Richard Chechile, PhD

HONORS AND AWARDS

2020 Third Prize, BU Grad. Prog. for Neuro. Interviews Poster Session

2017 Honorable Mention, NSF Graduate Research Fellowship Program

2017 Joanne Mary Sullivan Prize, Tufts University Psychology Department

2017 Barton Term Scholar for Arts and Sciences, Tufts University

2016 SpaceX People's Choice Award, Out for Undergrad Conference

2016 Greg Ellenoff Internship Grant, Tufts University Career Center

2016 Psi Chi Honor Society, Tufts University Chapter

PUBLICATIONS

Selected manuscript PDFs are available at https://www.tmmorin.com/work

Morin, T.M., Chang, A.E., Ma, W., McGuire, J.T. & Stern, C.E. (2021). Dynamic network analysis demonstrates the formation of stable functional networks during rule learning. *Cerebral Cortex*. https://doi.org/10.1093/cercor/bhab175

Gilbert, T.M., Zurcher, N.R., Wu, C.J., Bhanot, A., Hightower, B.G., Kim, M., Albrecht, D.S., Wey, H.Y., Schroeder, F.A., Rodriguez-Thompson, A., **Morin, T.M.**, Hart, K.L., Pellegrini, A.M., Riley, M.M., Wang, C., Stufflebeam, S.M., Haggarty, S.J., Holt, D.J., Loggia, M.L., Perlis, R.H., Brown, H.E., Roffman, J.L., Hooker, J.M. (2019). PET neuroimaging reveals histone deacetylase dysregulation in schizophrenia. *The Journal of Clinical Investigation*. https://doi.org/10.1172/JCI123743

Strebl, M.G., Campbell, A., Zhao, W.N., Riley, M.M., Chindavong, P., **Morin, T.M.**, Haggarty, S.J., Wagner, F.F., Ritter, T., Hooker, J.M. (2017). HDAC6 Brain Mapping with [^{18}F]Bavarostat Enabled by a Ru-Mediated Deoxyfluorination. *ACS Central Science*. 3(9), 1006-1014 http:/dx.doi.org/ 10.1021/acscentsci.7b00274

Placzek, M.S., Zhao, W., Wey, H.Y., **Morin, T.M.**, & Hooker, J.M. (2015). PET neurochemical imaging modes. *Seminars in Nuclear Medicine*, 46(1), 20-27 http://dx.doi.org/10.1053/j.semnuclmed.2015.09.001

MANUSCRIPTS IN PREPARATION

Morin, T.M., Moore, K.N., Isenburg, K.I., Ma, W., & Stern, C.E. Functional reconfiguration of task-active frontoparietal cortex facilitates abstract reasoning. *(in prep.)*

Morin, T.M., Dunne, M.F., Chang, A.E., & Stern, C.E. Hierarchical gradients in prefrontal cortex and hippocampus support context-dependent rule learning *(in prep.)*

Isenburg, K.I., **Morin, T.M.**, Rosen, M.L., Somers, D.C., & Stern, C.E. Default mode precuneus and its role in long term memory-guided versus stimulus-guided attention. *(in prep.)*

CONFERENCE POSTERS & PRESENTATIONS

Selected poster PDFs and presentation slides are available at https://www.tmmorin.com/work

Isenburg, K., **Morin, T.M.**, Rosen, M.L., Somers, D.C., & Stern, C.E. *Network interactions during long-term memory guided versus stimulus-guided attention in humans*. Society for Neuroscience. 2021. (Online Meeting, Due to COVID-19) [Poster]

Liapis, S.S.P., **Morin, T.M.**, McGuire, J.T., & Stern, C.E. *The dimensionality of representational space calibrates to abstract reasoning complexity.* Organization for Human Brain Mapping. 2021. (Online Meeting, Due to COVID-19) [Poster]

Morin, T.M., Ma, W., Chang, A.E., & Stern, C.E. *Dynamic functional connectivity during context-dependent rule learning*. Organization for Human Brain Mapping. 2020. (Online Meeting, Due to COVID-19) [Poster]

Morin, T.M., Moore, K.N., & Stern, C.E. *An fMRI investigation of functional network connectivity during abstract reasoning*. Cognitive Neuroscience Society Annual Meeting. 2020. (Online Meeting, Due to COVID-19). [Poster]

Morin, T.M., Chang, A.E., & Stern, C.E. *Cortical contributions to perceptual and symbolic reasoning using a one-dimensional raven's progressive matrices task.* Society for Neuroscience. 2019. Chicago, IL. [Poster]

Ma, W., **Morin, T.M.**, Chang, A.E., & Stern, C.E. *An fMRI investigation of medial prefrontal network dynamics during a context-dependent rule learning task.* Society for Neuroscience. 2019. Chicago, IL. [Poster]

Morin, T.M. *Frontoparietal Control Network Contributions to Abstract Reasoning*. Boston University Graduate Program for Neuroscience Annual Retreat. 2019. Essex, MA. [Presentation]

Morin, T.M., Chang, A.E., & Stern, C.E. *An fMRI investigation of symbolic processing using a one-dimensional raven's progressive matrices task*. Henry I. Russek Student Achievement Day. 2019. Boston University, Boston, MA. [Poster]

Cohen, J.E., **Morin, T.M.**, & Stern, C.E. *Theta oscillations at critical junctures of overlapping mazes*. Cognitive Neuroscience Society Annual Meeting. 2018. Boston, MA. [Poster]

Morin, T.M. & Wey, H.Y. *Optimizing fPET-FDG*. Cognitive & Brain Science Senior Symposium. 2017. Tufts University, Medford, MA. [Poster]

Morin, T.M. *Branching Out: What a Tree Can Teach You About Your Brain?* Out For Undergrad Engineering Conference. 2016. Stanford University, Palo Alto, CA. [Presentation]

Morin, T.M. *Creating a Computer Simulation Tool for PET Neuroimaging*. Tufts University Undergraduate Research and Scholarship Symposium. 2016. Tufts University, Medford, MA. [Presentation]

TEACHING

2018-2022	Guest Lecturer, *Intro to Neuroimaging* Course: Introduction to Cognitive & Brain Sciences, Tufts University
2021	Guest Lecturer, *Cognitive Neuroscience of Reasoning* Course: Graduate Cognition & Behavior, Boston University
2017	Teaching Assistant Course: Introduction to Cognitive & Brain Science, Tufts University
2016	Teaching Assistant Course: American Sign Language I, II, and III, Tufts University

MENTORSHIP

2022	Carolyn Kinsella, *Boston University, Undergraduate RA*
2020-2021	Bliss Cui, *Boston University, Neuroscience Student Org. Mentee*
2020-2021	Jiahe Nu, *Boston University, High School RA, Undergraduate RA*
2019-2020	Roberto Luis-Fuentes, *Boston University, BME Senior Thesis Project*
2019-2020	Vincent Chang, *Boston University, BME Senior Thesis Project*
2019	Sheila Yee, *Boston University, Undergraduate Directed Study Student*
2018-2020	Weida Ma, *Boston University, Undergraduate RA, BME Senior Thesis*
2018	Neoreet Braha, *Boston University, Undergraduate Research Assistant*

ADDITIONAL EXPERIENCE

2020-2022	Graduate Coach, InGenius Prep | College Admissions Consulting
2021	Volunteer Editor, Application Statement Feedback Program
2017-2019	Volunteer Mentor to a High School Student, Big Brothers Big Sisters
2015-2017	Class of 2017 Representative, Tufts Psychology Society

SKILLS

Programming Languages

- Fluent in Python, R, MATLAB, Shell Scripting
- Comfortable with C, C++
- Experience with HTML/CSS

Neuroimaging & Experimental Software

- AFNI, FSL, Freesurfer, CONN Toolbox, PMOD
- BIDS-compatible pipelines including fMRIprep and NiBetaSeries
- PsychoPy; some experience with ePrime

Key Concepts

- Cognitive neuroscience of abstract reasoning, learning, and memory
- Network science and graph-based analysis of functional connectivity data
- Kinetic modeling and analysis of functional PET neuroimaging data
- fMRI and PET study design, data collection, and analysis